Non-universal avalanches and burstiness in brain network models

Géza Ódor EK-MFA Complex Systems Department, Budapest

Non-universal avalanches and burstiness in brain network models

Géza Ódor EK-MFA Complex Systems Department, Budapest

Theoretical research and experiments suggest that the brain operates at or near a **critical state** between sustained activity and an inactive phase, exhibiting optimal computational properties (see: *Beggs & Plenz J. Neurosci. 2003; Chialvo Nat. Phys. 2010; Haimovici et al. PRL 2013*)

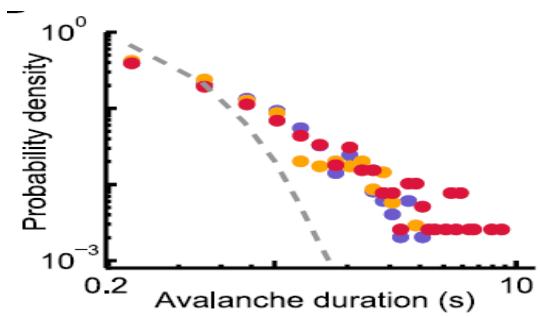

Non-universal avalanches and burstiness in brain network models

Géza Ódor EK-MFA Complex Systems Department, Budapest

Energiatudományi
Kutatóközpont

Theoretical research and experiments suggest that the brain operates at or near a **critical state** between sustained activity and an inactive phase, exhibiting optimal computational properties (see: *Beggs & Plenz J. Neurosci. 2003; Chialvo Nat. Phys. 2010; Haimovici et al. PRL 2013)*

↔ Neuro experiments show discontinuous transitions between up/down states

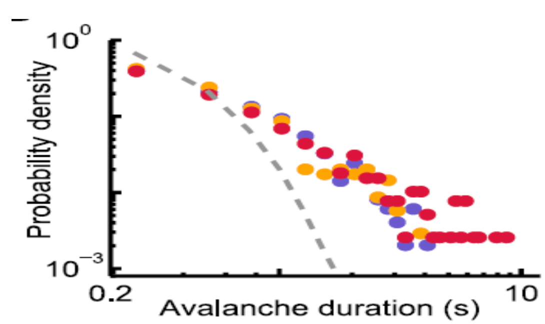

Non-universal avalanches and burstiness in brain network models

Géza Ódor EK-MFA Complex Systems Department, Budapest

Energiatudományi
Kutatóközpont

Theoretical research and experiments suggest that the brain operates at or near a **critical state** between sustained activity and an inactive phase, exhibiting optimal computational properties (see: *Beggs & Plenz J. Neurosci. 2003; Chialvo Nat. Phys. 2010; Haimovici et al. PRL 2013*)

↔ Neuro experiments show discontinuous transitions between up/down states

Quasistatic inhomogneity causes dynamical criticality in Griffiths phases

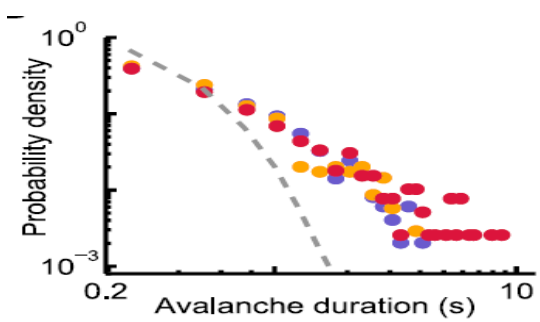

Non-universal avalanches and burstiness in brain network models

Géza Ódor EK-MFA Complex Systems Department, Budapest

Energiatudományi Kutatóközpont

Theoretical research and experiments suggest that the brain operates at or near a **critical state** between sustained activity and an inactive phase, exhibiting optimal computational properties (see: *Beggs & Plenz J. Neurosci. 2003; Chialvo Nat. Phys. 2010; Haimovici et al. PRL 2013*)

↔ Neuro experiments show discontinuous transitions between up/down states

Quasistatic inhomogneity causes dynamical criticality in Griffiths phases

→ Mixed order transition + Griffiths phase together

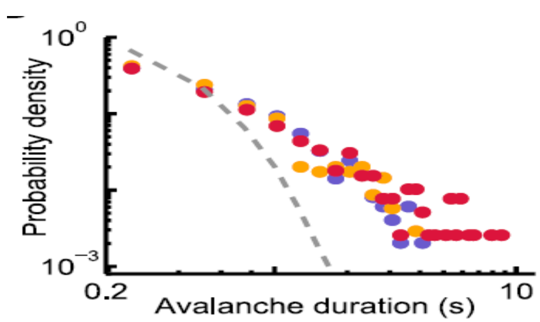

Brain experiments suggest power-law (critical?) activity avalanche behavior

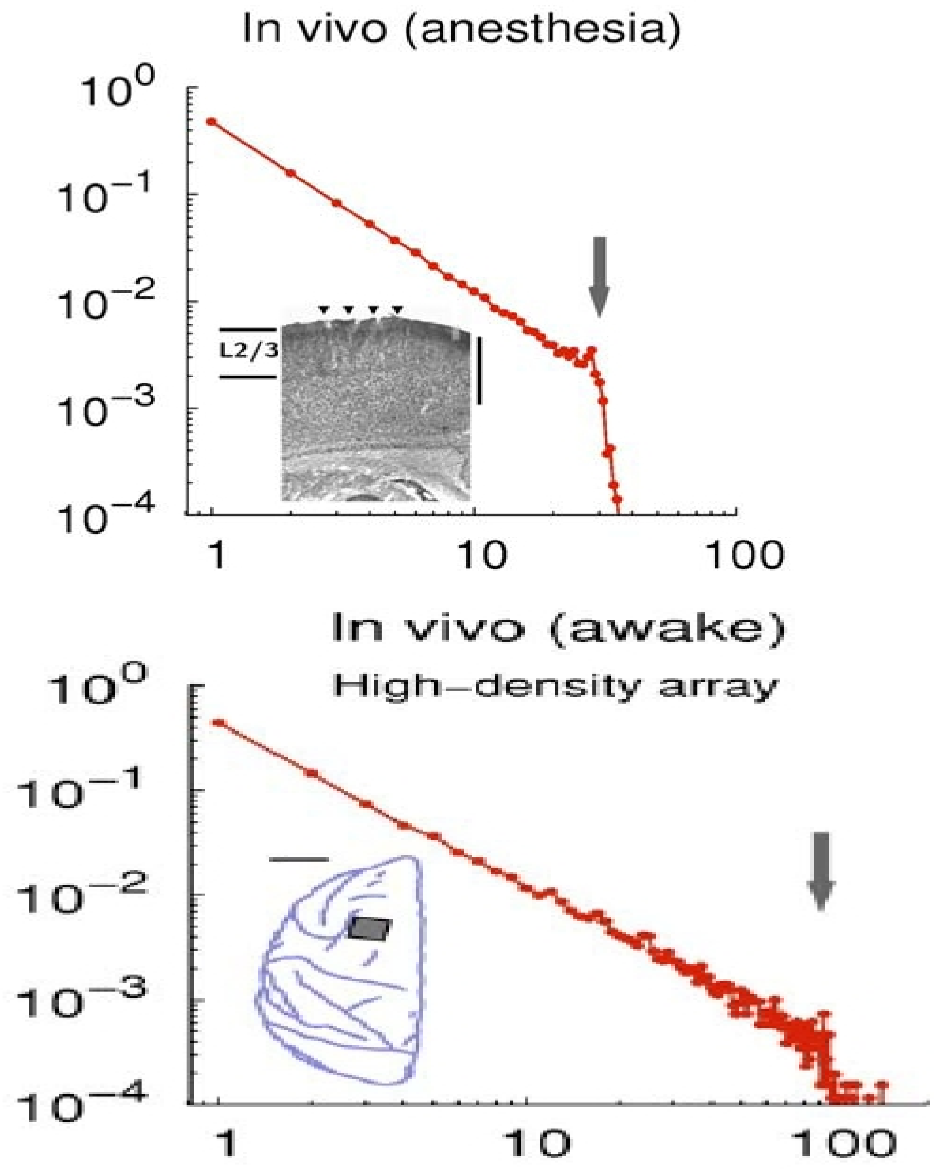

Brain experiments suggest power-law (critical?) activity avalanche behavior

Electrode LFP experiments

Since *Beggs* and *Plenz 2003*

For humans and animals

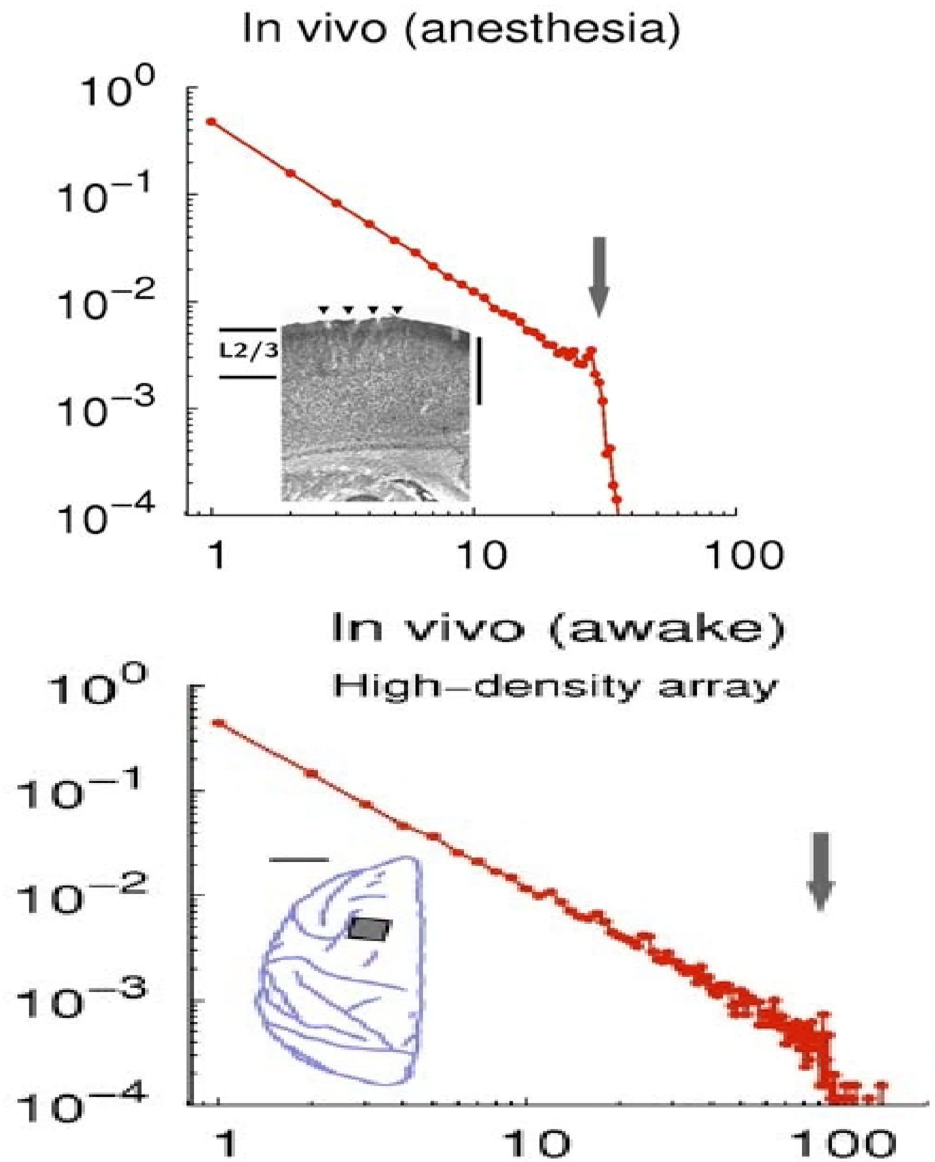

Brain experiments suggest power-law (critical?) activity avalanche behavior

Electrode LFP experiments

Since *Beggs* and *Plenz 2003*

For humans and animals

In vitro, for balanced excitatory/inhibitory states

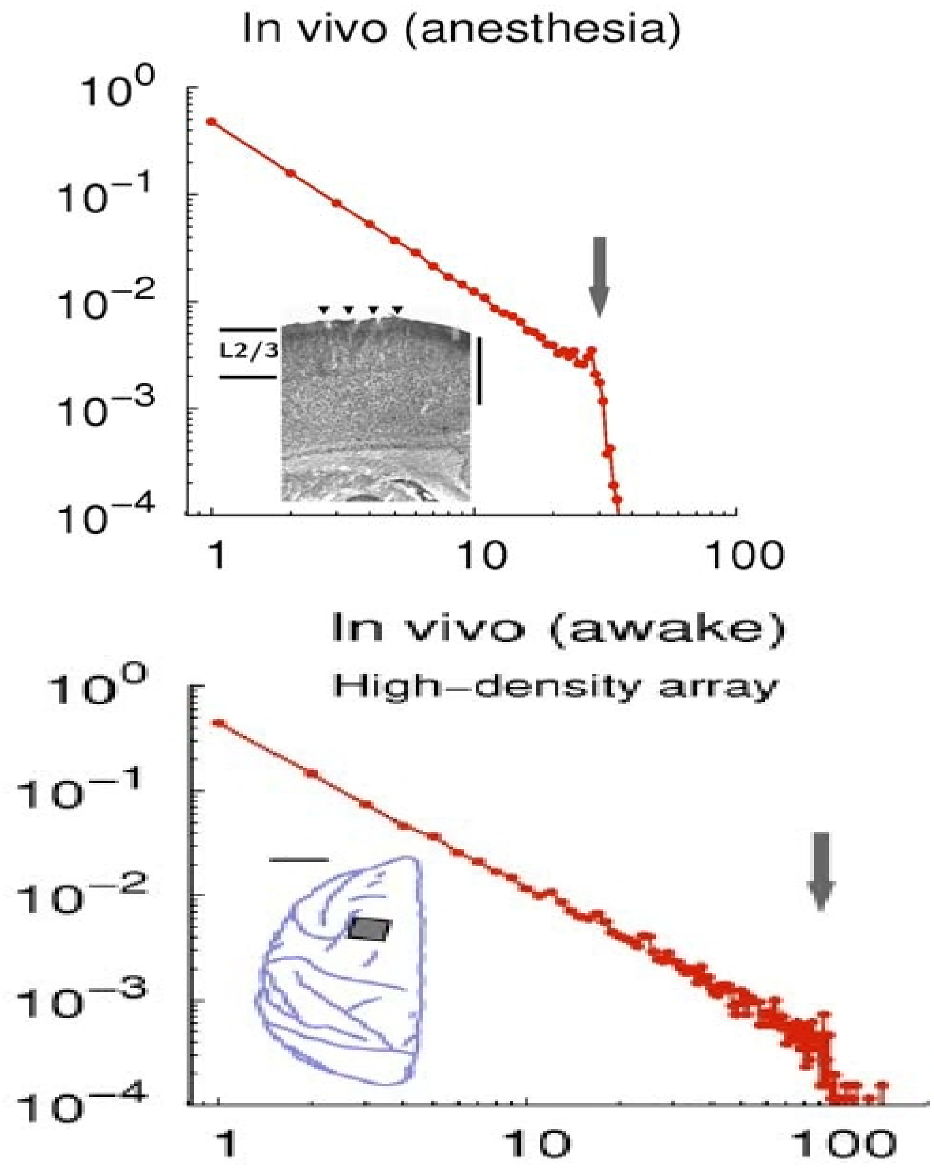

Brain experiments suggest power-law (critical?) activity avalanche behavior

Electrode LFP experiments

Since *Beggs* and *Plenz 2003*

For humans and animals

In vitro, for balanced excitatory/inhibitory states

Other experiments: fMRI, BOLD,

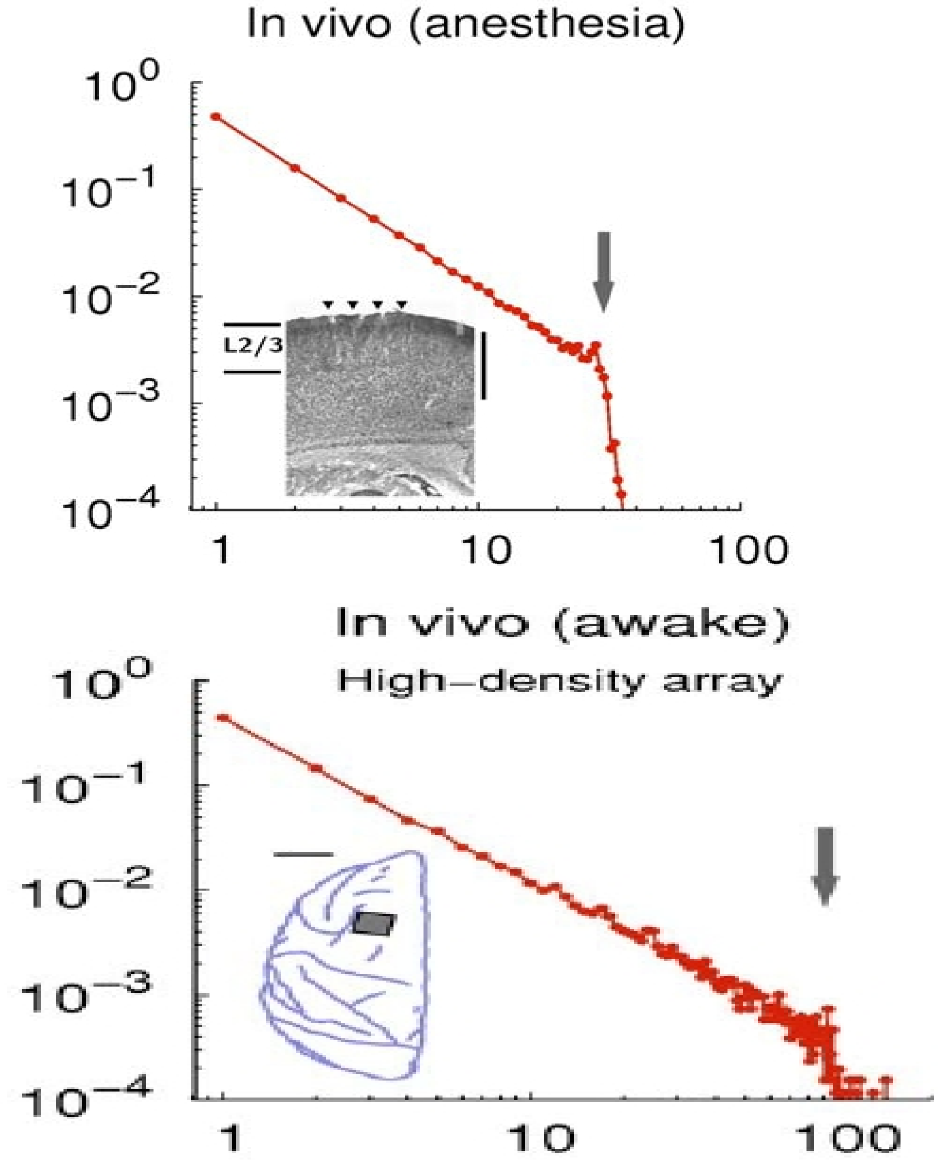

Brain experiments suggest power-law (critical?) activity avalanche behavior

Electrode LFP experiments

Since *Beggs* and *Plenz 2003*

For humans and animals

In vitro, for balanced excitatory/inhibitory states

Other experiments: fMRI, BOLD, Voltage imaging, calcium imaging, MEG, EEG, **L**ong-**R**ange **T**emporal **C**orrelations (**LRTC**).

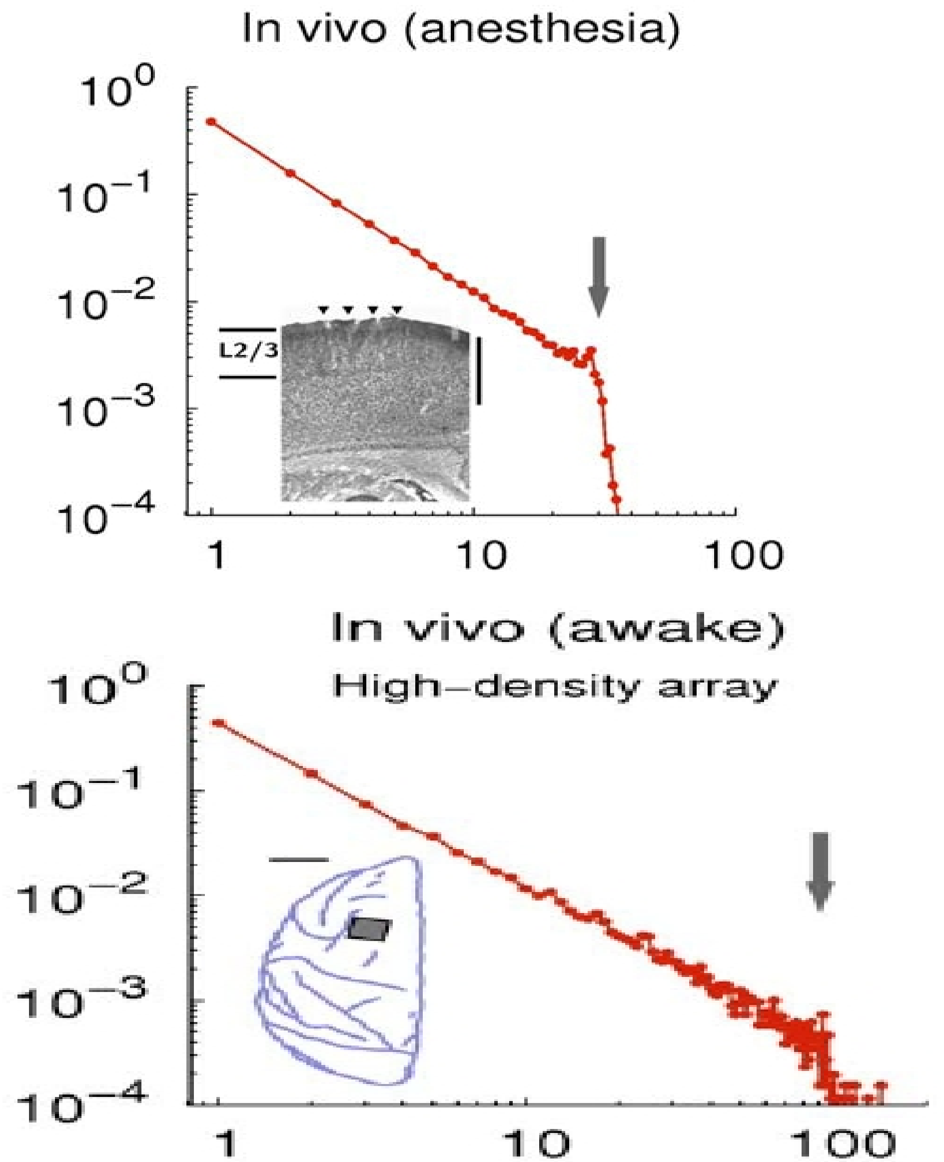

Brain experiments suggest power-law (critical?) activity avalanche behavior

Electrode LFP experiments

Since *Beggs* and *Plenz 2003*

For humans and animals

In vitro, for balanced excitatory/inhibitory states

Other experiments: fMRI, BOLD, Voltage imaging, calcium imaging, MEG, EEG, **L**ong-**R**ange **T**emporal **C**orrelations (**LRTC**).

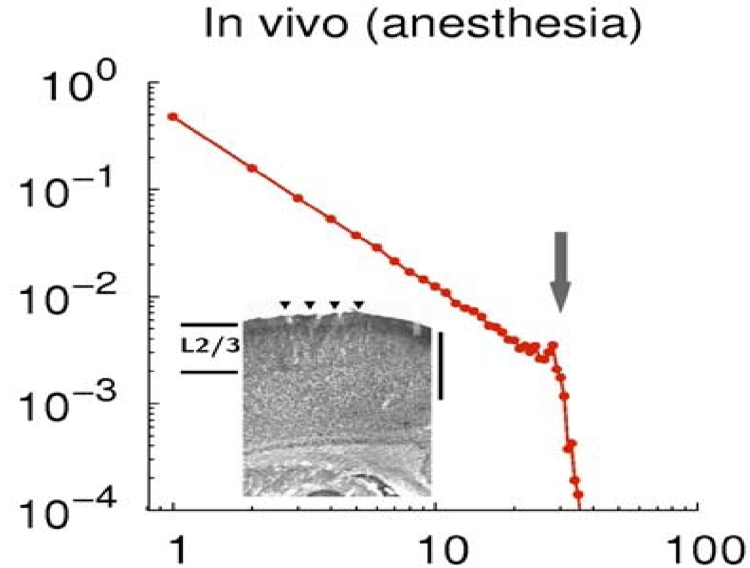

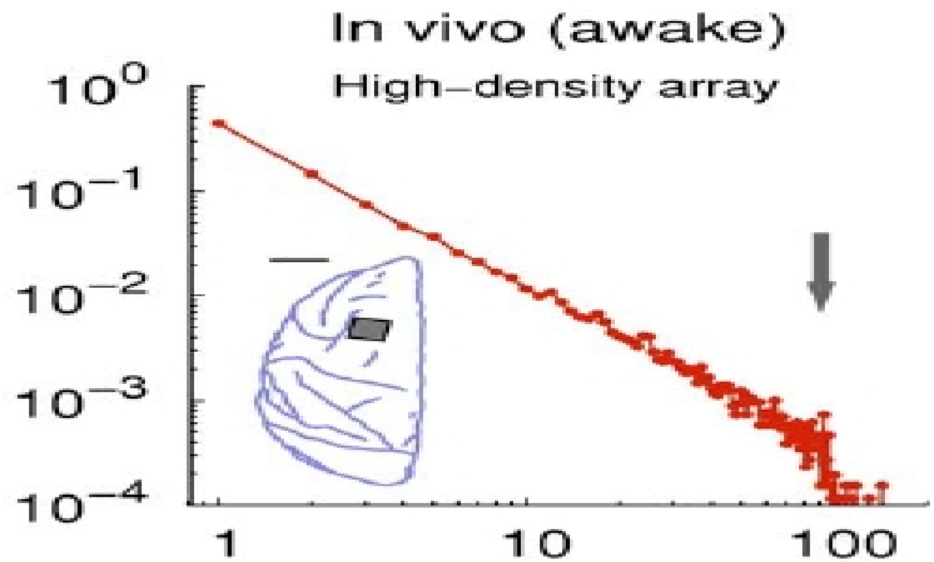

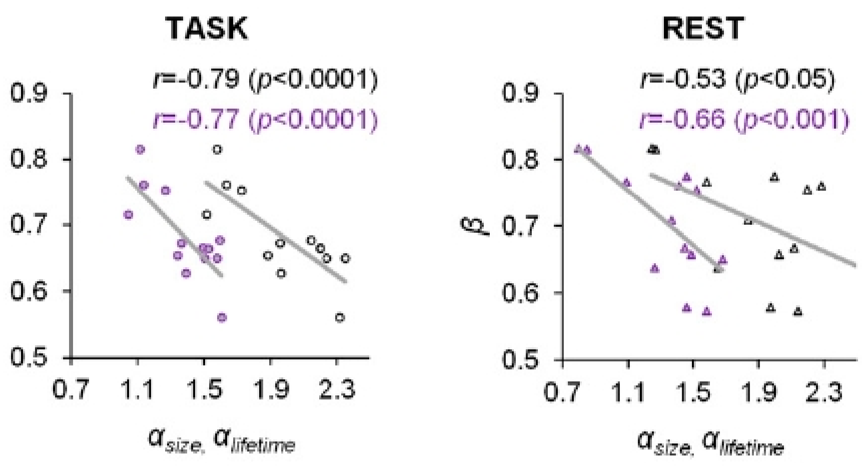

Brain experiments suggest power-law (critical?) activity avalanche behavior

Electrode LFP experiments

Since *Beggs* and *Plenz 2003*

For humans and animals

In vitro, for balanced excitatory/inhibitory states

Other experiments: fMRI, BOLD, Voltage imaging, calcium imaging, MEG, EEG, **L**ong-**R**ange **T**emporal **C**orrelations (**LRTC**).

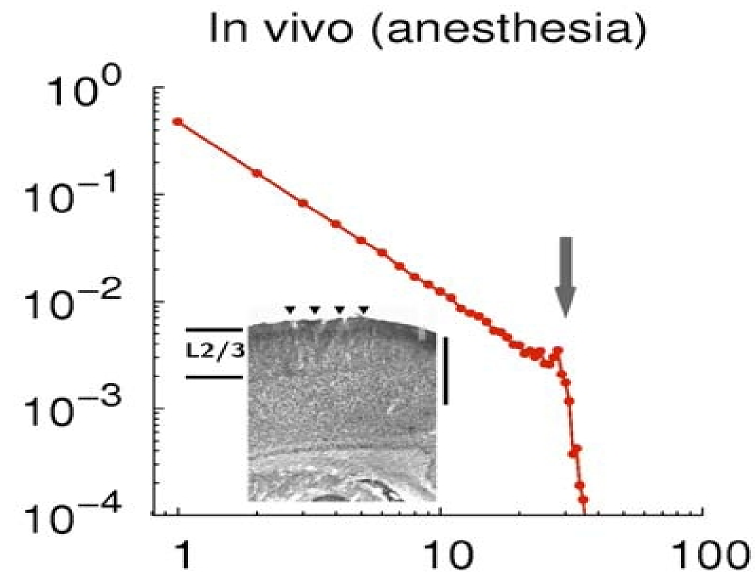

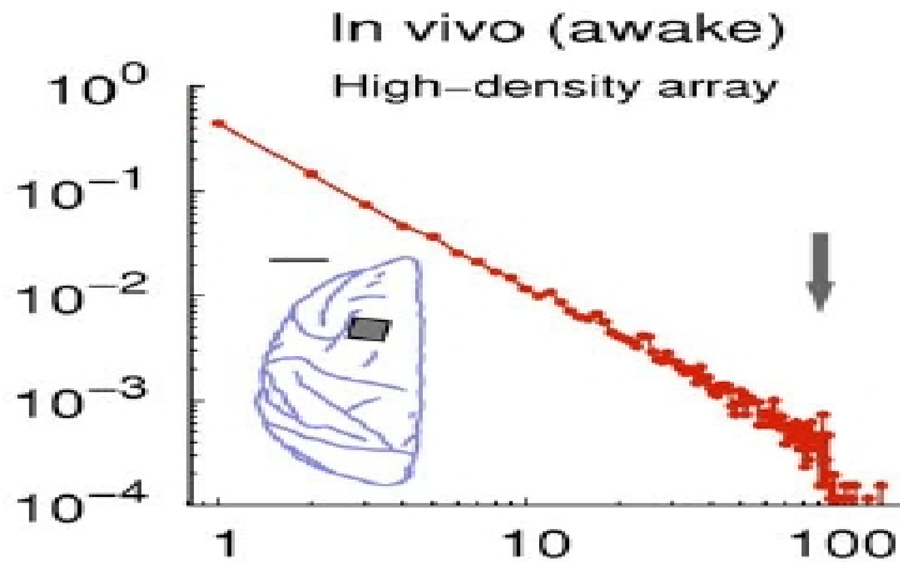

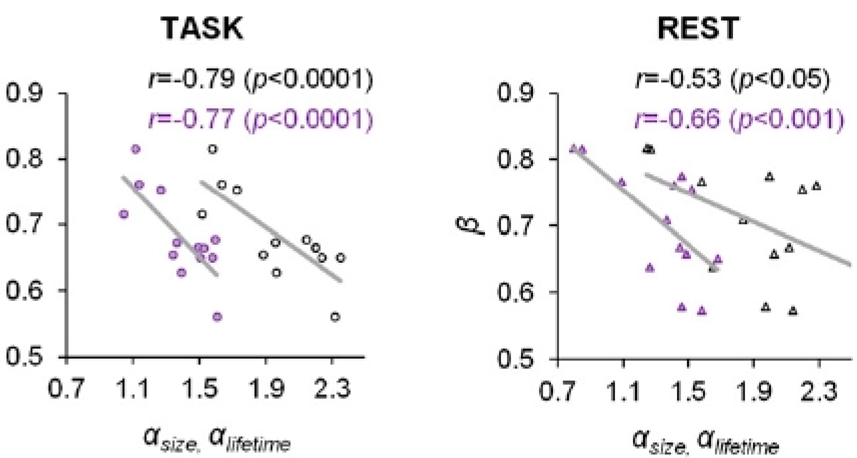

Nonuniversal critical exponents or Mean-field values : τ =1.5 τ_t=2 ?

Why would the brain be critical ?

Why would the brain be critical ?

Pros:

Diverging fluctuations →
High sensitivity to stimuli

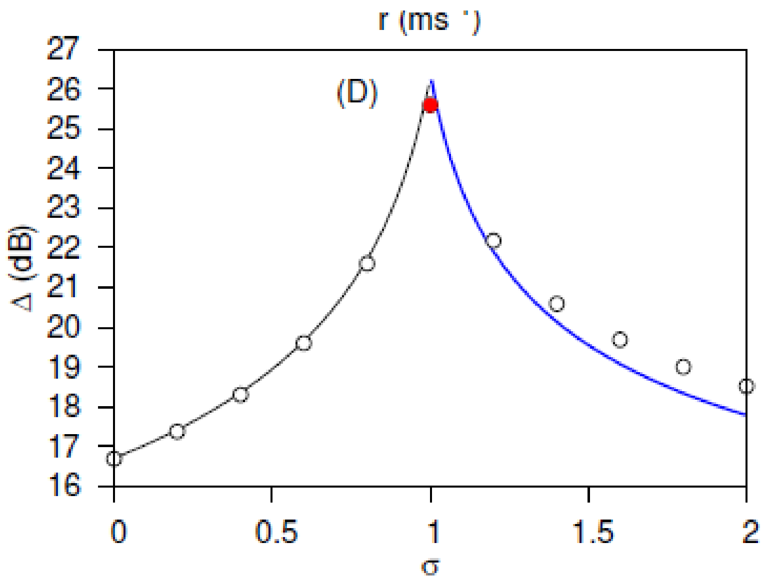

Why would the brain be critical ?

Pros:

Diverging fluctuations →
High sensitivity to stimuli

Diverging correlation functions →
Optimal transmission and
storage of information

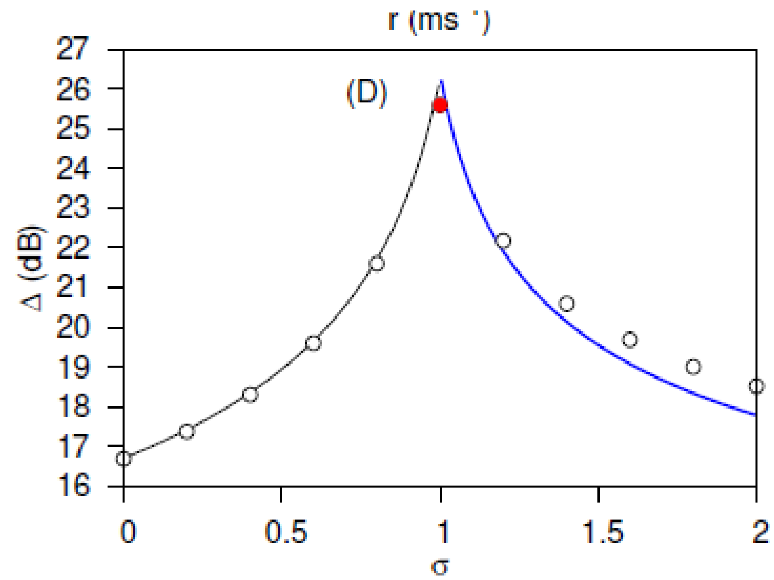

Why would the brain be critical ?

Pros:

Diverging fluctuations →
High sensitivity to stimuli

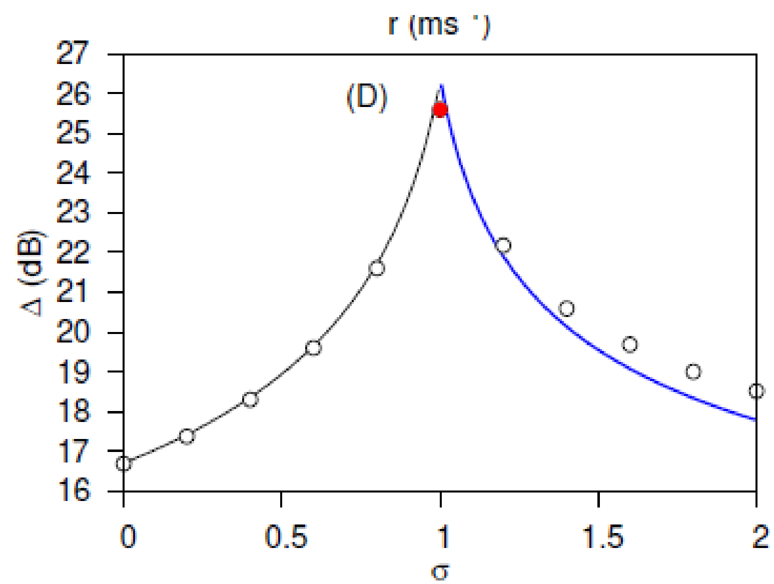

Diverging correlation functions →
Optimal transmission and
storage of information

Maximal information processing and computational
performance

Why would the brain be critical ?

Pros:

Diverging fluctuations →
High sensitivity to stimuli

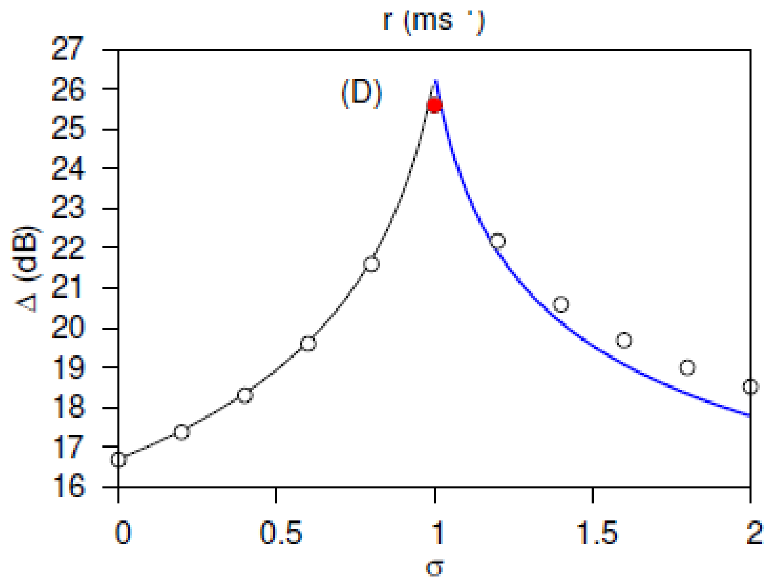

Diverging correlation functions →
Optimal transmission and storage of information

Maximal information processing and computational performance

Cons: Tuning to critical point is needed
Danger of super-critical (epileptic) behavior

Why would the brain be critical ?

Pros:

Diverging fluctuations →
High sensitivity to stimuli

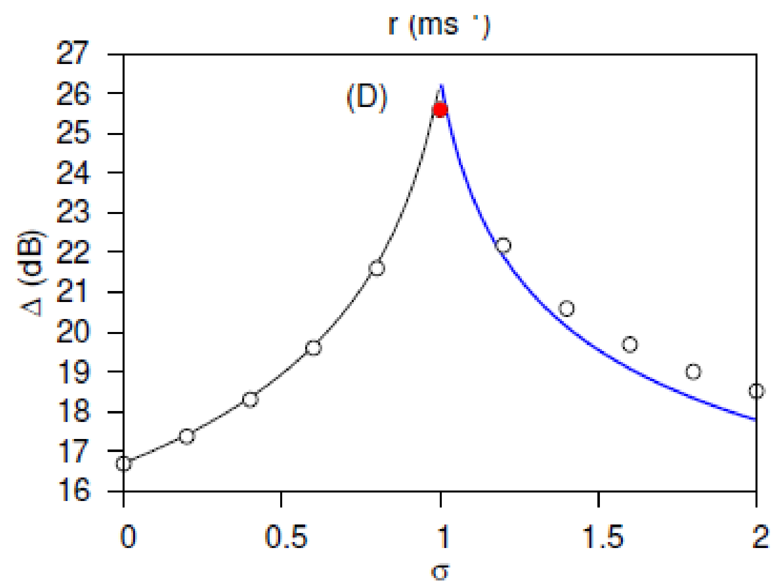

Diverging correlation functions →
Optimal transmission and
storage of information

Maximal information processing and computational performance

Cons: Tuning to critical point is needed
Danger of super-critical (epileptic) behavior

Self-organization to criticality (SOC) ?

Discrete dynamical model on networks

Discrete dynamical model on networks

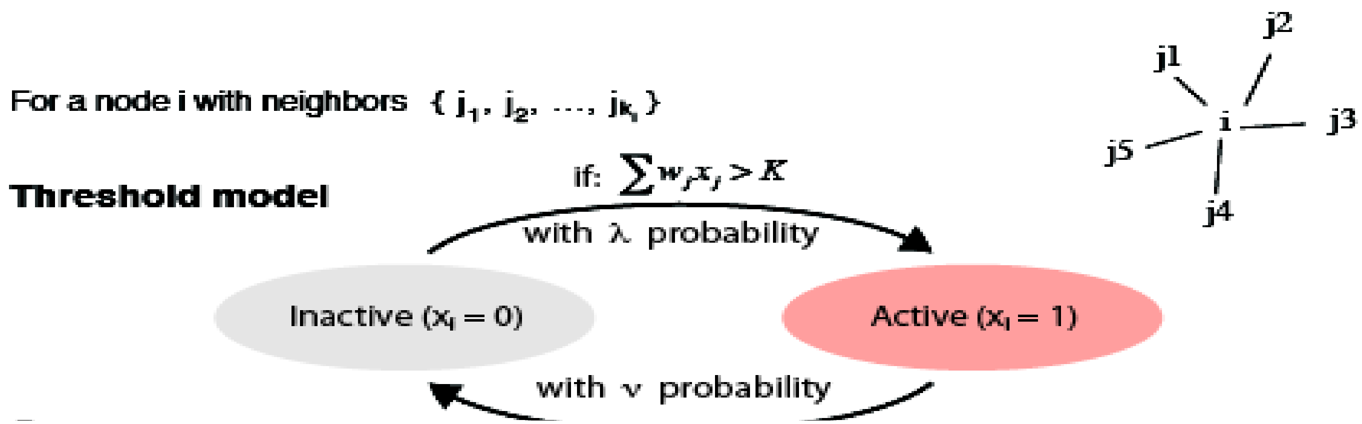

Discrete dynamical model on networks

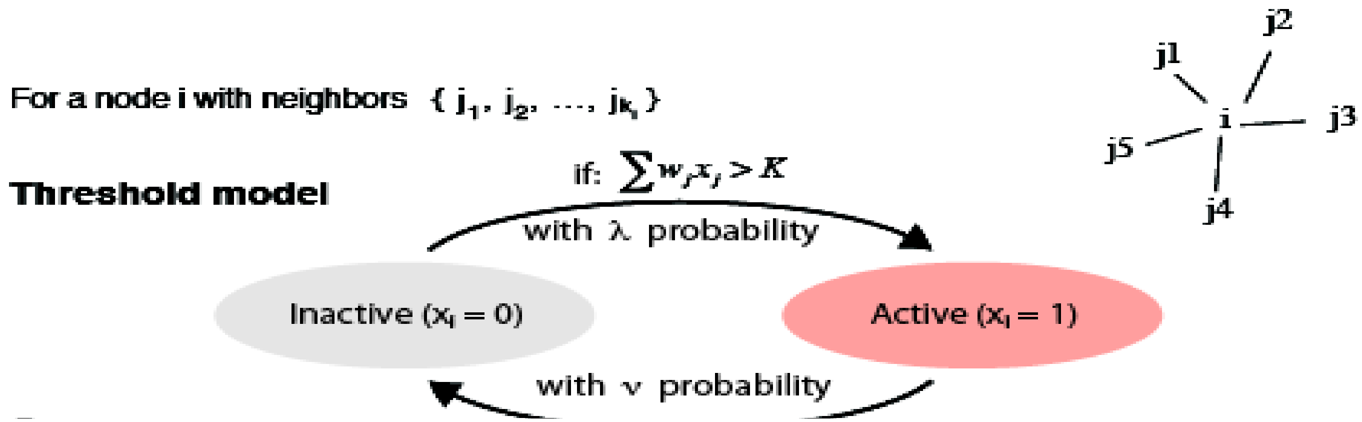

Higher order interactions!

Discrete dynamical model on networks

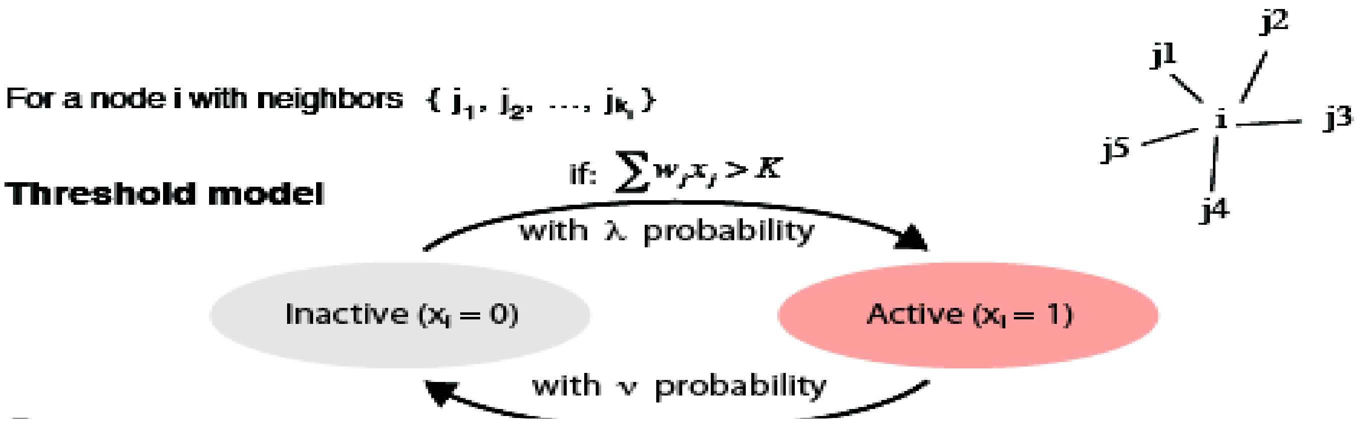

Higher order interactions!

Order parameter : density of active sites (ρ *)*

Discrete dynamical model on networks

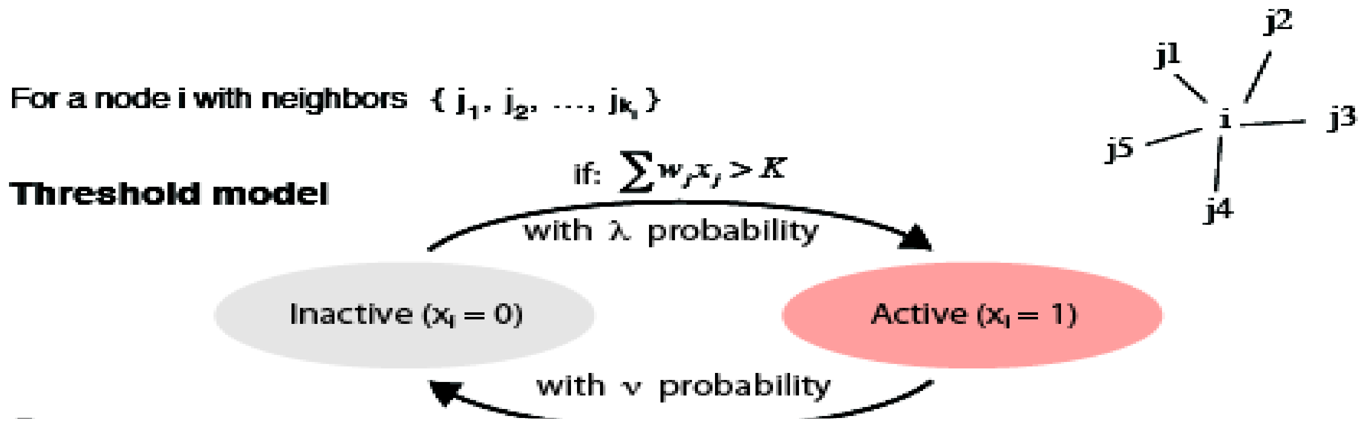

Higher order interactions!

Order parameter : density of active sites (ρ)

Mean field for reaction diffusion systems : mA → (m+k)A, nA → (n-l)A
For m > n : ***first order phase transition*** *see: GÓ: RMP 76 (2004) 663.*

Discrete dynamical model on networks

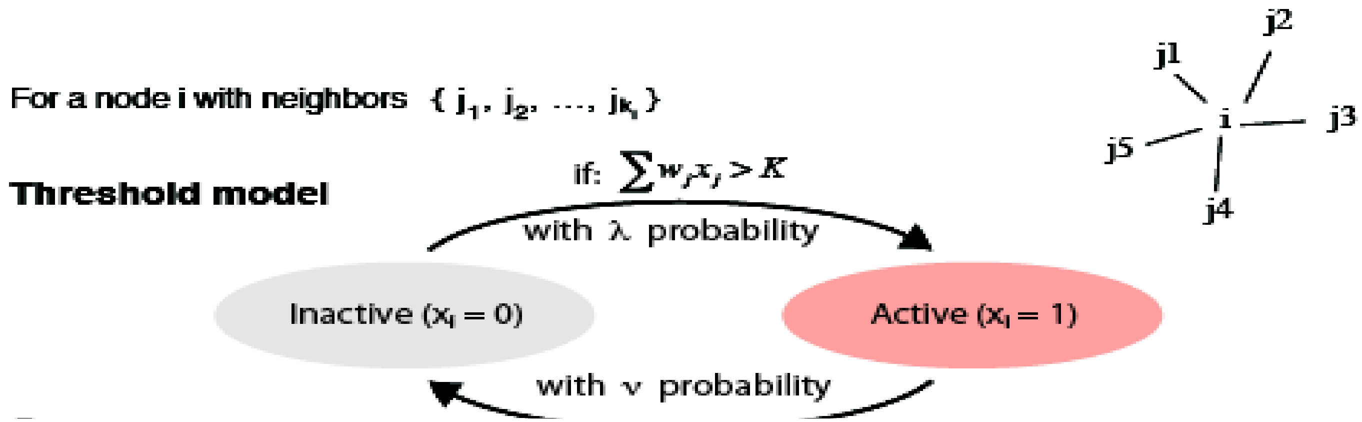

Higher order interactions!

Order parameter : density of active sites (ρ)

Mean field for reaction diffusion systems : mA → (m+k)A, nA → (n-l)A
*For m > n : **first order phase transition** see: GÓ: RMP 76 (2004) 663.*

*On **low dimensional** regular, Euclidean lattice: **DP** critical point : $\lambda_c > 0$ between inactive and active phases (GÓ: PRE 67 (2003) 056114.)*

Discrete dynamical model on networks

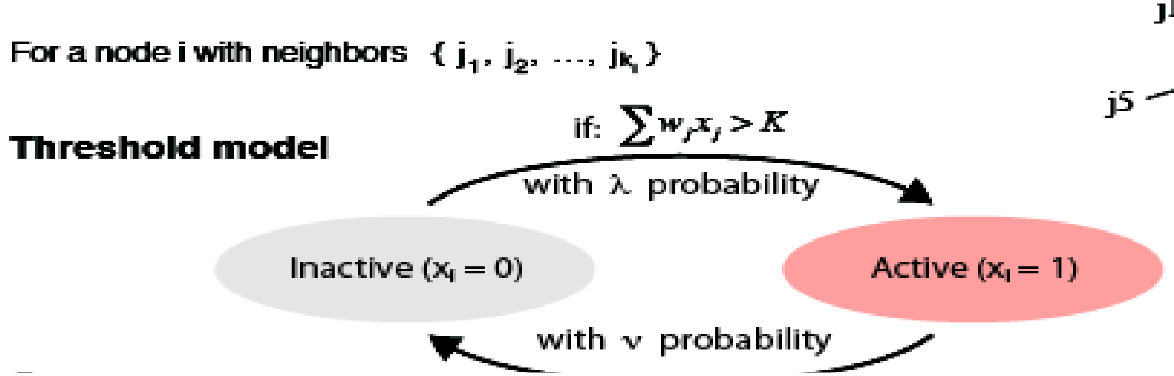

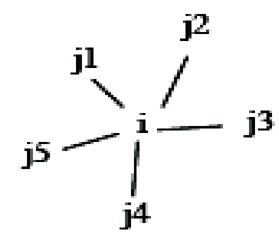

Order parameter : density of active sites (ρ)

Higher order interactions!

Mean field for reaction diffusion systems : mA → (m+k)A, nA → (n-l)A
For m > n : ***first order phase transition*** *see: GÓ: RMP 76 (2004) 663.*

On ***low dimensional*** *regular, Euclidean lattice:* ***DP*** *critical point : $\lambda_c > 0$ between inactive and active phases (GÓ: PRE 67 (2003) 056114.)*

In case of quenched heterogeneity: Griffiths Phase

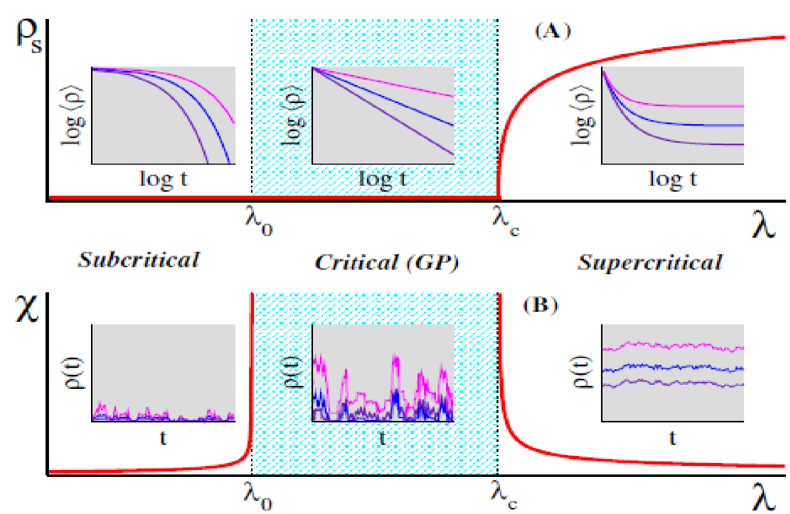

Discrete dynamical model on networks

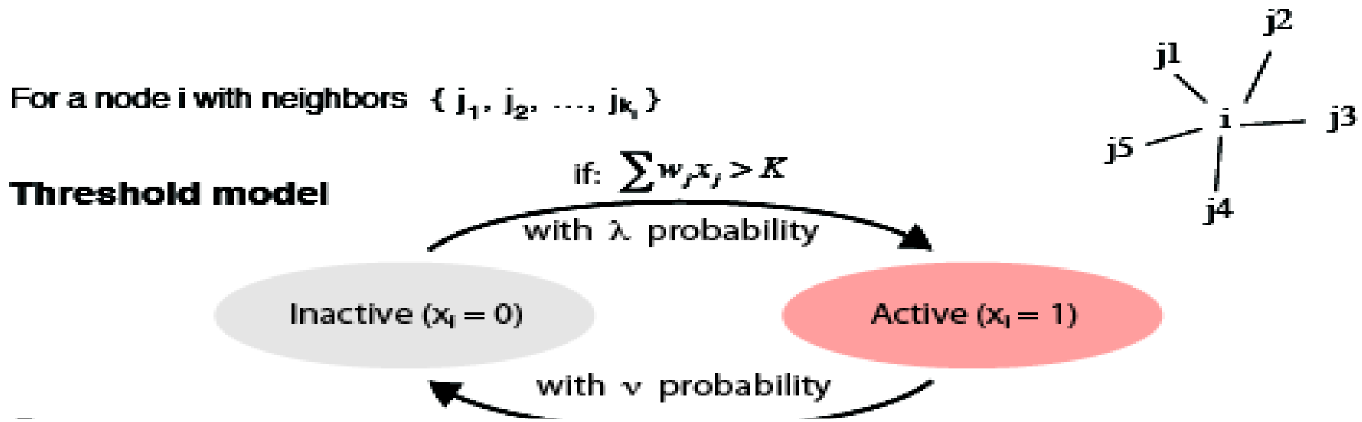

Order parameter : density of active sites (ρ)

Higher order interactions!

Mean field for reaction diffusion systems : mA → (m+k)A, nA → (n-l)A
For m > n : ***first order phase transition*** *see: GÓ: RMP 76 (2004) 663.*

On ***low dimensional*** *regular, Euclidean lattice:* ***DP*** *critical point : $\lambda_c > 0$ between inactive and active phases (GÓ: PRE 67 (2003) 056114.)*

In case of quenched heterogeneity: Griffiths Phase

PRL 105, 128701 (2010)

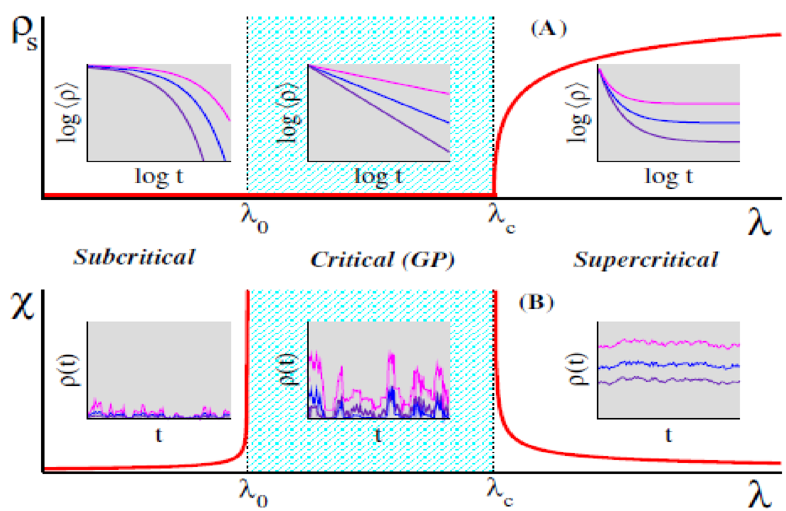

Rare **R**egion theory for **quench disordered CP**

CP: infect with prob λ, heal with prob 1-λ

Rare **R**egion theory for **quench disordered** **CP**

CP: infect with prob λ, heal with prob 1-λ

- *Fixed (quenched) disorder/impurity*

changes the local birth rate

$\Rightarrow \lambda_c > \lambda_c^0$

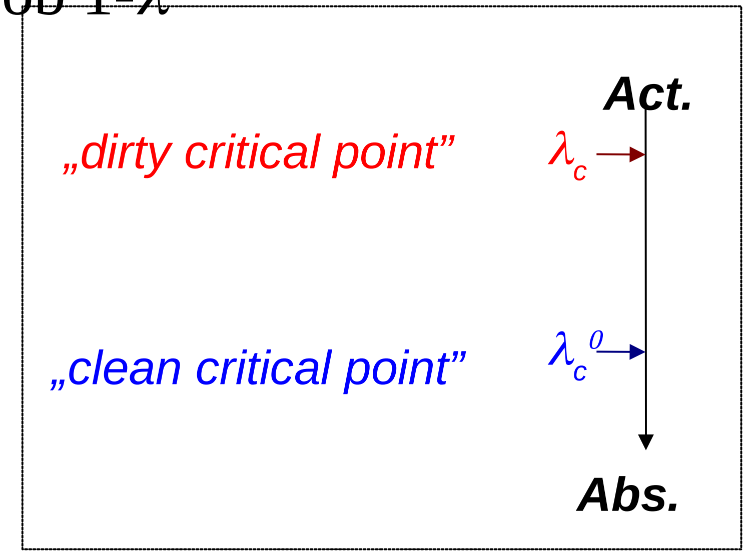

Rare **R**egion theory for quench disordered **CP**

CP: infect with prob λ, heal with prob 1-λ

- *Fixed (quenched) disorder/impurity*

  changes the local birth rate

$\Rightarrow \lambda_c > \lambda_c^0$

- ***Locally active****, but arbitrarily large*

  Rare Regions

  in the inactive phase due to the inhomogeneities

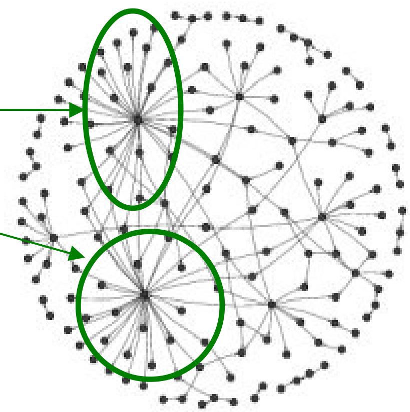

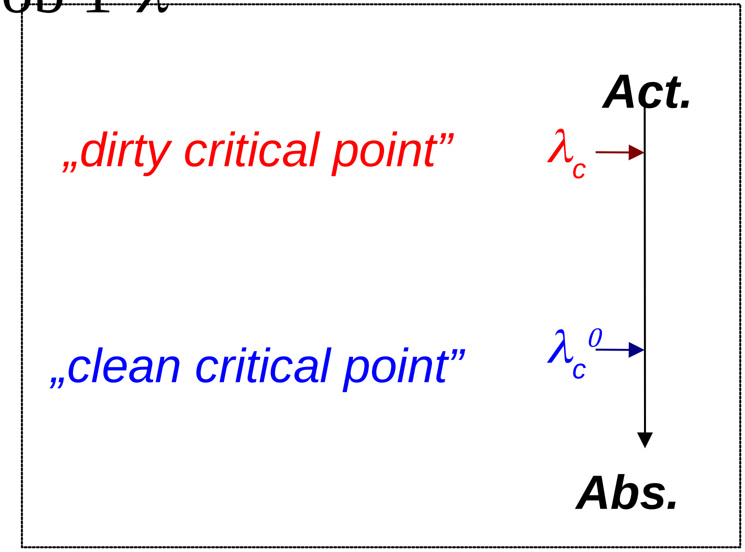

Rare **R**egion theory for quench disordered **CP**

CP: infect with prob λ, heal with prob 1-λ

- *Fixed (quenched) disorder/impurity*

  changes the local birth rate

  $\Rightarrow \lambda_c > \lambda_c^0$

- ***Locally active**, but arbitrarily large*

  Rare Regions

  in the inactive phase
  due to the inhomogeneities

- *Probability of RR of size L_R:*

  $w(L_R) \sim \exp(-c\, L_R)$

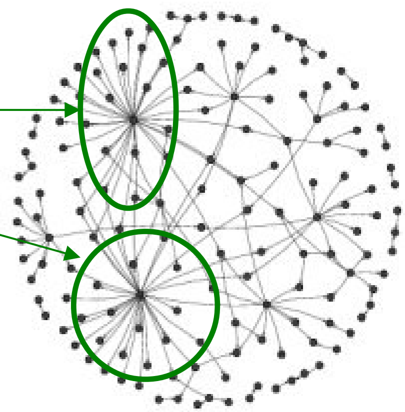

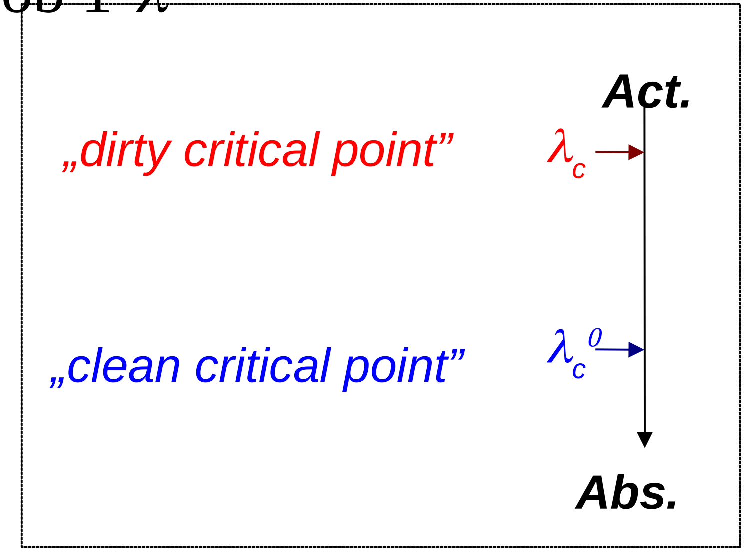

Rare Region theory for quench disordered CP

CP: infect with prob λ, heal with prob 1-λ

- *Fixed (quenched) disorder/impurity*

  changes the local birth rate

  $\Rightarrow \lambda_c > \lambda_c^0$

- ***Locally active***, *but arbitrarily large*

  Rare Regions

  in the inactive phase due to the inhomogeneities

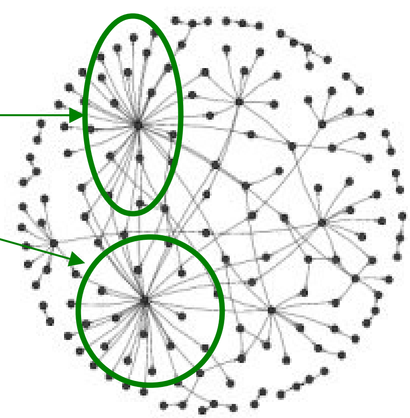

- *Probability of RR of size L_R:*

  $w(L_R) \sim \exp(-c\, L_R)$

  contribute to the density: $\rho(t) \sim \int dL_R\ L_R\ w(L_R)\ \exp[-t/\tau(L_R)]$

Act.

„dirty critical point" λ_c

„clean critical point" λ_c^0

Abs.

Rare Region theory for quench disordered CP

CP: infect with prob λ, heal with prob $1-\lambda$

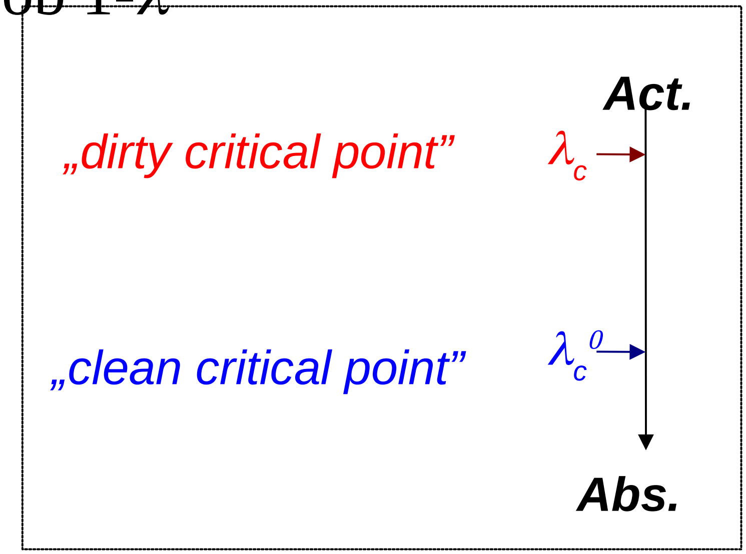

- *Fixed (quenched) disorder/impurity*

  changes the local birth rate

  $\Rightarrow \lambda_c > \lambda_c^0$

- ***Locally active****, but arbitrarily large*

  Rare Regions

  in the inactive phase
  due to the inhomogeneities

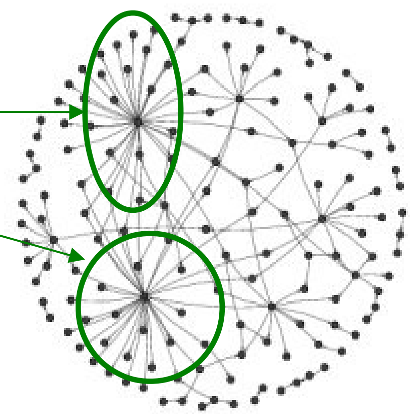

- *Probability of RR of size L_R:*

  $w(L_R) \sim \exp(-c\, L_R)$

  contribute to the density: $\rho(t) \sim \int dL_R\; L_R\; w(L_R)\; \exp[-t/\tau(L_R)]$

- ***For*** $\lambda < \lambda_c^0$ *: conventional (exponentially fast) decay*

Rare **R**egion theory for **quench disordered CP**

CP: infect with prob λ, heal with prob 1-λ

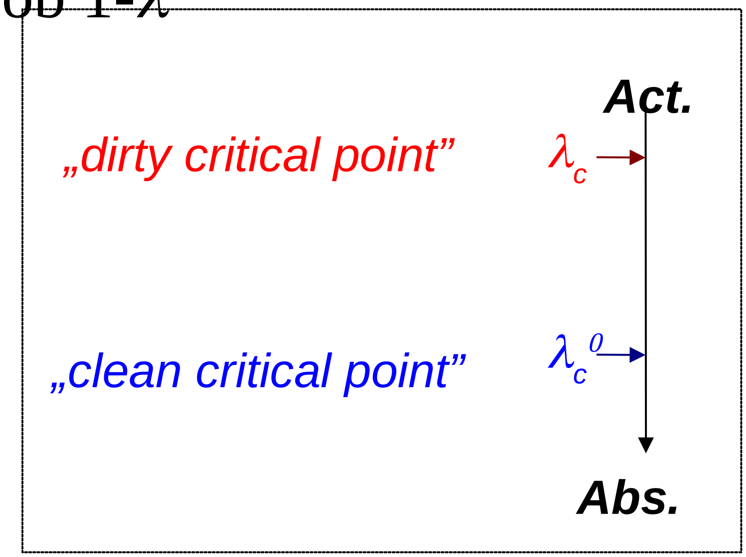

- *Fixed (quenched) disorder/impurity*

  changes the local birth rate

  $\Rightarrow \lambda_c > \lambda_c^0$

- ***Locally active**, but arbitrarily large*

  Rare Regions

  in the inactive phase due to the inhomogeneities

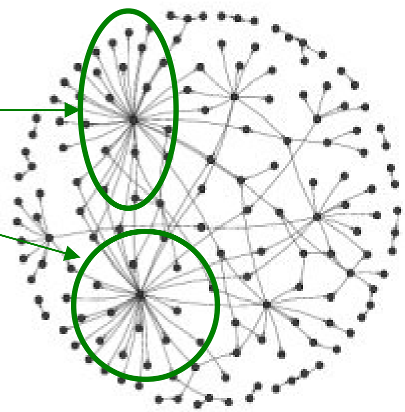

- *Probability of RR of size L_R:*

  $w(L_R) \sim \exp(-c\, L_R)$

  contribute to the density: $\rho(t) \sim \int dL_R\; L_R\; w(L_R)\; \exp[-t/\tau(L_R)]$

- ***For*** $\lambda < \lambda_c^0$ *: conventional (exponentially fast) decay*
- ***At*** λ_c^0 *the characteristic time scales as:* $\tau(L_R) \sim L_R^{\,Z}$ $\Rightarrow$ *saddle point analysis:*

  $\ln \rho(t) \sim t^{\,d/(d+Z)}$ *stretched exponential*

Rare Region theory for quench disordered CP

CP: infect with prob λ, heal with prob $1-\lambda$

- *Fixed (quenched) disorder/impurity*

  changes the local birth rate

  $\Rightarrow \lambda_c > \lambda_c^0$

- ***Locally active**, but arbitrarily large*

  Rare Regions

  in the inactive phase
  due to the inhomogeneities

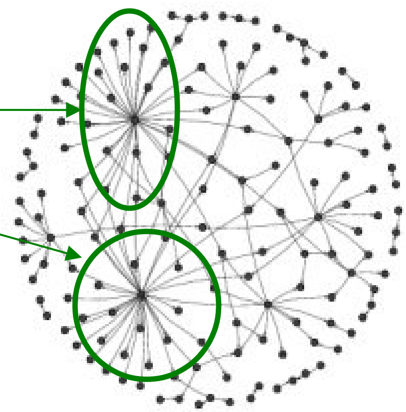

„dirty critical point” λ_c

„clean critical point” λ_c^0

Act.

GP

Abs.

- *Probability of RR of size L_R:*

  $w(L_R) \sim \exp(-c\, L_R)$

  contribute to the density: $\rho(t) \sim \int dL_R \; L_R \; w(L_R) \; \exp[-t/\tau(L_R)]$

- ***For*** $\lambda < \lambda_c^0$ *: conventional (exponentially fast) decay*

- ***At*** λ_c^0 *the characteristic time scales as:* $\tau(L_R) \sim L_R^{\,z} \Rightarrow$ *saddle point analysis:*

  $\ln \rho(t) \sim t^{d/(d+Z)}$ *stretched exponential*

- ***For*** $\lambda_c^0 < \lambda < \lambda_c$ *:* $\tau(L_R) \sim \exp(b\, L_R)$*:* ***Griffiths Phase***

Rare Region theory for quench disordered CP

CP: infect with prob λ, heal with prob 1-λ

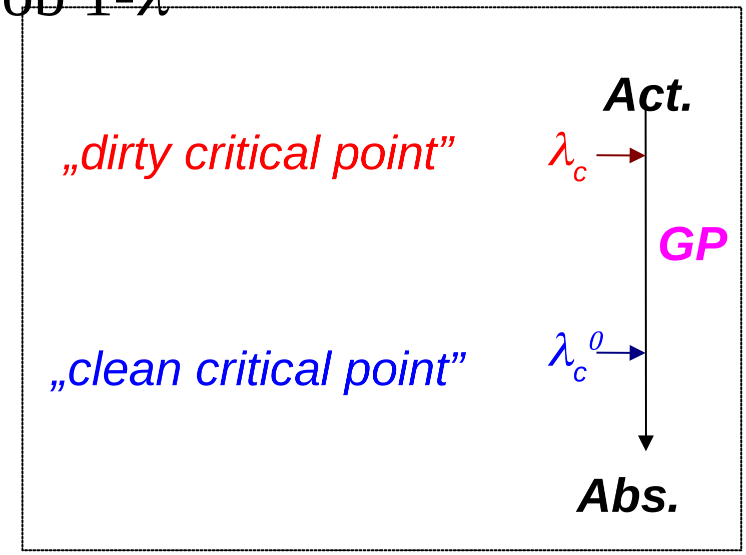

- *Fixed (quenched) disorder/impurity*

  changes the local birth rate

  $\Rightarrow \lambda_c > \lambda_c^0$

- ***Locally active***, *but arbitrarily large*

  Rare Regions

  in the inactive phase
  due to the inhomogeneities

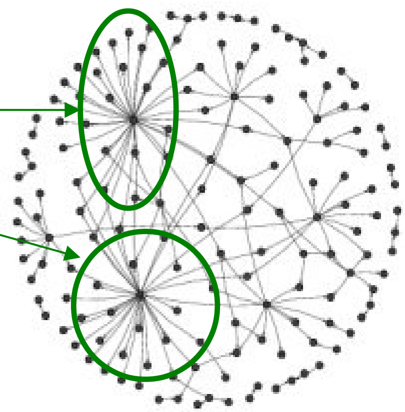

- *Probability of RR of size L_R:*

  $w(L_R) \sim \exp(-c\, L_R)$

  contribute to the density: $\rho(t) \sim \int dL_R\ L_R\ w(L_R)\ \exp[-t/\tau(L_R)]$

- ***For*** $\lambda < \lambda_c^0$ *: conventional (exponentially fast) decay*
- ***At*** λ_c^0 *the characteristic time scales as:* $\tau(L_R) \sim L_R^{\,Z} \Rightarrow$ *saddle point analysis:*

  $\ln \rho(t) \sim t^{\,d/(d+Z)}$ *stretched exponential*

- ***For*** $\lambda_c^0 < \lambda < \lambda_c$ *:* $\tau(L_R) \sim \exp(b\, L_R)$*:* ***Griffiths Phase***

  $\rho(t) \sim t^{-c/b}$ *continuously changing exponents*

Rare Region theory for quench disordered CP

CP: infect with prob λ, heal with prob $1-\lambda$

- *Fixed (quenched) disorder/impurity*

  changes the local birth rate

  $\Rightarrow \lambda_c > \lambda_c^0$

- ***Locally active***, *but arbitrarily large*

  Rare Regions

  in the inactive phase

  due to the inhomogeneities

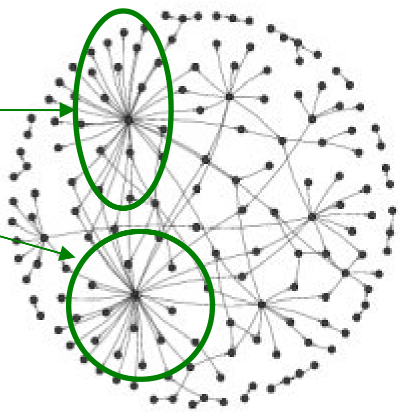

„dirty critical point” λ_c

Act.

GP

„clean critical point” λ_c^0

Abs.

- *Probability of RR of size* L_R:

  $w(L_R) \sim \exp(-c\, L_R)$

  contribute to the density: $\rho(t) \sim \int dL_R \; L_R \; w(L_R) \; \exp[-t/\tau(L_R)]$

- **For** $\lambda < \lambda_c^0$: *conventional (exponentially fast) decay*
- **At** λ_c^0 *the characteristic time scales as:* $\tau(L_R) \sim L_R^{\,Z} \Rightarrow$ *saddle point analysis:*

  $\ln \rho(t) \sim t^{d/(d+Z)}$ *stretched exponential*

- **For** $\lambda_c^0 < \lambda < \lambda_c$: $\tau(L_R) \sim \exp(b\, L_R)$: ***Griffiths Phase***

  $\rho(t) \sim t^{-c/b}$ *continuously changing exponents*

- **At** λ_c : *b may diverge* $\rightarrow$ $\rho(t) \sim \ln(t)^{-\alpha}$ *Infinite randomness fixed point scaling*

Rare Region theory for quench disordered CP

CP: infect with prob λ, heal with prob 1-λ

- *Fixed (quenched) disorder/impurity*

  changes the local birth rate

  $\Rightarrow \lambda_c > \lambda_c^0$

- ***Locally active***, *but arbitrarily large*

  Rare Regions

  in the inactive phase
  due to the inhomogeneities

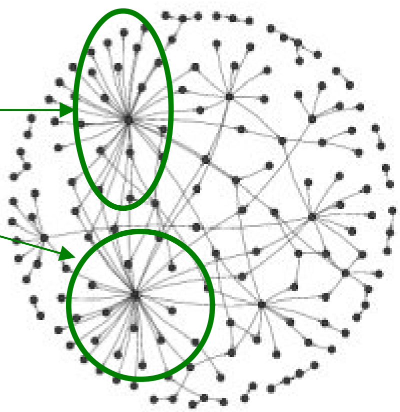

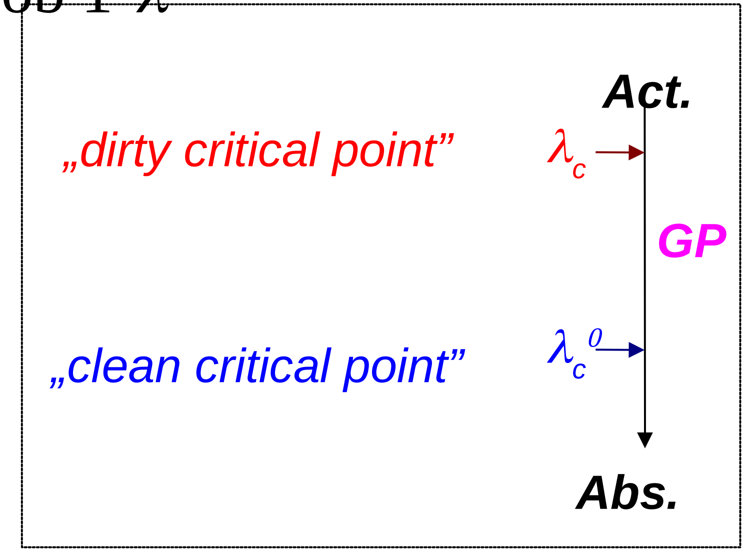

- *Probability of RR of size L_R:*

  $w(L_R) \sim \exp(-c\, L_R)$

  contribute to the density: $\rho(t) \sim \int dL_R \; L_R \; w(L_R) \; \exp[-t/\tau(L_R)]$

- ***For*** $\lambda < \lambda_c^0$ *: conventional (exponentially fast) decay*

- ***At*** λ_c^0 *the characteristic time scales as:* $\tau(L_R) \sim L_R^{\,Z} \Rightarrow$ *saddle point analysis:*

  $\ln \rho(t) \sim t^{\,d/(d+Z)}$ *stretched exponential*

- ***For*** $\lambda_c^0 < \lambda < \lambda_c$ *:* $\tau(L_R) \sim \exp(b\, L_R)$*:* ***Griffiths Phase***

  $\rho(t) \sim t^{\,-c/b}$ *continuously changing exponents*

- ***At*** λ_c *: b may diverge* $\rightarrow$ $\rho(t) \sim \ln(t)^{-\alpha}$ *Infinite randomness fixed point scaling*

- **GP: Dynamical (scaling) criticality + susceptibility diverges**

Open Connectome Large Human graphs

Open Connectome Large Human graphs

Diffusion and structural MRI images with

$1\ mm^3$ voxel resolution :

$10^5 – 10^6$ nodes

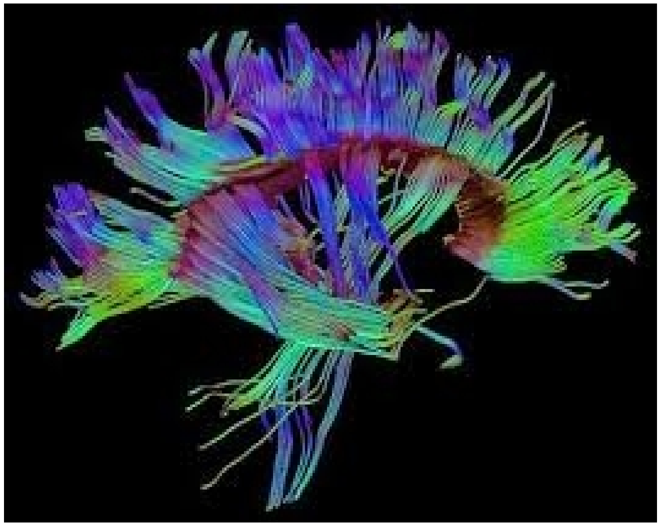

Open Connectome Large Human graphs

Diffusion and structural MRI images with
1 mm^3 voxel resolution :
$10^5 – 10^6$ nodes

Hierarchical modular graphs

Open Connectome Large Human graphs

Diffusion and structural MRI images with
- *1 mm*^{3} voxel resolution :
- $10^5 – 10^6$ nodes

Hierarchical modular graphs

Top level: *70* brain region (Desikan atlas)

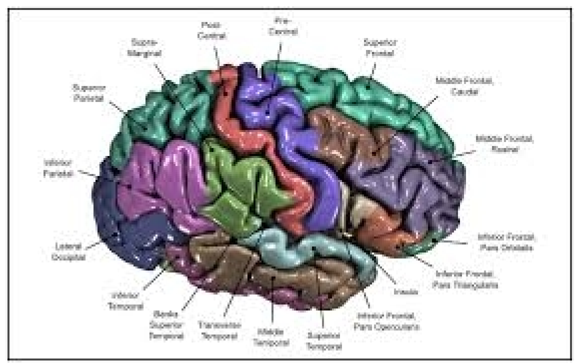

Open Connectome Large Human graphs

Diffusion and structural MRI images with
$1\ mm^3$ voxel resolution :
$10^5 – 10^6$ nodes

Hierarchical modular graphs

Top level: *70* brain region (Desikan atlas)

Lower levels: Deterministic tractography: Fiber Assignment by Continuous Tracking (FACT) algorithm

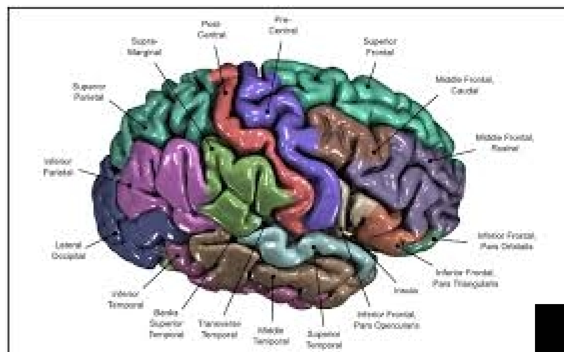

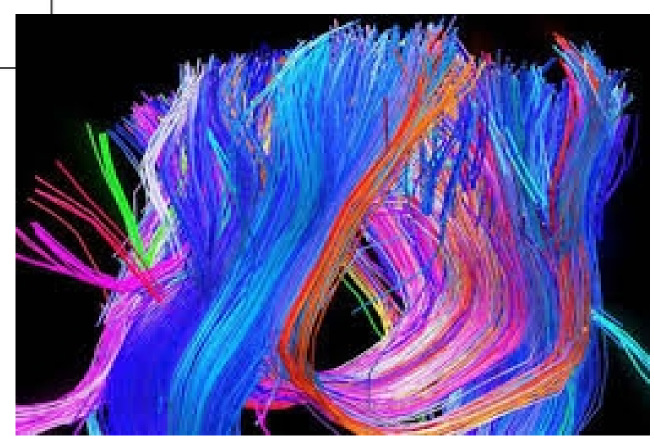

Open Connectome Large Human graphs

Diffusion and structural MRI images with
1 mm^3 voxel resolution :
10^5 – 10^6 nodes

Hierarchical modular graphs

Top level: *70* brain region (Desikan atlas)

Lower levels: Deterministic tractography: Fiber Assignment by Continuous Tracking (FACT) algorithm

Map : voxel → vertex (~ 10^7)

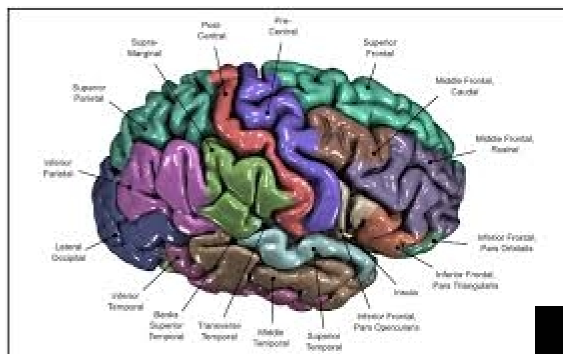

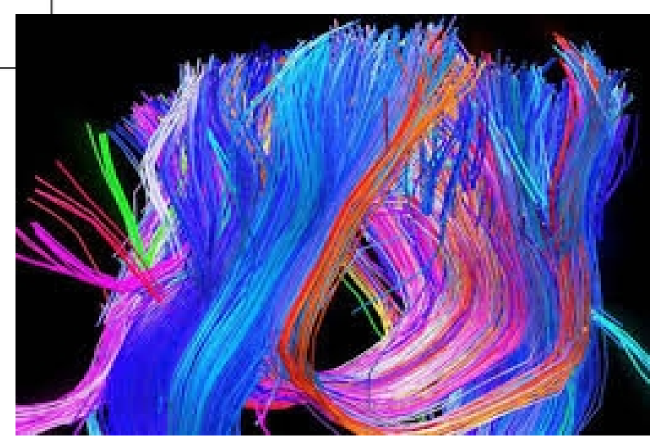

Open Connectome Large Human graphs

Diffusion and structural MRI images with
1 mm^3 voxel resolution :
10^5 – 10^6 nodes

Hierarchical modular graphs

Top level: *70* brain region (Desikan atlas)

Lower levels: Deterministic tractography: Fiber Assignment by Continuous Tracking (FACT) algorithm

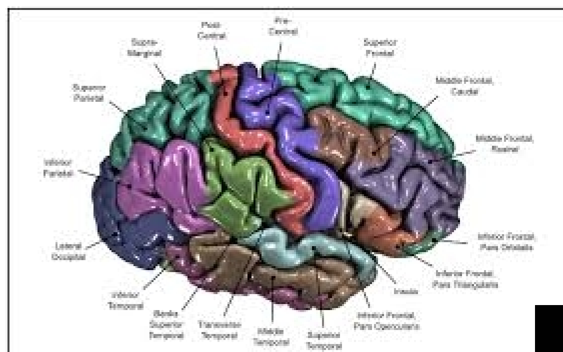

Map : voxel → vertex (~ 10^7)

fiber → edge (~ 10^{10})

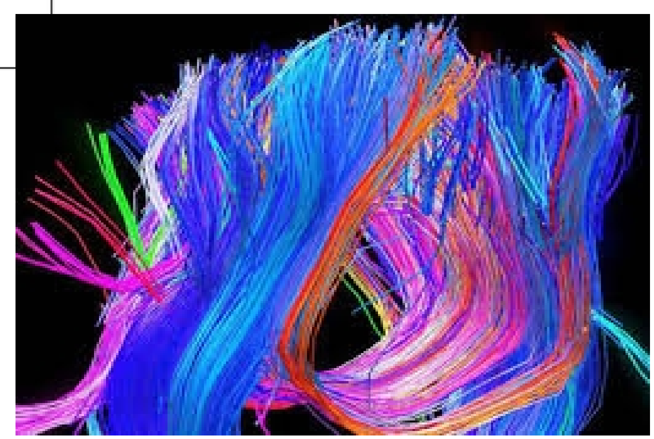

Open Connectome Large Human graphs

Diffusion and structural MRI images with
$1\ mm^3$ voxel resolution :
$10^5 – 10^6$ nodes

Hierarchical modular graphs

Top level: *70* brain region (Desikan atlas)

Lower levels: Deterministic tractography: Fiber Assignment by Continuous Tracking (FACT) algorithm

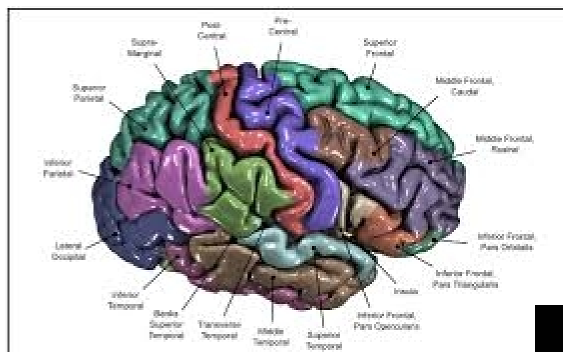

Map : voxel → vertex ($\sim 10^7$)

fiber → edge ($\sim 10^{10}$)

+ noise reduction → graph

undirected, weighted

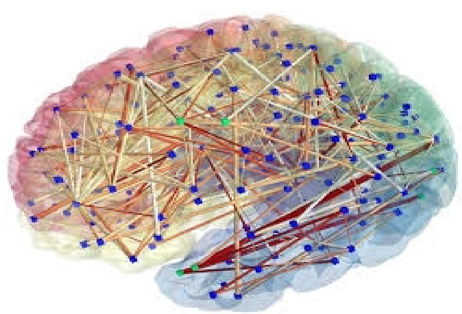

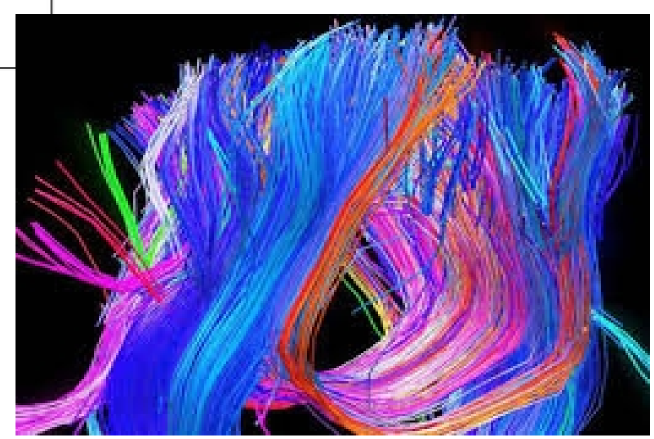

Open Connectome Large Human graphs

Diffusion and structural MRI images with
$1\ mm^3$ voxel resolution :
$10^5 – 10^6$ nodes

Hierarchical modular graphs

Top level: *70* brain region (Desikan atlas)

Lower levels: Deterministic tractography: Fiber Assignment by Continuous Tracking (FACT) algorithm

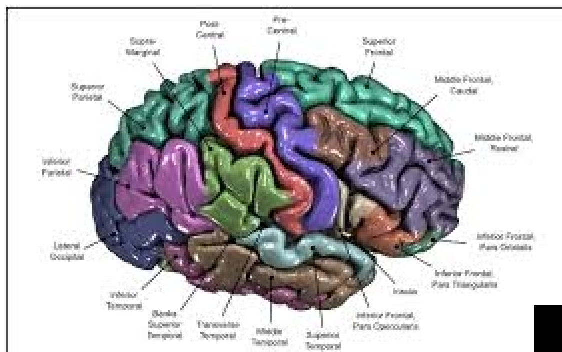

Map : voxel → vertex (~ *10^7*)

fiber → edge (~ *10^{10}*)

+ noise reduction → graph

undirected, weighted

Graph dimension: d < 4

MG, GO Sci.Rep. 2016

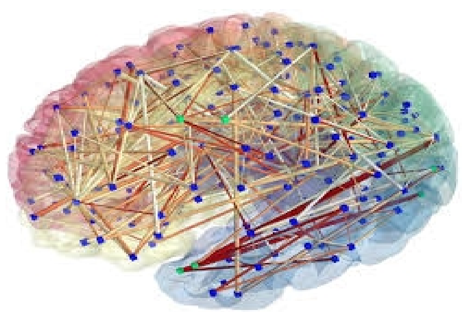

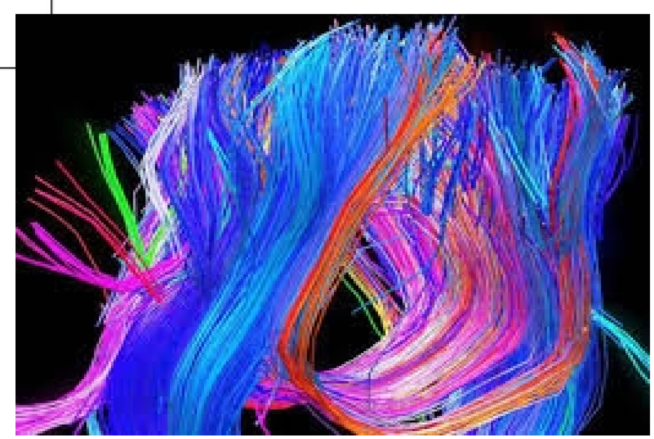

Threshold model simulations on an OCP graph

Threshold model simulations on an OCP graph

KKI-18 graph: *836733* vertex, *8 x 10⁷* weighted, undirected edges

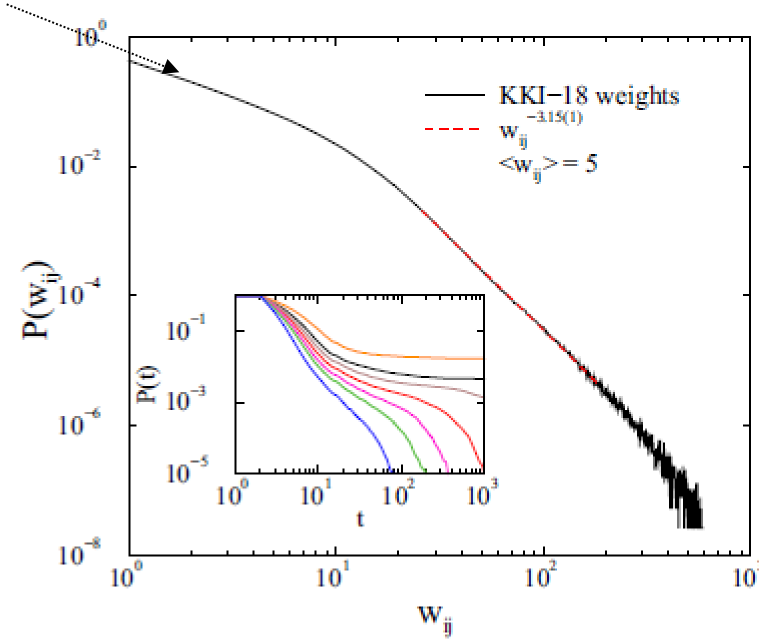

FIG. 1. Link weight probability density function of the KKI-18 OCP graph. Dashed line: a PL fit for intermediate w_{ij}'s. Inset: survival probability in the $K = 6$ threshold model near the transition point for $\lambda = 0.003$, $\nu = 0.3, 0.4, 0.45, 0.5, 0.55, 0.6, 0.7$ (top to bottom curves).

Threshold model simulations on an OCP graph

KKI-18 graph: *836733* vertex, *8 x 10⁷* weighted, undirected edges

Cluster spreading simulations from randomly selected active nodes

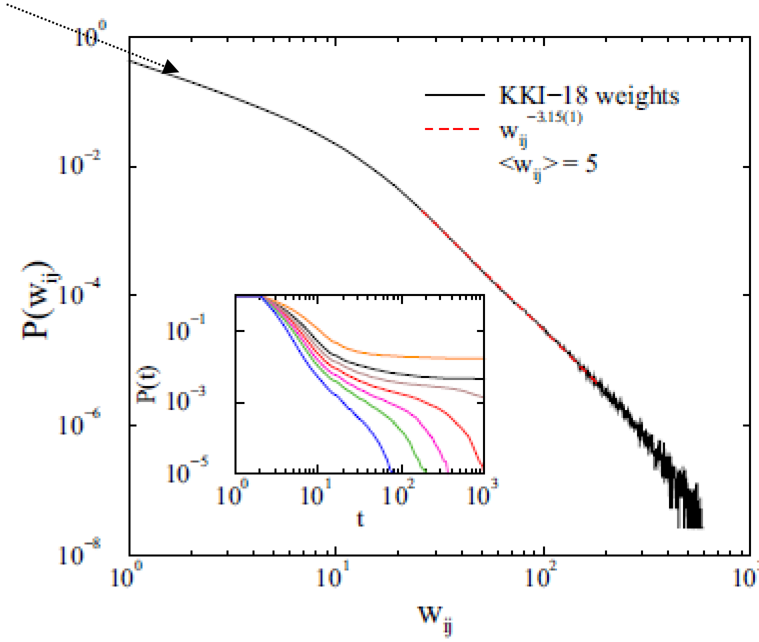

FIG. 1. Link weight probability density function of the KKI-18 OCP graph. Dashed line: a PL fit for intermediate w_{ij}'s. Inset: survival probability in the $K = 6$ threshold model near the transition point for $\lambda = 0.003$, $\nu = 0.3, 0.4, 0.45, 0.5, 0.55, 0.6, 0.7$ (top to bottom curves).

Threshold model simulations on an OCP graph

KKI-18 graph: *836733* vertex, *8 x 10⁷* weighted, undirected edges

Cluster spreading simulations from randomly selected active nodes

Survival probability: $P(t) \propto t^{-\delta}$

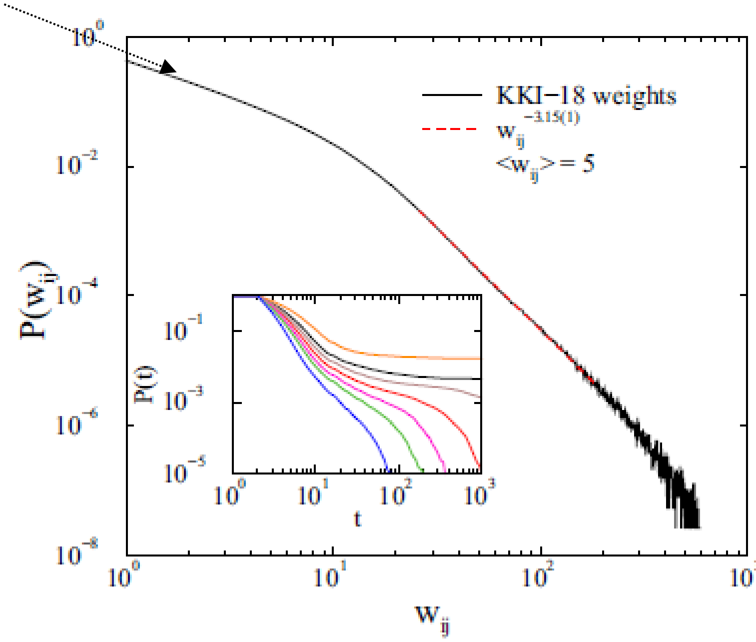

FIG. 1. Link weight probability density function of the KKI-18 OCP graph. Dashed line: a PL fit for intermediate w_{ij}'s. Inset: survival probability in the $K = 6$ threshold model near the transition point for $\lambda = 0.003$, $\nu = 0.3, 0.4, 0.45, 0.5, 0.55, 0.6, 0.7$ (top to bottom curves).

Threshold model simulations on an OCP graph

KKI-18 graph: *836733* vertex, *8 x 10*^{7} weighted, undirected edges

Cluster spreading simulations from randomly selected active nodes

Survival probability: $P(t) \propto t^{-\delta}$

Does not show critical region,

but discontinuous phase transition

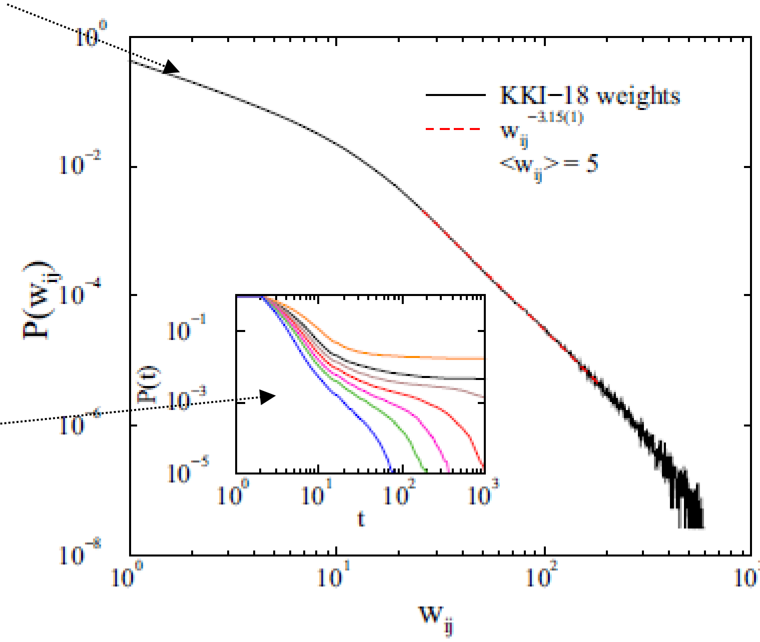

FIG. 1. Link weight probability density function of the KKI-18 OCP graph. Dashed line: a PL fit for intermediate w_{ij}'s. Inset: survival probability in the $K = 6$ threshold model near the transition point for $\lambda = 0.003$, $\nu = 0.3, 0.4, 0.45, 0.5, 0.55, 0.6, 0.7$ (top to bottom curves).

Threshold model simulations on an OCP graph

KKI-18 graph: *836733* vertex, *8 x 10⁷* weighted, undirected edges

Cluster spreading simulations from randomly selected active nodes

Survival probability: $P(t) \propto t^{-\delta}$

Does not show critical region,

but discontinuous phase transition

→ Inherent disorder of KKI-18 can't round the phase transition,
No Griffiths Phase, Hub effects!

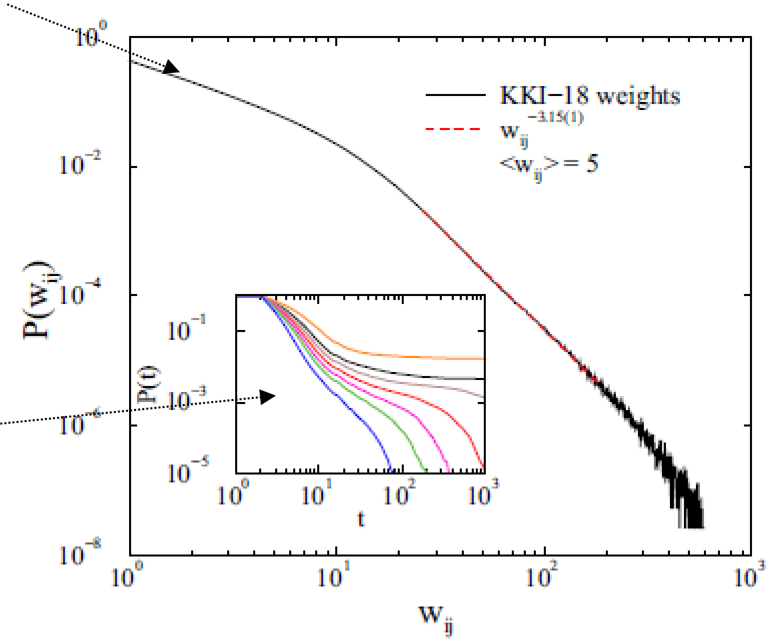

FIG. 1. Link weight probability density function of the KKI-18 OCP graph. Dashed line: a PL fit for intermediate w_{ij}'s. Inset: survival probability in the $K = 6$ threshold model near the transition point for $\lambda = 0.003$, $\nu = 0.3, 0.4, 0.45, 0.5, 0.55, 0.6, 0.7$ (top to bottom curves).

Threshold model simulations on an OCP graph

KKI-18 graph: *836733* vertex, *8 x 10⁷* weighted, undirected edges

Cluster spreading simulations from
randomly selected active nodes

Survival probability: $P(t) \propto t^{-\delta}$

Does not show critical region,

but discontinuous phase transition

→ Inherent disorder of KKI-18 can't
round the phase transition,
No Griffiths Phase, Hub effects!

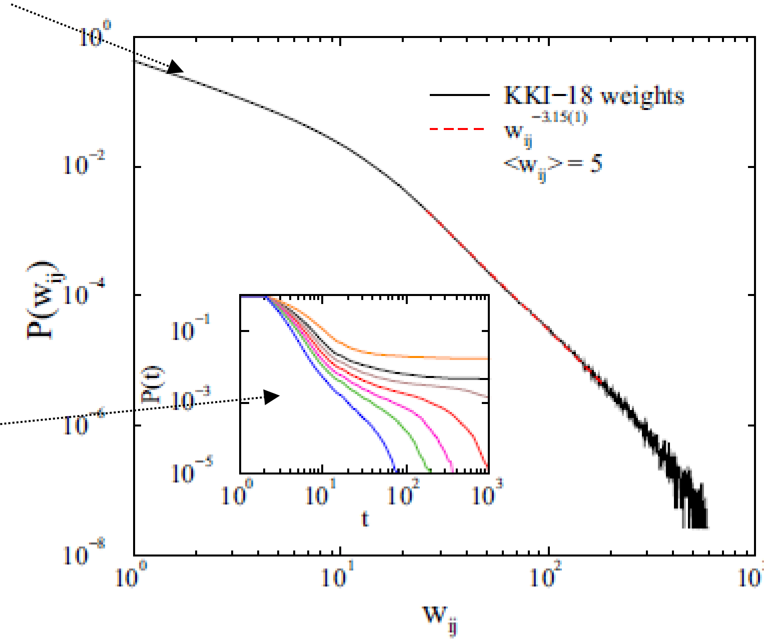

FIG. 1. Link weight probability density function of the KKI-18 OCP graph. Dashed line: a PL fit for intermediate w_{ij}'s. Inset: survival probability in the $K = 6$ threshold model near the transition point for $\lambda = 0.003$, $\nu = 0.3, 0.4, 0.45, 0.5, 0.55, 0.6, 0.7$ (top to bottom curves).

Relative Threshold model :
incoming weights normalized by the sum :
to model homogeneous sensitivity of nodes $w'_{i,j} = w_{i,j} / \sum_{j \in \text{neighb. of } i} w_{i,j}$.

Threshold model simulations on an OCP graph

KKI-18 graph: *836733* vertex, *8 x 10*[7] weighted, undirected edges

Cluster spreading simulations from randomly selected active nodes

Survival probability: $P(t) \propto t^{-\delta}$

Does not show critical region,

but discontinuous phase transition

→ Inherent disorder of KKI-18 can't round the phase transition,
No Griffiths Phase, Hub effects!

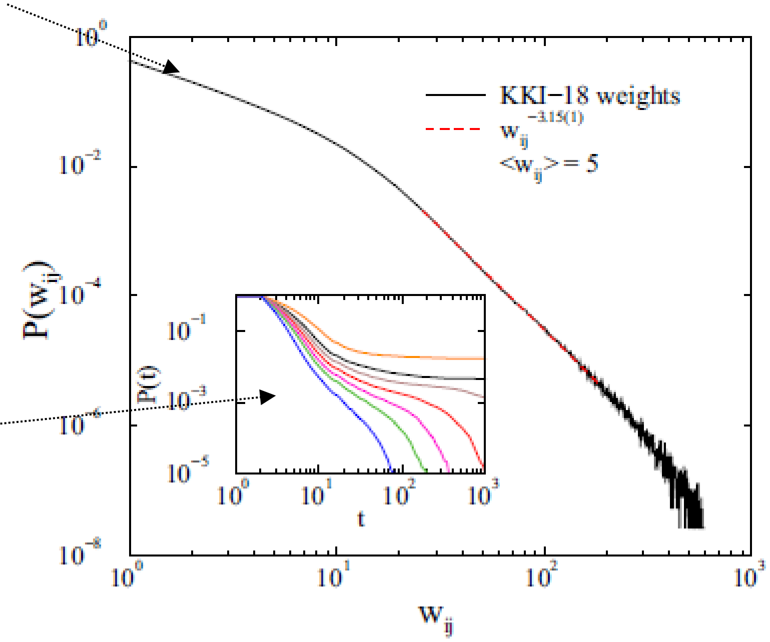

FIG. 1. Link weight probability density function of the KKI-18 OCP graph. Dashed line: a PL fit for intermediate w_{ij}'s. Inset: survival probability in the $K = 6$ threshold model near the transition point for $\lambda = 0.003$, $\nu = 0.3, 0.4, 0.45, 0.5, 0.55, 0.6, 0.7$ (top to bottom curves).

Relative Threshold model :
incoming weights normalized by the sum : to model homogeneous sensitivity of nodes

$$w'_{i,j} = w_{i,j} / \sum_{j \in \text{neighb. of } i} w_{i,j}.$$

Inhibition: randomly selected weights are flipped to negative (quenched)

$$w'_{i,j} = -w'_{i,j}.$$

Avalanche size distribution compared to experiments

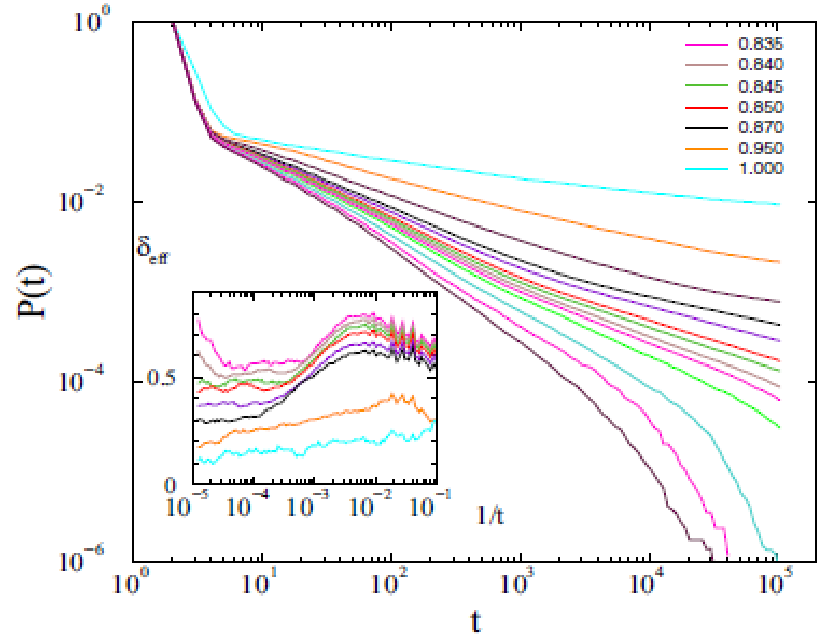

FIG. 2. Avalanche survival distribution of the relative threshold model with $K = 0.25$, for $\nu = 0.95$ and $\lambda = 0.8, 0.81, 0.82, 0.83, 0.835, 0.84, 0.845, 0.85, 0.86, 0.87, 0.9, 0.95, 1$ (bottom to top curves). Inset: Local slopes of the same from $\lambda = 0.835$ to $\lambda = 1$ (top to bottom curves). Griffiths effect manifests by slopes reaching a constant value as $1/t \to 0$.

Avalanche size distribution compared to experiments

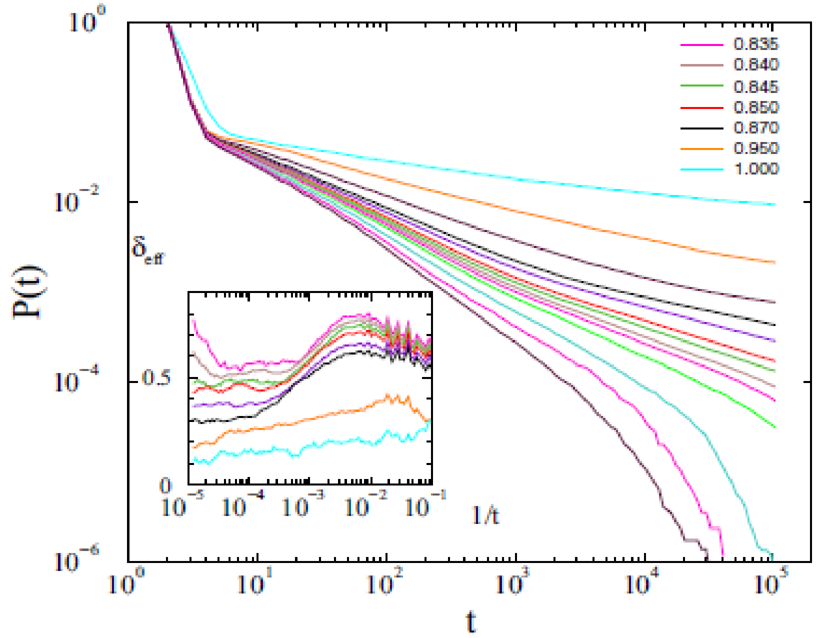

FIG. 2. Avalanche survival distribution of the relative threshold model with $K = 0.25$, for $\nu = 0.95$ and $\lambda = 0.8, 0.81, 0.82, 0.83, 0.835, 0.84, 0.845, 0.85, 0.86, 0.87, 0.9, 0.95, 1$ (bottom to top curves). Inset: Local slopes of the same from $\lambda = 0.835$ to $\lambda = 1$ (top to bottom curves). Griffiths effect manifests by slopes reaching a constant value as $1/t \to 0$.

Autocorrelations show the same
→ "Burstyness"

Avalanche size distribution compared to experiments

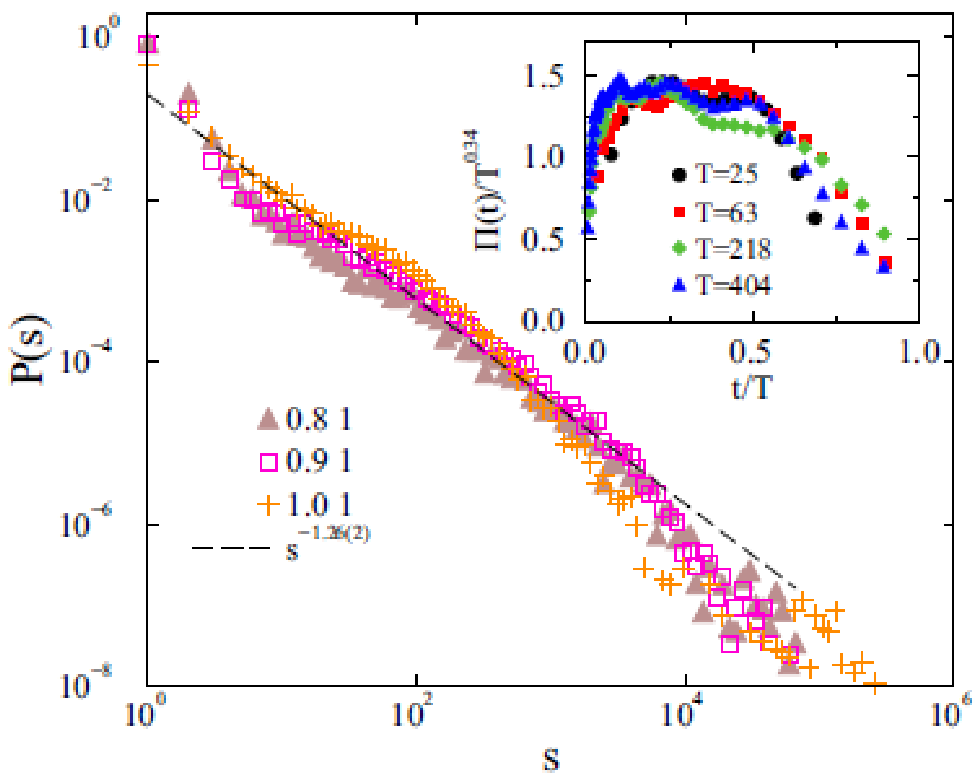

FIG. 3. Avalanche size distribution of the relative threshold model with $K=0.25$, for $\nu=1$ and $\lambda=1,0.9,0.8$. Dashed line: PL fit to the $\lambda=0.8$ case. Inset: Avalanche shape collapse for $T=25,63,218,404$ at $\lambda=0.86$ and $\nu=0.95$.

$$p(s) \propto s^{-\tau}$$

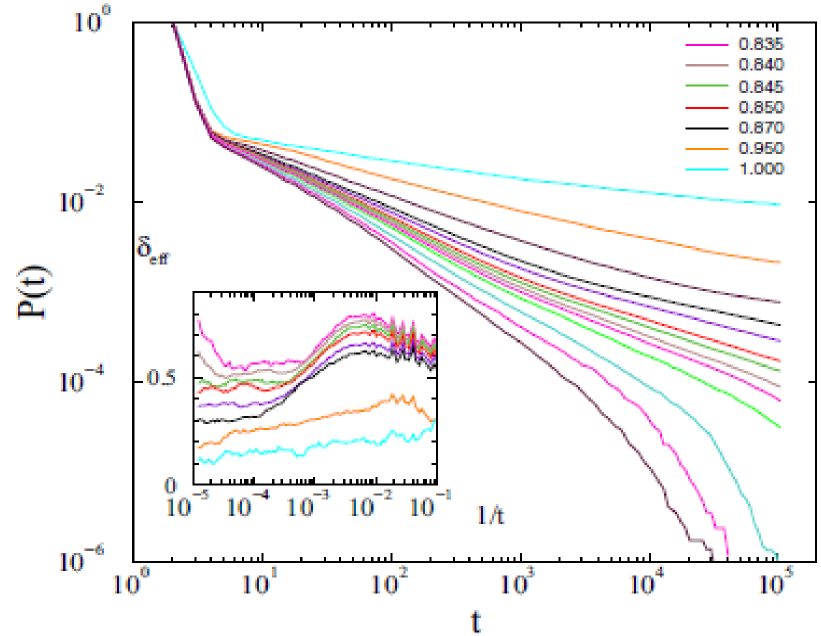

FIG. 2. Avalanche survival distribution of the relative threshold model with $K=0.25$, for $\nu=0.95$ and $\lambda=0.8, 0.81, 0.82, 0.83, 0.835, 0.84, 0.845, 0.85, 0.86, 0.87, 0.9, 0.95, 1$ (bottom to top curves). Inset: Local slopes of the same from $\lambda=0.835$ to $\lambda=1$ (top to bottom curves). Griffiths effect manifests by slopes reaching a constant value as $1/t \to 0$.

Autocorrelations show the same
→ "Burstyness"

Avalanche size distribution compared to experiments

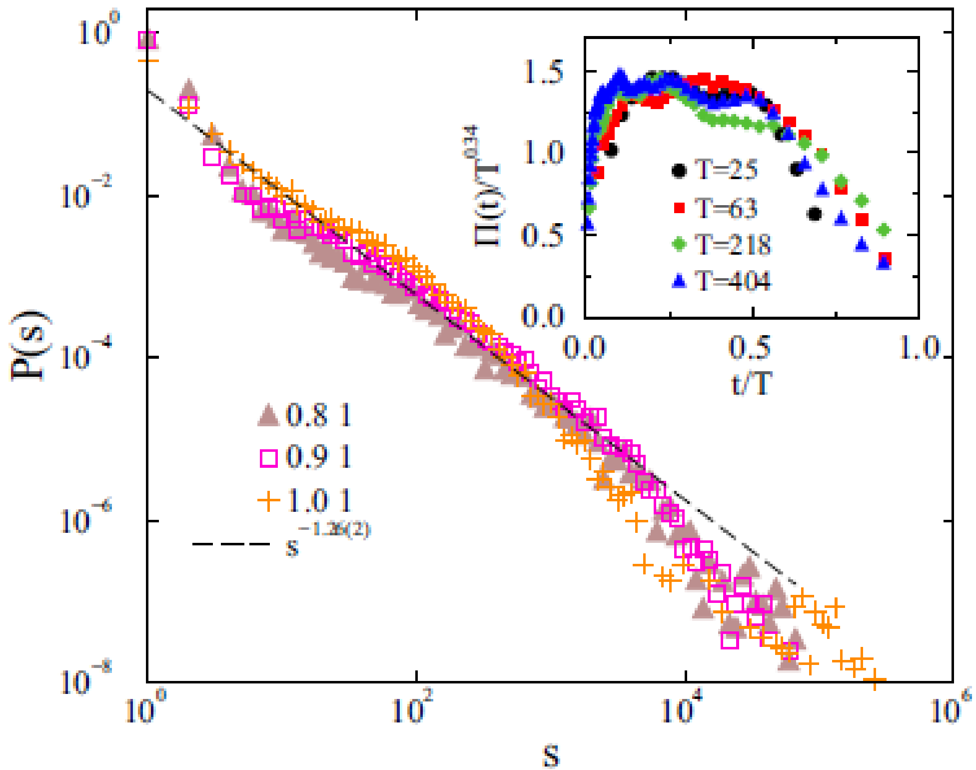

FIG. 3. Avalanche size distribution of the relative threshold model with $K = 0.25$, for $\nu = 1$ and $\lambda = 1, 0.9, 0.8$. Dashed line: PL fit to the $\lambda = 0.8$ case. Inset: Avalanche shape collapse for $T = 25, 63, 218, 404$ at $\lambda = 0.86$ and $\nu = 0.95$.

$$p(s) \propto s^{-\tau}$$

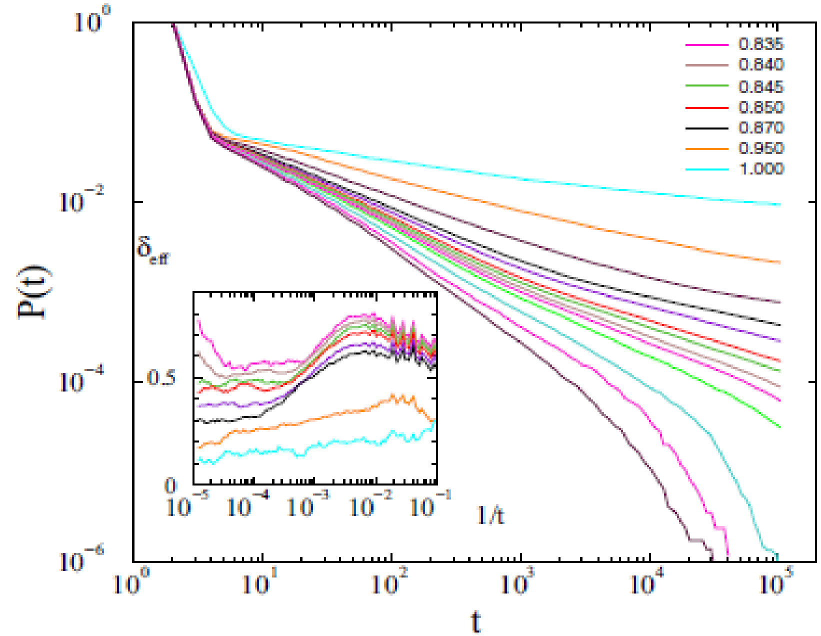

FIG. 2. Avalanche survival distribution of the relative threshold model with $K = 0.25$, for $\nu = 0.95$ and $\lambda = 0.8, 0.81, 0.82, 0.83, 0.835, 0.84, 0.845, 0.85, 0.86, 0.87, 0.9, 0.95, 1$ (bottom to top curves). Inset: Local slopes of the same from $\lambda = 0.835$ to $\lambda = 1$ (top to bottom curves). Griffiths effect manifests by slopes reaching a constant value as $1/t \to 0$.

Scaling near experimental values in the Griffiths Phase (*GO PRE 2016*)

Autocorrelations show the same → "Burstyness"

Robustness of Griffiths effects in homeostatic connectome threshold models

G. Ó, Phys. Rev. E 98 (2018) 042126

Robustness of Griffiths effects in homeostatic connectome threshold models

G. Ó, Phys. Rev. E 98 (2018) 042126

Addition of a third (refractive) state does not destroy GP

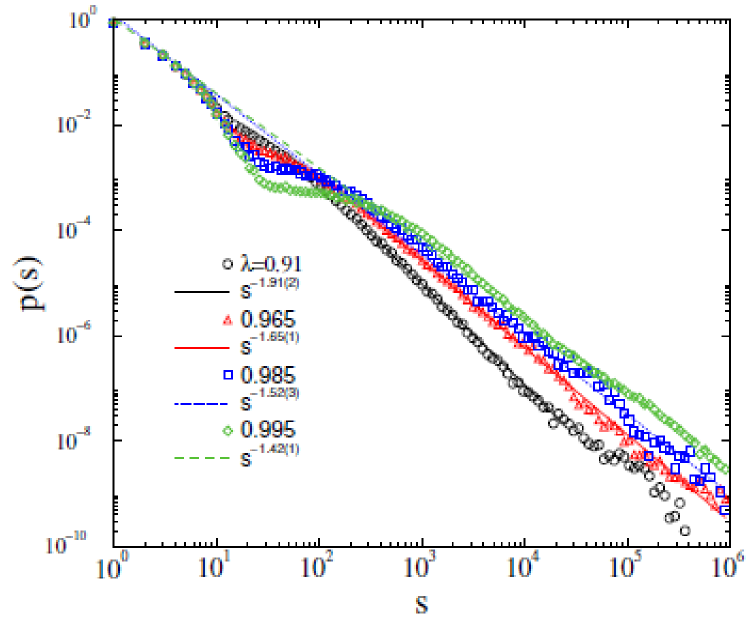

FIG. 3: Avalanche size distribution in the relative threshold model with refractory states, for $K = 0.2$, $\nu = 1$ and $\lambda = 0.91, 0.965, 0.985, 0.995$ (bottom to top symbols). Lines: PL fits for $10^2 < s < 10^5$, for these curves as shown by the legends.

Robustness of Griffiths effects in homeostatic connectome threshold models

G. Ó, Phys. Rev. E 98 (2018) 042126

Addition of a third (refractive) state does not destroy GP

Time dependent threshold model : GP shrinks, but survives for weak variations

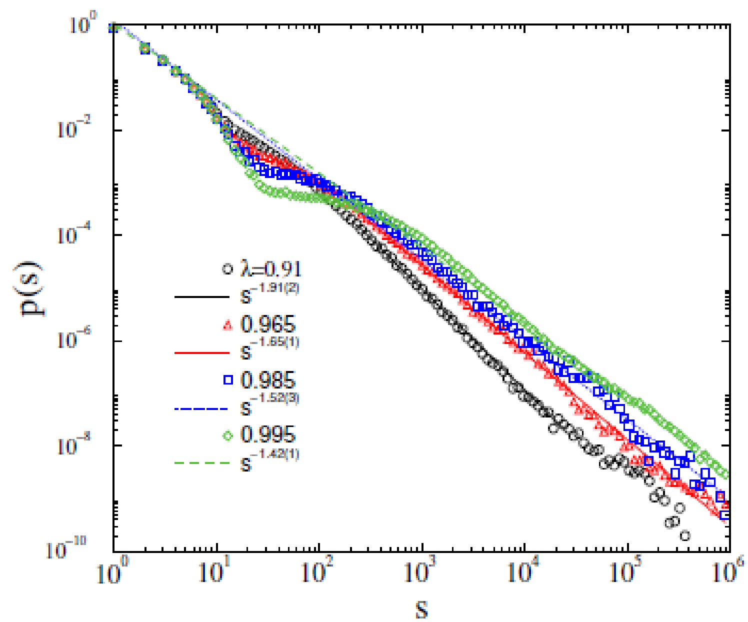

FIG. 3: Avalanche size distribution in the relative threshold model with refractory states, for $K = 0.2$, $\nu = 1$ and $\lambda = 0.91, 0.965, 0.985, 0.995$ (bottom to top symbols). Lines: PL fits for $10^2 < s < 10^5$, for these curves as shown by the legends.

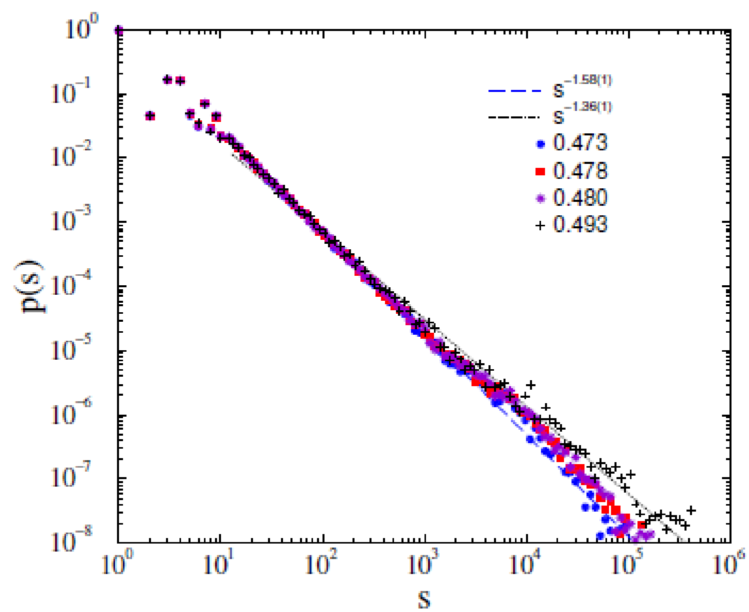

FIG. 10: Avalanche size distribution of the time dependent relative threshold model with 30% inhibitory links at $K = 0.1$, $\Delta K = 0.01$, $\nu = 0.95$ and $\lambda = 0.473, 0.478, 0.480, 0.493$ (bottom to top symbols) Dashed lines: PL fits for the tails of the $\lambda = 0.473$ and $\lambda = 0.493$ curves (bottom to top).

Hierarchical **M**odular **N**etwork topology motivated by connectomes

Hierarchical **M**odular **N**etwork topology motivated by connectomes

HMN2d:

Exponentially decaying connection probabilities with the levels l :

$$p_l \approx \langle k \rangle (1/2)^{s\,l}$$

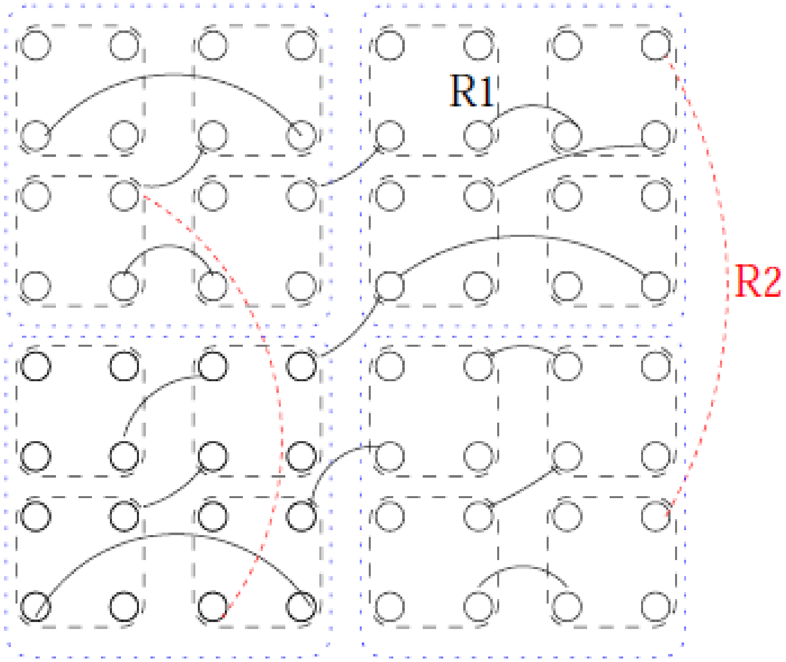

FIG. 1: Two lowest levels of the hierarchical network construction with 4 nodes/module. Dashed lines: $l = l_1$, dotted lines: $l = l_2$. The solid lines denoted R1 are randomly chosen connections within the bottom level (fully connected) modules, while those denoted R2 provide random connections on the next level. Links can be directed.

Hierarchical **M**odular **N**etwork topology motivated by connectomes

HMN2d:

Exponentially decaying connection probabilities with the levels l :

$$p_l \approx \langle k \rangle (½)^{s\,l}$$

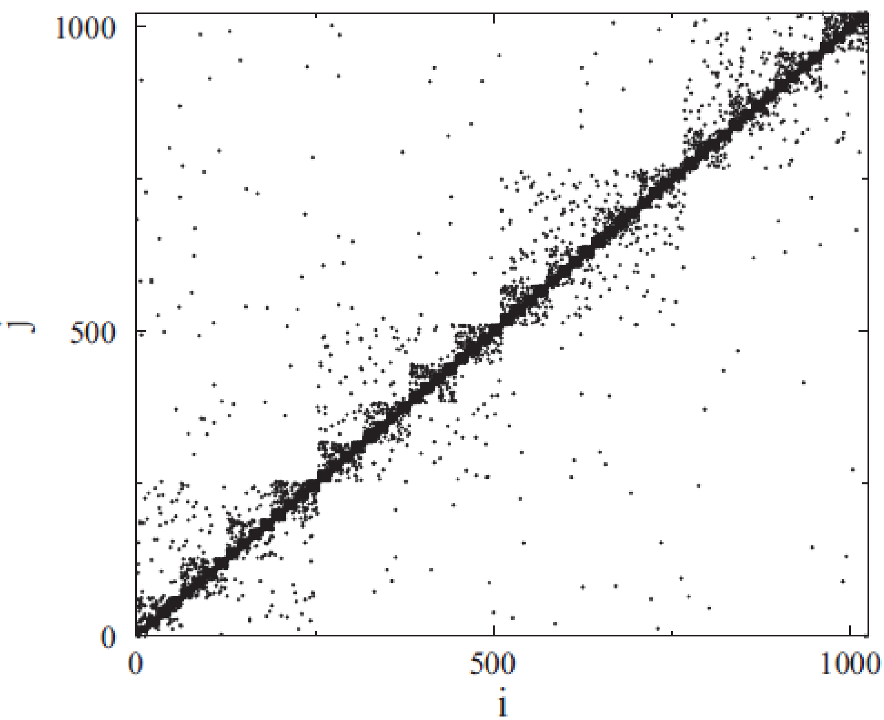

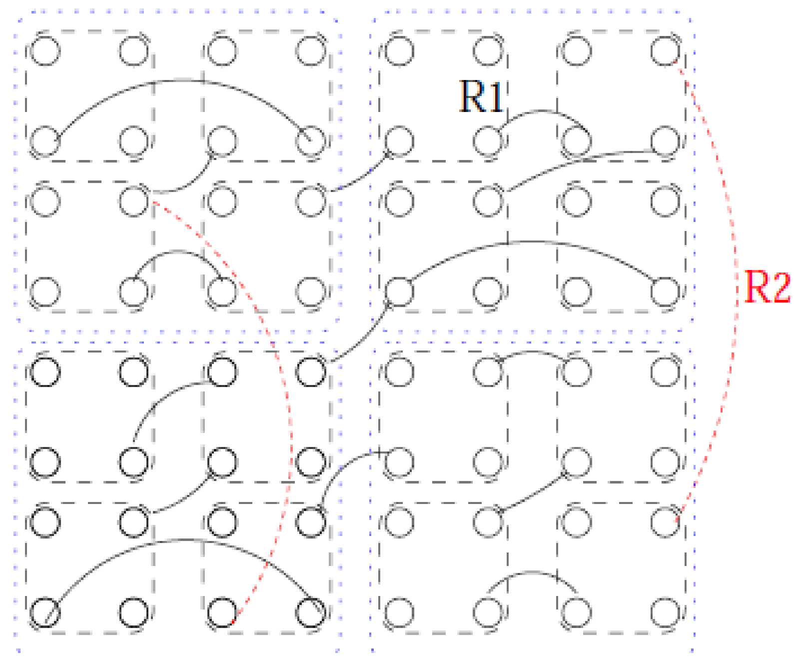

FIG. 1: Two lowest levels of the hierarchical network construction with 4 nodes/module. Dashed lines: $l = l_1$, dotted lines: $l = l_2$. The solid lines denoted R1 are randomly chosen connections within the bottom level (fully connected) modules, while those denoted R2 provide random connections on the next level. Links can be directed.

Hierarchical **M**odular **N**etwork topology motivated by connectomes

HMN2d:

Exponentially decaying connection probabilities with the levels l :

$p_l \approx \langle k \rangle (1/2)^{s\, l}$ $\qquad R \simeq 2^l$,

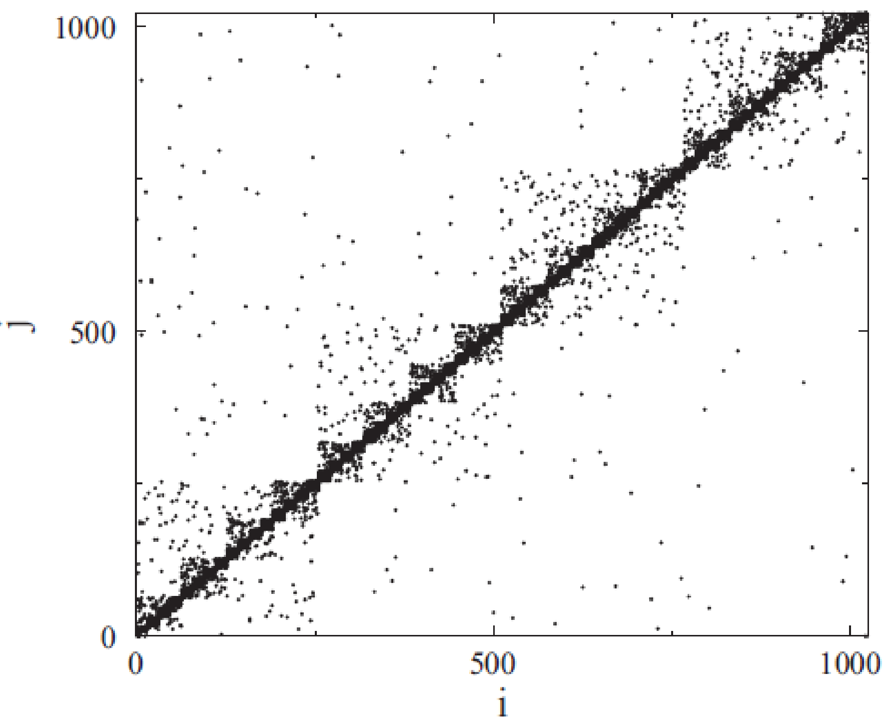

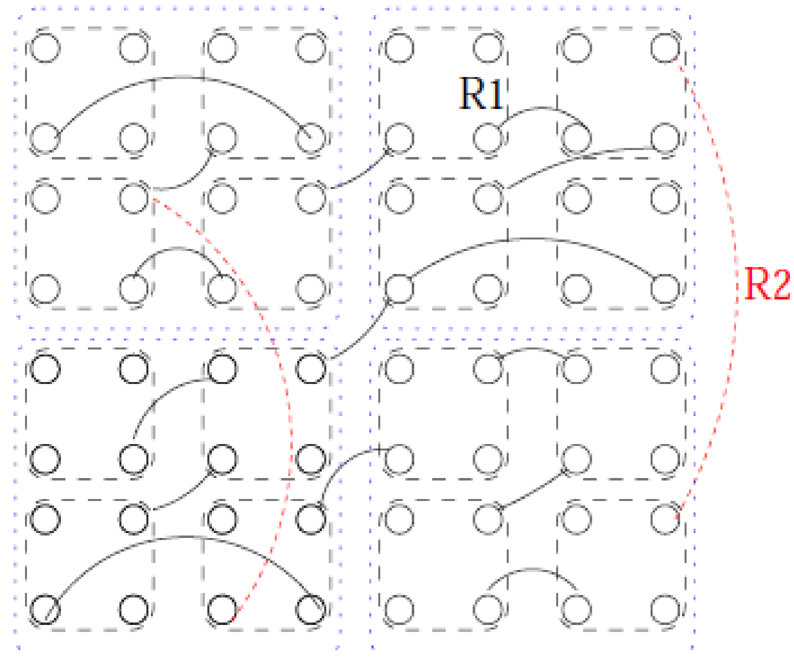

FIG. 1: Two lowest levels of the hierarchical network construction with 4 nodes/module. Dashed lines: $l = l_1$, dotted lines: $l = l_2$. The solid lines denoted R1 are randomly chosen connections within the bottom level (fully connected) modules, while those denoted R2 provide random connections on the next level. Links can be directed.

Hierarchical **M**odular **N**etwork topology motivated by connectomes

HMN2d:

Exponentially decaying connection probabilities with the levels l :

$$p_l \approx \langle k \rangle (1/2)^{s\, l} \qquad R \simeq 2^l,$$

related to networks with long edge probabilities:

$$p(R) \sim \langle k \rangle R^{-s}$$

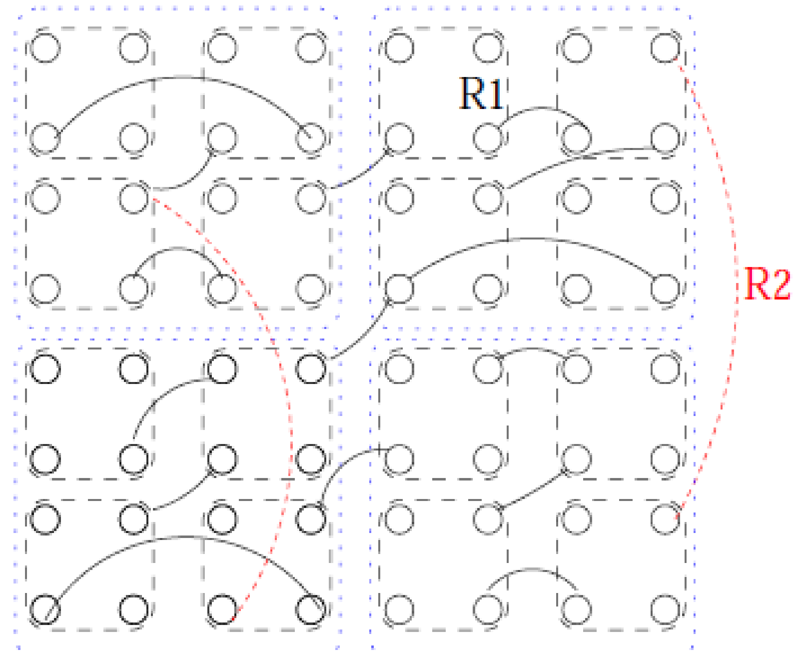

FIG. 1: Two lowest levels of the hierarchical network construction with 4 nodes/module. Dashed lines: $l = l_1$, dotted lines: $l = l_2$. The solid lines denoted R1 are randomly chosen connections within the bottom level (fully connected) modules, while those denoted R2 provide random connections on the next level. Links can be directed.

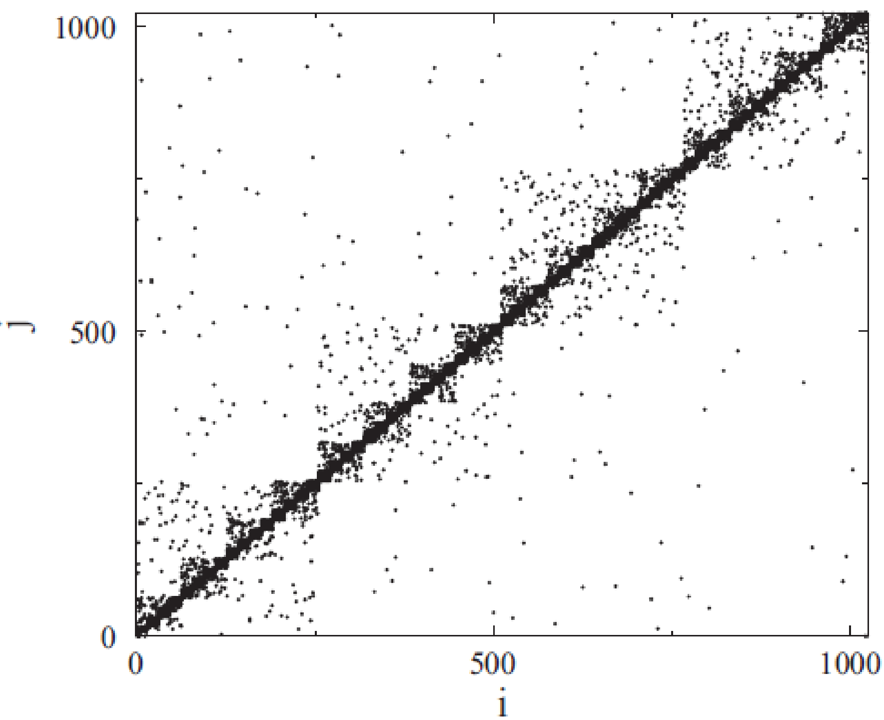

Hierarchical **M**odular **N**etwork topology motivated by connectomes

HMN2d:

Exponentially decaying connection probabilities with the levels l :

$$p_l \approx \langle k \rangle (1/2)^{s\,l} \qquad R \simeq 2^l,$$

related to networks with long edge probabilities:

$$p(R) \sim \langle k \rangle R^{-s}$$

where **Griffiths Phase** is present

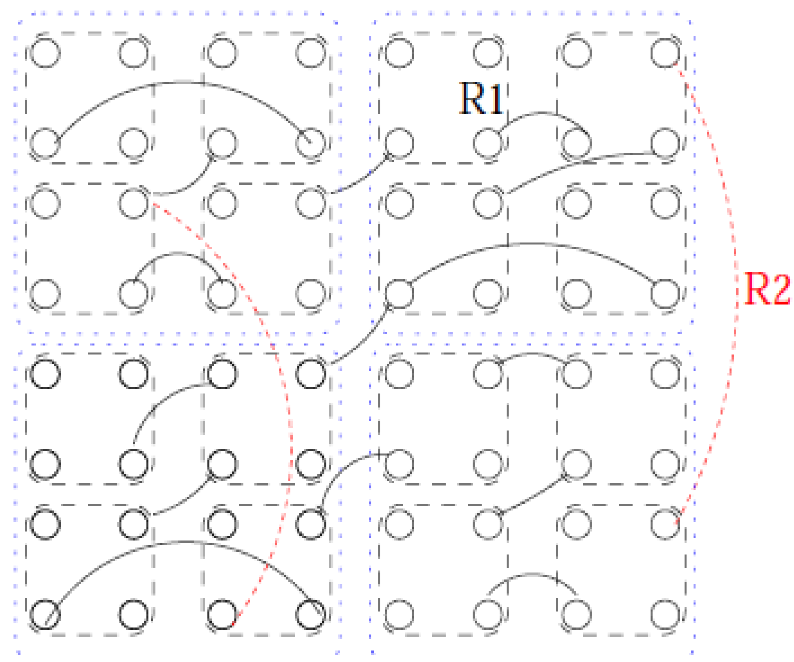

FIG. 1: Two lowest levels of the hierarchical network construction with 4 nodes/module. Dashed lines: $l = l_1$, dotted lines: $l = l_2$. The solid lines denoted R1 are randomly chosen connections within the bottom level (fully connected) modules, while those denoted R2 provide random connections on the next level. Links can be directed.

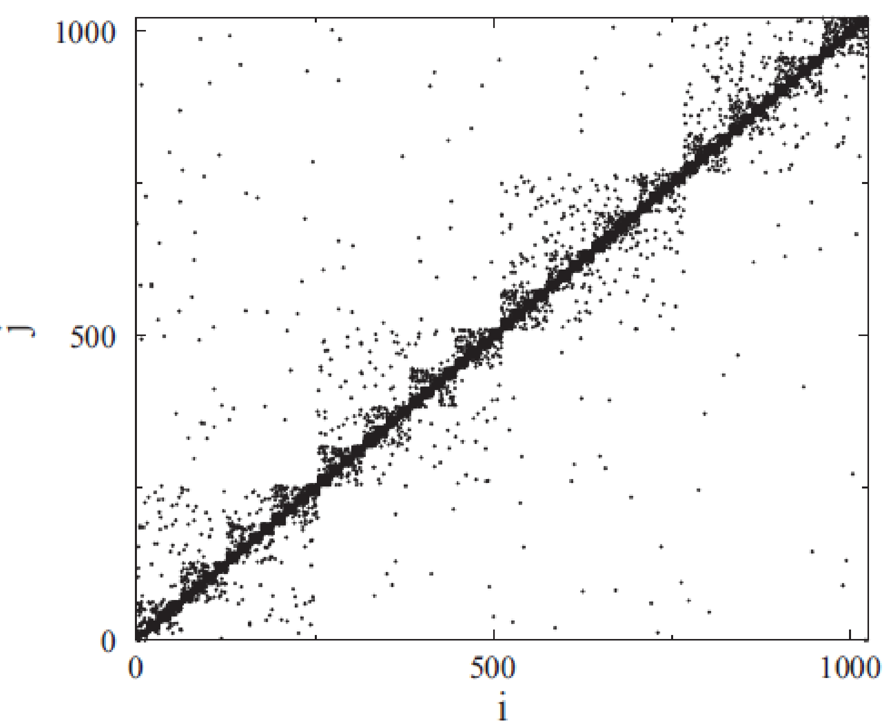

Network metrics

Network metrics

Topological dimension : $N(r) \sim r^{d}$

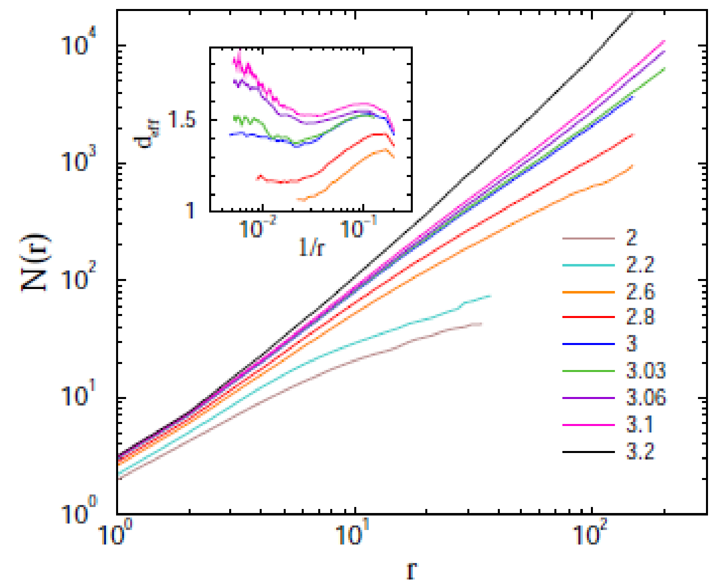

FIG. 3: Number of nodes within chemical distance r in HMN2d networks with $s = 4$ and $l = 9$ levels. Different curves correspond to different $\langle k \rangle$-s. Inset: local slopes d_{eff} of the $N(r)$ curves, defined in Eq. 4.

Network metrics

Topological dimension : $N(r) \sim r^{d}$

Effective dimension:

$$d_{\text{eff}} = \frac{\ln[N(r))/N(r')]}{\ln(r/r')}$$

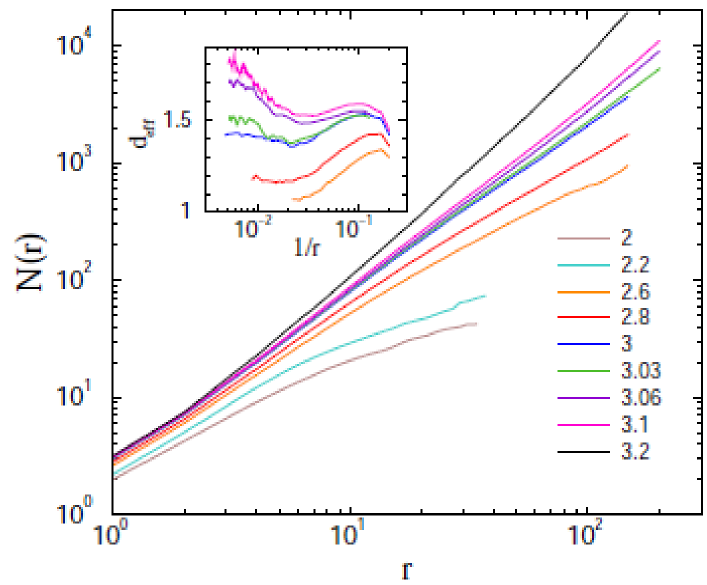

FIG. 3: Number of nodes within chemical distance r in HMN2d networks with $s = 4$ and $l = 9$ levels. Different curves correspond to different $\langle k \rangle$-s. Inset: local slopes d_{eff} of the $N(r)$ curves, defined in Eq. 4.

Network metrics

Topological dimension : $N(r) \sim r^{d}$

Effective dimension:
$$d_{\rm eff} = \frac{\ln[N(r))/N(r')]}{\ln(r/r')}$$

Breadth-first search results, in agreement with the

1d networks with power-law ranged, long edges:

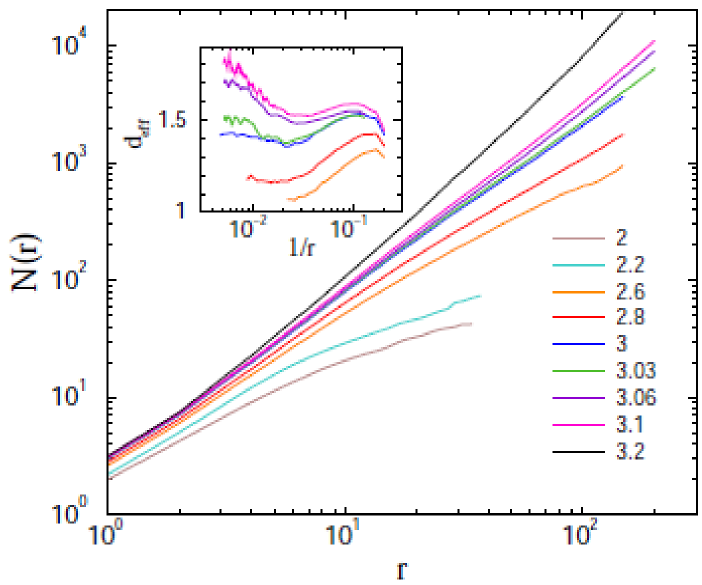

FIG. 3: Number of nodes within chemical distance r in HMN2d networks with $s = 4$ and $l = 9$ levels. Different curves correspond to different $\langle k \rangle$-s. Inset: local slopes d_{eff} of the $N(r)$ curves, defined in Eq. 4.

Network metrics

Topological dimension : $N(r) \sim r^{\,d}$

Effective dimension:

$$d_{\text{eff}} = \frac{\ln[N(r))/N(r')]}{\ln(r/r')}$$

Breadth-first search results, in agreement with the

1d networks with power-law ranged, long edges:

For $s = 4$: $\langle k \rangle$ dependent continuously changing

finite dimensions

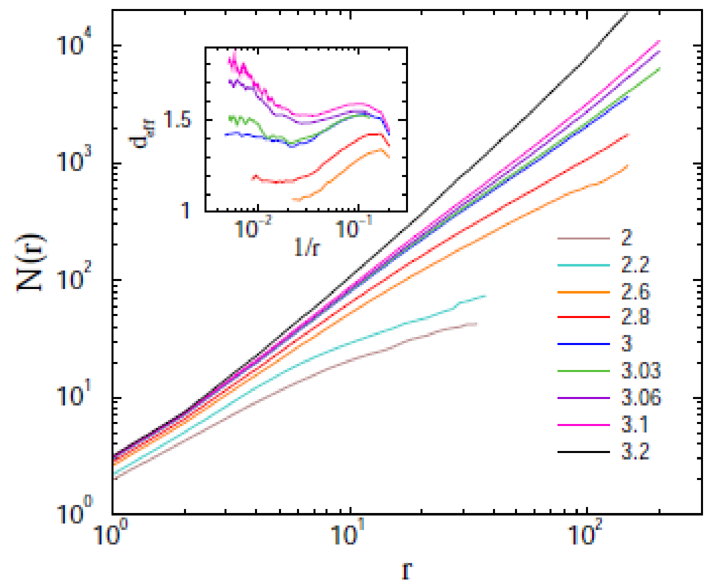

FIG. 3: Number of nodes within chemical distance r in HMN2d networks with $s = 4$ and $l = 9$ levels. Different curves correspond to different $\langle k \rangle$-s. Inset: local slopes d_{eff} of the $N(r)$ curves, defined in Eq. 4.

Network metrics

Topological dimension : $N(r) \sim r^{d}$

Effective dimension:

$$d_{\text{eff}} = \frac{\ln[N(r))/N(r')]}{\ln(r/r')}$$

Breadth-first search results, in agreement with the

1d networks with power-law ranged, long edges:

For $s = 4$: $<k>$ dependent continuously changing finite dimensions

For $s < 4$ small-world networks, $d \to \infty$

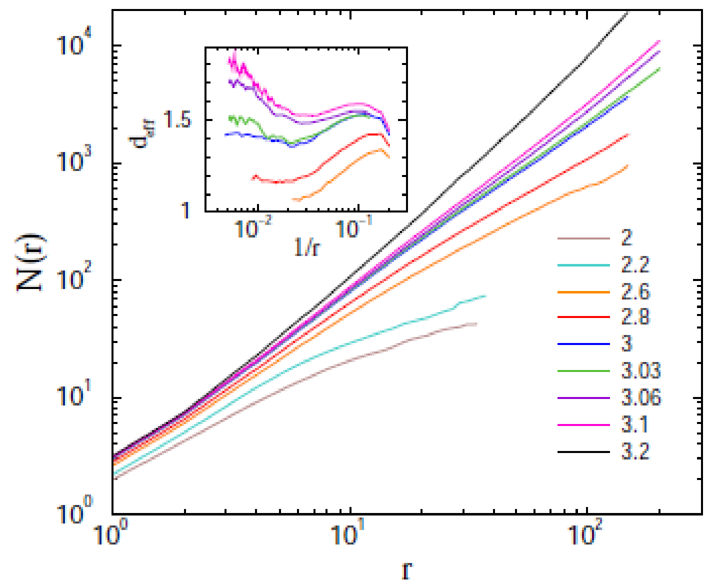

FIG. 3: Number of nodes within chemical distance r in HMN2d networks with $s = 4$ and $l = 9$ levels. Different curves correspond to different $\langle k \rangle$-s. Inset: local slopes d_{eff} of the $N(r)$ curves, defined in Eq. 4.

Network metrics

Topological dimension : $N(r) \sim r^{\,d}$

Effective dimension: $$d_{\mathrm{eff}} = \frac{\ln[N(r))/N(r')]}{\ln(r/r')}$$

Breadth-first search results, in agreement with the

1d networks with power-law ranged, long edges:

For $s = 4$: $<k>$ dependent continuously changing finite dimensions

For $s < 4$ small-world networks, $d \to \infty$

For $s > 4$ $d \to 1$, fast decaying long links

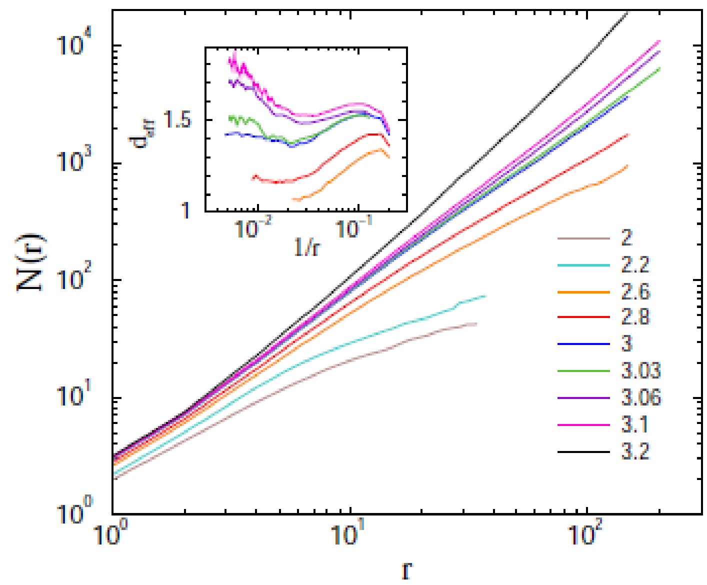

FIG. 3: Number of nodes within chemical distance r in HMN2d networks with $s = 4$ and $l = 9$ levels. Different curves correspond to different $\langle k \rangle$-s. Inset: local slopes d_{eff} of the $N(r)$ curves, defined in Eq. 4.

Network metrics

Topological dimension : $N(r) \sim r^{d}$

Effective dimension: $$d_{\text{eff}} = \frac{\ln[N(r))/N(r')]}{\ln(r/r')}$$

Breadth-first search results, in agreement with the

1d networks with power-law ranged, long edges:

For $s = 4$: $<k>$ dependent continuously changing finite dimensions →

For $s < 4$ small-world networks, $d \to \infty$

For $s > 4$ $d \to 1$, fast decaying long links

We study $s = 3$ *now* in more detail

+ lattice connectedness at: $l = 1$

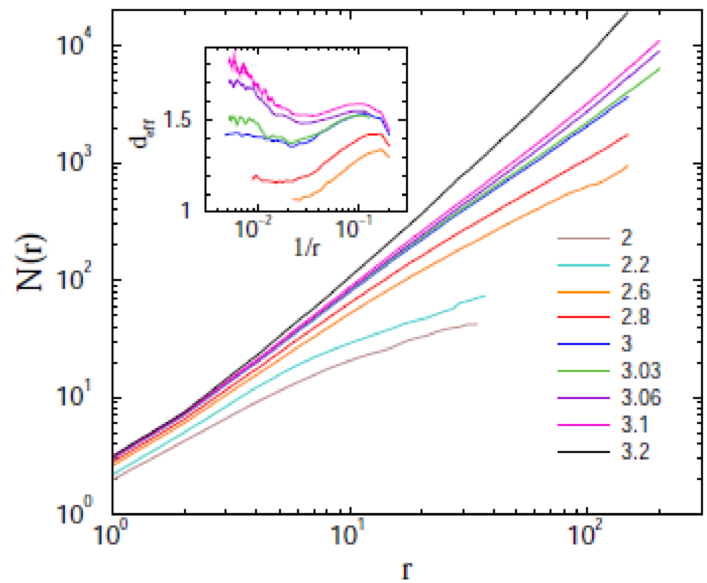

FIG. 3: Number of nodes within chemical distance r in HMN2d networks with $s = 4$ and $l = 9$ levels. Different curves correspond to different $\langle k \rangle$-s. Inset: local slopes d_{eff} of the $N(r)$ curves, defined in Eq. 4.

Network metrics

Topological dimension : $N(r) \sim r^{d}$

Effective dimension: $$d_{\text{eff}} = \frac{\ln[N(r))/N(r')]}{\ln(r/r')}$$

Breadth-first search results, in agreement with the

1d networks with power-law ranged, long edges:

For $s = 4$: $\langle k \rangle$ dependent continuously changing finite dimensions →

For $s < 4$ small-world networks, $d \to \infty$

For $s > 4$ $d \to 1$, fast decaying long links

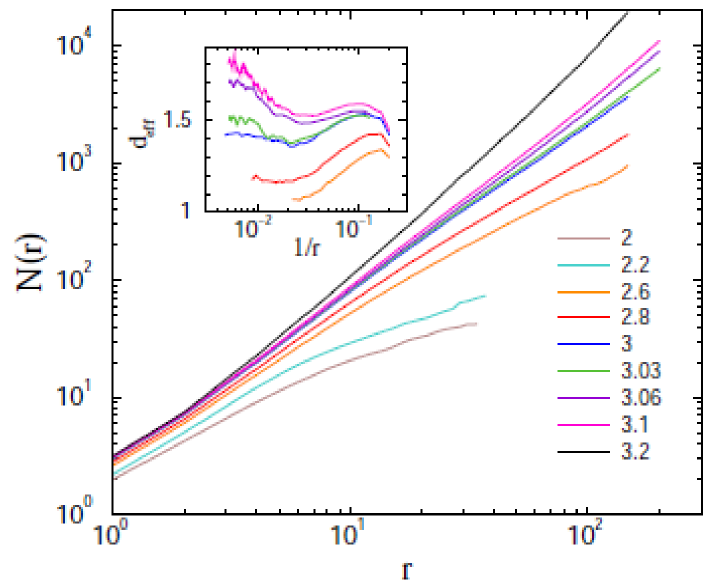

FIG. 3: Number of nodes within chemical distance r in HMN2d networks with $s = 4$ and $l = 9$ levels. Different curves correspond to different $\langle k \rangle$-s. Inset: local slopes d_{eff} of the $N(r)$ curves, defined in Eq. 4.

We study $s = 3$ *now* in more detail

+ lattice connectedness at: $l = 1$

$d_{eff} > 4$ → **mean-field behavior expected !**

Mean-field behavior of the *K=2* threshold model

Mean-field behavior of the *K=2* threshold model

Two-state system: $x_i = 0, 1$ (inactive, active)

Mean-field behavior of the *K*=*2* threshold model

Two-state system: $x_i = 0, 1$ (inactive, active)

- Conditional activation rule: $\sum_j x_j w_{i,j} \geq K$ (w_{ij} weight of interaction)

Mean-field behavior of the $K=2$ threshold model

Two-state system: $x_i = 0, 1$ (inactive, active)

• Conditional activation rule: $\sum_j x_j w_{i,j} \geq K$ (w_{ij} weight of interaction)

If this is true:

– nodes become active with activation probability: Λ

Mean-field behavior of the $K=2$ threshold model

Two-state system: $x_i = 0, 1$ (inactive, active)

• Conditional activation rule: $\sum_j x_j w_{i,j} \geq K$ (w_{ij} weight of interaction)

If this is true:

– nodes become active with activation probability: Λ

Otherwise:

– Nodes become inactive with deactivation probability: $\nu = 1 - \Lambda$

Mean-field behavior of the *K=2* threshold model

Two-state system: $x_i = 0, 1$ (inactive, active)

• Conditional activation rule: $\sum_j x_j w_{i,j} \geq K$ (w_{ij} weight of interaction)

If this is true:

– nodes become active with activation probability: Λ

Otherwise:

– Nodes become inactive with deactivation probability: $\nu = 1 - \Lambda$

Mean-field approximation: probability of site activation: ρ and a pair of nodes can be selected in a $(N-1)(N-2)/2$ way. The creation rate is:

$$\frac{1}{2}(N-1)(N-2)\Lambda\rho^2(1-\rho)$$

Mean-field behavior of the $K=2$ threshold model

Two-state system: $x_i = 0, 1$ (inactive, active)

• Conditional activation rule: $\sum_j x_j w_{i,j} \geq K$ (w_{ij} weight of interaction)

If this is true:

– nodes become active with activation probability: Λ

Otherwise:

– Nodes become inactive with deactivation probability: $\nu = 1 - \Lambda$

Mean-field approximation: probability of site activation: ρ and a pair of nodes can be selected in a $(N\text{-}1)(N\text{-}2)/2$ way. The creation rate is:

$$\frac{1}{2}(N-1)(N-2)\Lambda\rho^2(1-\rho)$$

Calling: $\lambda = (N - 1)(N - 2)\,\Lambda/2$, for a full graph of N nodes

Mean-field behavior of the $K=2$ threshold model

Two-state system: $x_i = 0, 1$ (inactive, active)

• Conditional activation rule: $\sum_j x_j w_{i,j} \geq K$ (w_{ij} weight of interaction)

If this is true:

– nodes become active with activation probability: Λ

Otherwise:

– Nodes become inactive with deactivation probability: $\nu = 1 - \Lambda$

Mean-field approximation: probability of site activation: $\boldsymbol{\rho}$ and a pair of nodes can be selected in a $(N-1)(N-2)/2$ way. The creation rate is:

$$\frac{1}{2}(N-1)(N-2)\Lambda\rho^2(1-\rho)$$

Calling: $\lambda = (N - 1)(N - 2)\,\Lambda/2$, for a full graph of N nodes

$$\frac{d\rho}{dt} = \lambda\,\rho^2(1-\rho) - \nu\,\rho$$

Mean-field behavior of the *K=2* threshold model

Two-state system: $x_i = 0, 1$ (inactive, active)

• Conditional activation rule: $\sum_j x_j w_{i,j} \geq K$ (w_{ij} weight of interaction)

If this is true:

– nodes become active with activation probability: Λ

Otherwise:

– Nodes become inactive with deactivation probability: $\nu = 1 - \Lambda$

Mean-field approximation: probability of site activation: $\boldsymbol{\rho}$ and a pair of nodes can be selected in a $(N\text{-}1)(N\text{-}2)/2$ way. The creation rate is:

$$\frac{1}{2}(N-1)(N-2)\Lambda\rho^2(1-\rho)$$

Calling: $\lambda = (N - 1)(N - 2)\,\Lambda/2$, for a full graph of N nodes

$$\frac{d\rho}{dt} = \lambda\,\rho^2(1-\rho) - \nu\,\rho$$

Real and positive solution for $\lambda > 4/5$: $\Lambda_c = \frac{8}{5(N-1)(N-2)}$

Mean-field behavior of the K=2 threshold model

Two-state system: $x_i = 0, 1$ (inactive, active)

• Conditional activation rule: $\sum_j x_j w_{i,j} \geq K$ (w_{ij} weight of interaction)

If this is true:

– nodes become active with activation probability: Λ

Otherwise:

– Nodes become inactive with deactivation probability: $\nu = 1 - \Lambda$

Mean-field approximation: probability of site activation: ρ and a pair of nodes can be selected in a $(N-1)(N-2)/2$ way. The creation rate is:

$$\frac{1}{2}(N-1)(N-2)\Lambda\rho^2(1-\rho)$$

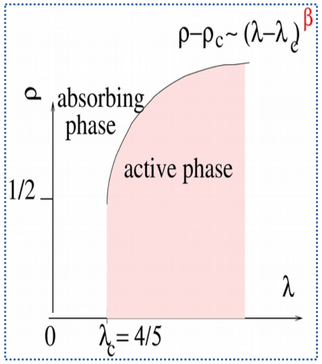

Calling: $\lambda = (N-1)(N-2)\,\Lambda/2$, for a full graph of N nodes

$$\frac{d\rho}{dt} = \lambda\,\rho^2(1-\rho) - \nu\,\rho$$

Real and positive solution for $\lambda > 4/5$: $\Lambda_c = \frac{8}{5(N-1)(N-2)}$

Mean-field behavior of the *K=2* threshold model

Two-state system: $x_i = 0, 1$ (inactive, active)

• Conditional activation rule: $\sum_j x_j w_{i,j} \geq K$ (w_{ij} weight of interaction)

If this is true:

– nodes become active with activation probability: Λ

Otherwise:

– Nodes become inactive with deactivation probability: $\nu = 1 - \Lambda$

Mean-field approximation: probability of site activation: ρ and a pair of nodes can be selected in a $(N-1)(N-2)/2$ way. The creation rate is:

$$\frac{1}{2}(N-1)(N-2)\Lambda\rho^2(1-\rho)$$

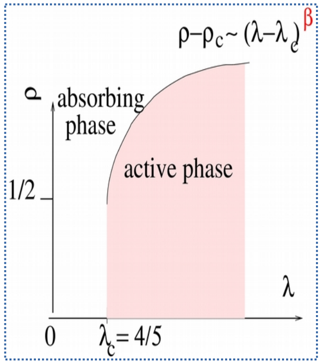

Calling: $\lambda = (N-1)(N-2)\Lambda/2$, for a full graph of N nodes

$$\frac{d\rho}{dt} = \lambda\, \rho^2(1-\rho) - \nu\, \rho$$

Real and positive solution for $\lambda > 4/5$: $\Lambda_c = \frac{8}{5(N-1)(N-2)}$

At the discontinuous transition PL decay: $\rho(t) - \rho_c \sim t^{-1}$ and

Mean-field behavior of the *K=2* threshold model

Two-state system: $x_i = 0, 1$ (inactive, active)

• Conditional activation rule: $\sum_j x_j w_{i,j} \geq K$ (w_{ij} weight of interaction)

If this is true:

– nodes become active with activation probability: Λ

Otherwise:

– Nodes become inactive with deactivation probability: $\nu = 1 - \Lambda$

Mean-field approximation: probability of site activation: ρ and a pair of nodes can be selected in a $(N-1)(N-2)/2$ way. The creation rate is:

$$\frac{1}{2}(N-1)(N-2)\Lambda\rho^2(1-\rho)$$

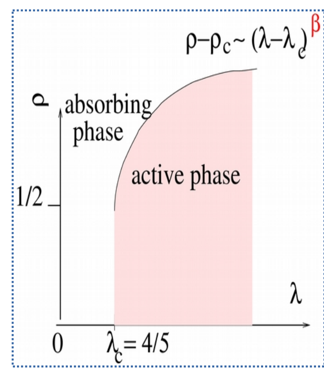

Calling: $\lambda = (N-1)(N-2)\Lambda/2$, for a full graph of N nodes

$$\frac{d\rho}{dt} = \lambda\, \rho^2(1-\rho) - \nu\, \rho$$

Real and positive solution for $\lambda > 4/5$: $\Lambda_c = \frac{8}{5(N-1)(N-2)}$

At the discontinuous transition PL decay: $\rho(t) - \rho_c \sim t^{-1}$ and $(\rho - \rho_c) \propto (\lambda - \lambda_c)^{1/2}$.

K=2 threshold model on HMN2d

K=2 threshold model on HMN2d

By running the model on the HMN2d graphs : discontinuous transition + PLs with continuously varying exponents

K=2 threshold model on HMN2d

By running the model on the HMN2d graphs : discontinuous transition + PLs with continuously varying exponents

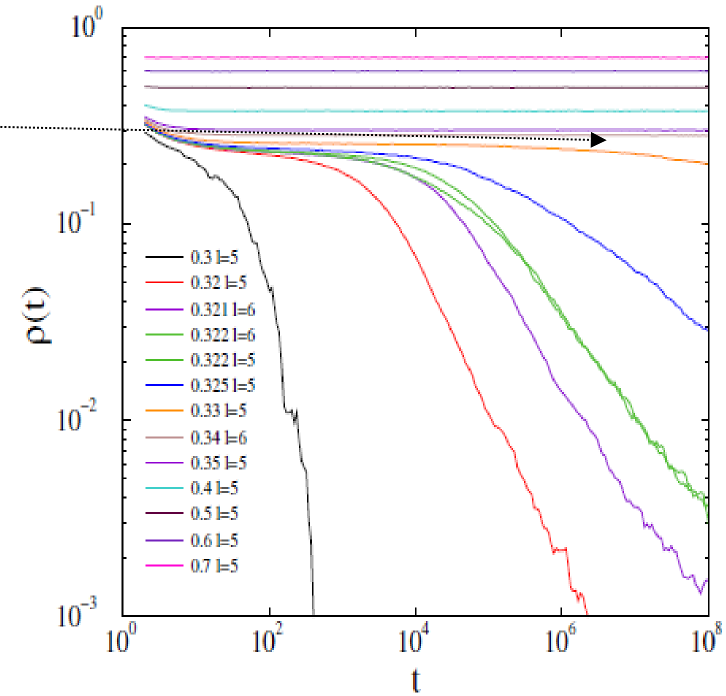

Fig. 1. Evolution of the activity for different control parameter λ in case of start from fully active state in a threshold model running on hierarchical modular graphs. One can see a discontinuous transition to a Griffiths Phase (from Ref. [4]).

K=2 threshold model on HMN2d

By running the model on the HMN2d graphs : discontinuous transition + PLs with continuously varying exponents

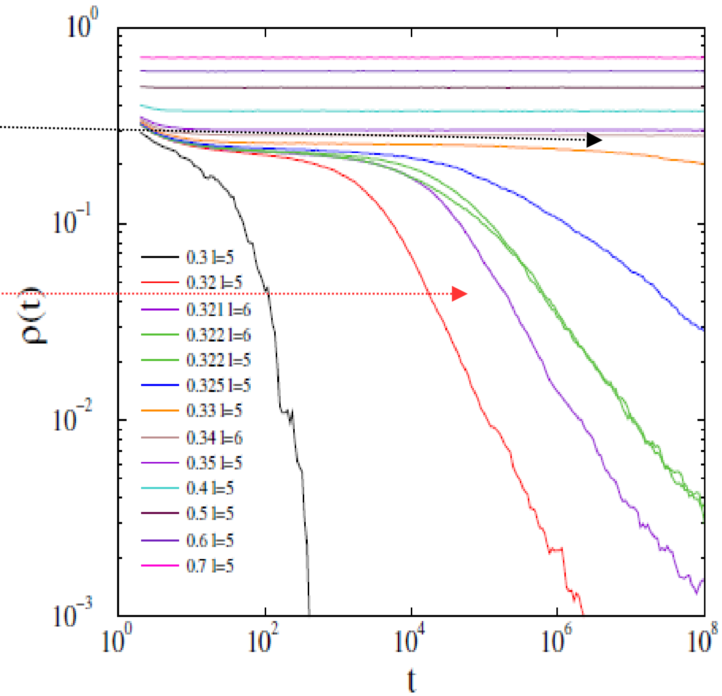

Fig. 1. Evolution of the activity for different control parameter λ in case of start from fully active state in a threshold model running on hierarchical modular graphs. One can see a discontinuous transition to a Griffiths Phase (from Ref. [4]).

K=2 threshold model on HMN2d

By running the model on the HMN2d graphs : discontinuous transition + PLs with continuously varying exponents

→ **Griffiths Phase**: below λ_c

n sized **dynamically fragmented** modules create active Rare Regions

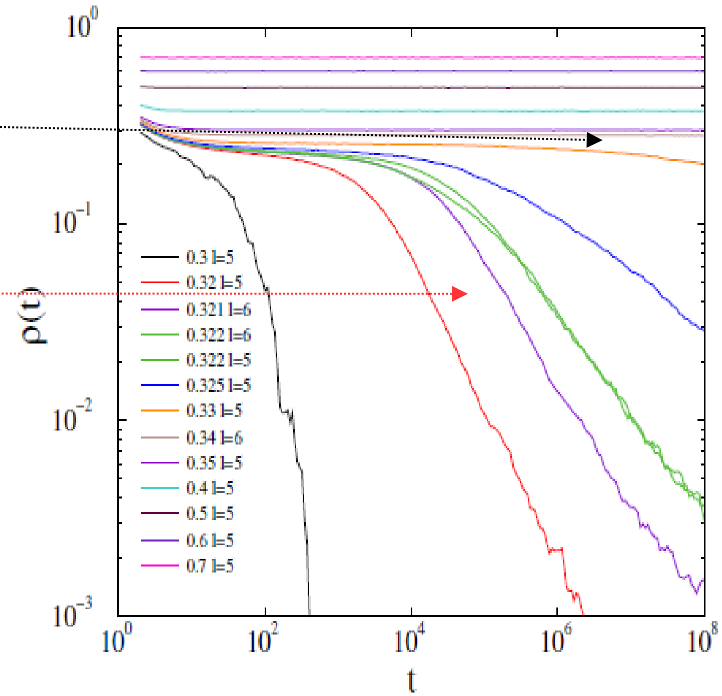

Fig. 1. Evolution of the activity for different control parameter λ in case of start from fully active state in a threshold model running on hierarchical modular graphs. One can see a discontinuous transition to a Griffiths Phase (from Ref. [4]).

K=2 threshold model on HMN2d

By running the model on the HMN2d graphs : discontinuous transition + PLs with continuously varying exponents

→ **Griffiths Phase**: below λ_c

n sized **dynamically fragmented** modules create active Rare Regions with probability: $p(n) \sim p_l \sim c^{\,4-l}$

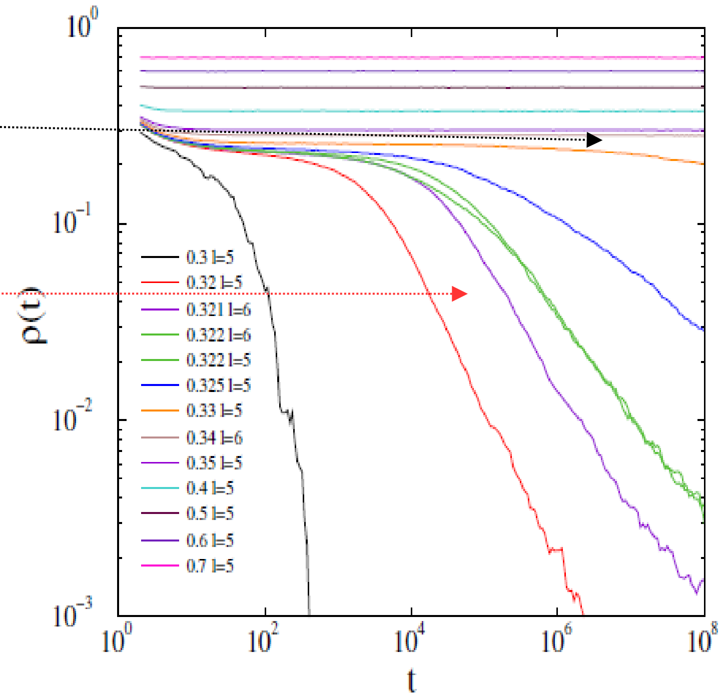

Fig. 1. Evolution of the activity for different control parameter λ in case of start from fully active state in a threshold model running on hierarchical modular graphs. One can see a discontinuous transition to a Griffiths Phase (from Ref. [4]).

K=2 threshold model on HMN2d

By running the model on the HMN2d graphs : discontinuous transition + PLs with continuously varying exponents

→ **Griffiths Phase**: below λ_c

n sized **dynamically fragmented** modules create active Rare Regions with probability: $p(n) \sim p_l \sim c^{4-l}$

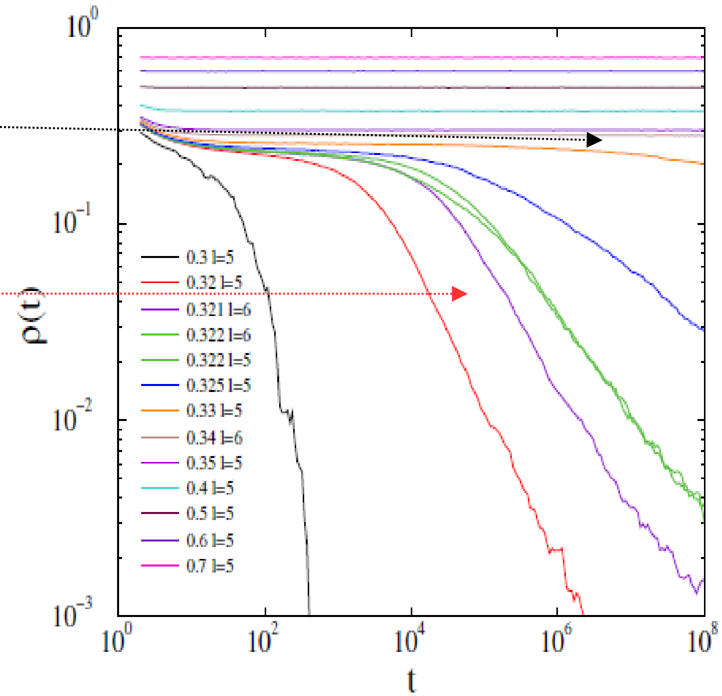

Fig. 1. Evolution of the activity for different control parameter λ in case of start from fully active state in a threshold model running on hierarchical modular graphs. One can see a discontinuous transition to a Griffiths Phase (from Ref. [4]).

K=2 threshold model on HMN2d

By running the model on the HMN2d graphs : discontinuous transition + PLs with continuously varying exponents

→ **Griffiths Phase**: below λ_c

n sized **dynamically fragmented** modules create active Rare Regions with probability: $p(n) \sim p_l \sim c^{\,4-l}$

and decay slowly with $\tau \sim exp(b\, n)$

The density of active sites:

$$\rho(t) \sim \int dn \;\; n \;\; p(n) \;\; exp\,[-t\,/\tau(\,n\,)]$$

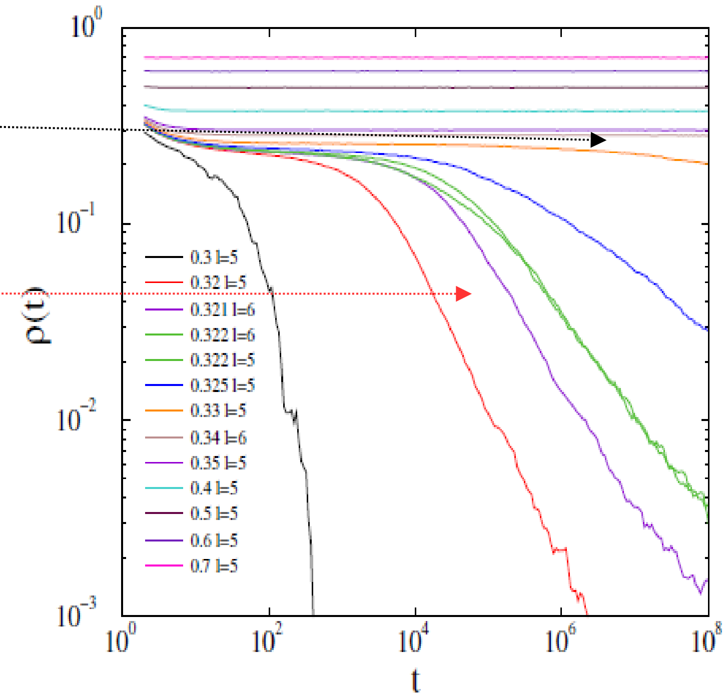

Fig. 1. Evolution of the activity for different control parameter λ in case of start from fully active state in a threshold model running on hierarchical modular graphs. One can see a discontinuous transition to a Griffiths Phase (from Ref. [4]).

K=2 threshold model on HMN2d

By running the model on the HMN2d graphs : discontinuous transition + PLs with continuously varying exponents

→ **Griffiths Phase**: below λ_c

n sized **dynamically fragmented** modules create active Rare Regions with probability: $p(n) \sim p_l \sim c^{\,4-l}$

and decay slowly with $\tau \sim exp(b\, n)$

The density of active sites:

$$\rho(t) \sim \int dn \;\; n \;\; p(n) \;\; exp\,[-t\,/\tau(\,n\,)]$$

For $\lambda_c^{\,0} < \lambda < \lambda_c \;:\; \rho(t) \sim t^{\,-c/b}$

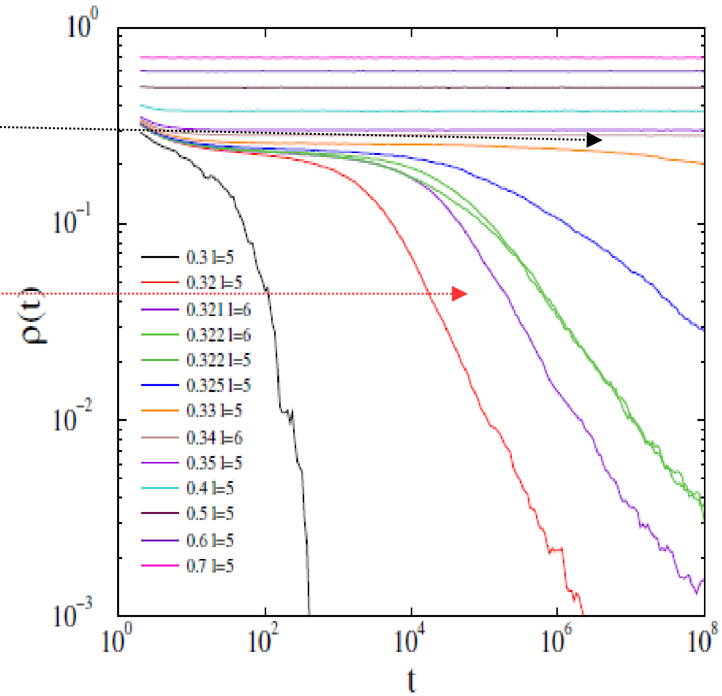

Fig. 1. Evolution of the activity for different control parameter λ in case of start from fully active state in a threshold model running on hierarchical modular graphs. One can see a discontinuous transition to a Griffiths Phase (from Ref. [4]).

MEASUREMENTS

- Density of active nodes $\rho(t) = 1/N \sum_{i=1}^{N} x_i$
- A single pair of active nodes can trigger an avalanche of duration T and spatiotemporal size $s = \sum_{i=1}^{N} \sum_{t=1}^{T} x_i$. It allows us to compute:
  - **probability density functions of avalanche sizes** $p(s)$
  - **final survival time distributions** $p(t)$

MEASUREMENTS

- Density of active nodes $\rho(t) = 1/N \sum_{i=1}^{N} x_i$
- A single pair of active nodes can trigger an avalanche of duration T and spatiotemporal size $s = \sum_{i=1}^{N} \sum_{t=1}^{T} x_i$. It allows us to compute:
  - **probability density functions of avalanche sizes** $p(s)$
  - **final survival time distributions** $p(t)$

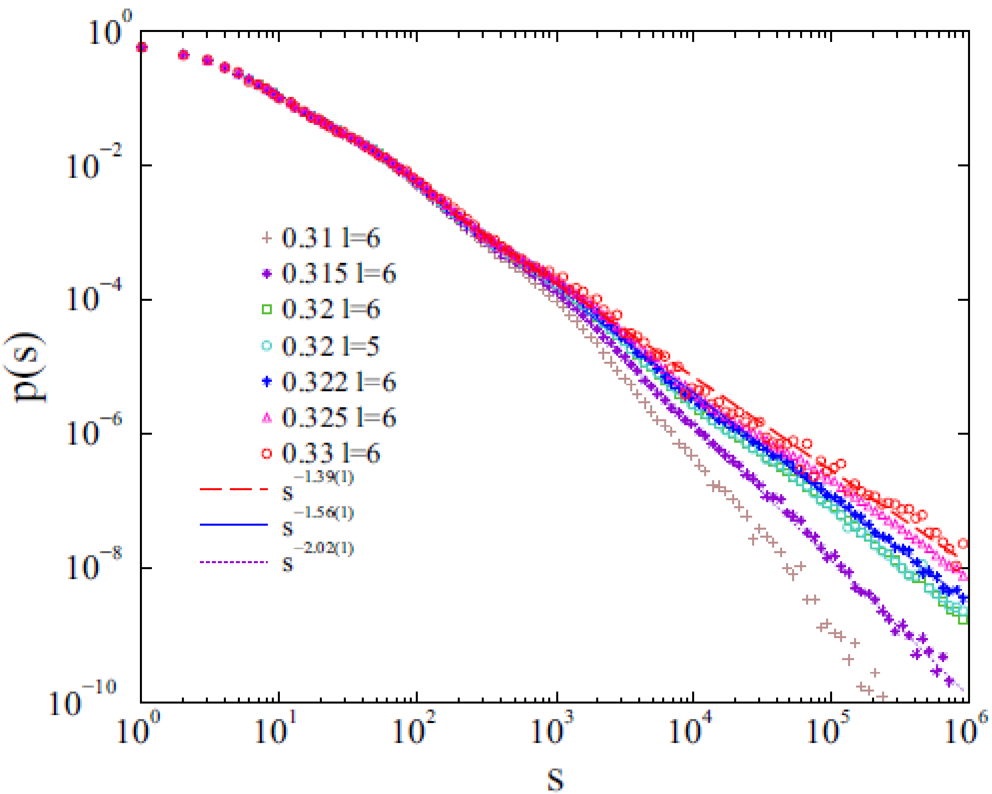

FIG. 3. Avalanche size distributions at different λ branching rates, denoted by the symbols, in the presence of excitatory links in the HMN2d with $l = 5, 6$ levels. From top to bottom curves: $\lambda = 0.33$, 0.325, 0.322, 0.32 ($l = 5$ cyan and $l = 6$ green), 0.315, 0.31. Dashed lines show PL fits for the tails: $s > 1000$ at $\lambda = 0.315$, 0.322, 0.33.

MEASUREMENTS

- Density of active nodes $\rho(t) = 1/N \sum_{i=1}^{N} x_i$
- A single pair of active nodes can trigger an avalanche of duration T and spatiotemporal size $s = \sum_{i=1}^{N} \sum_{t=1}^{T} x_i$. It allows us to compute:
  - **probability density functions of avalanche sizes** $p(s)$
  - **final survival time distributions** $p(t)$

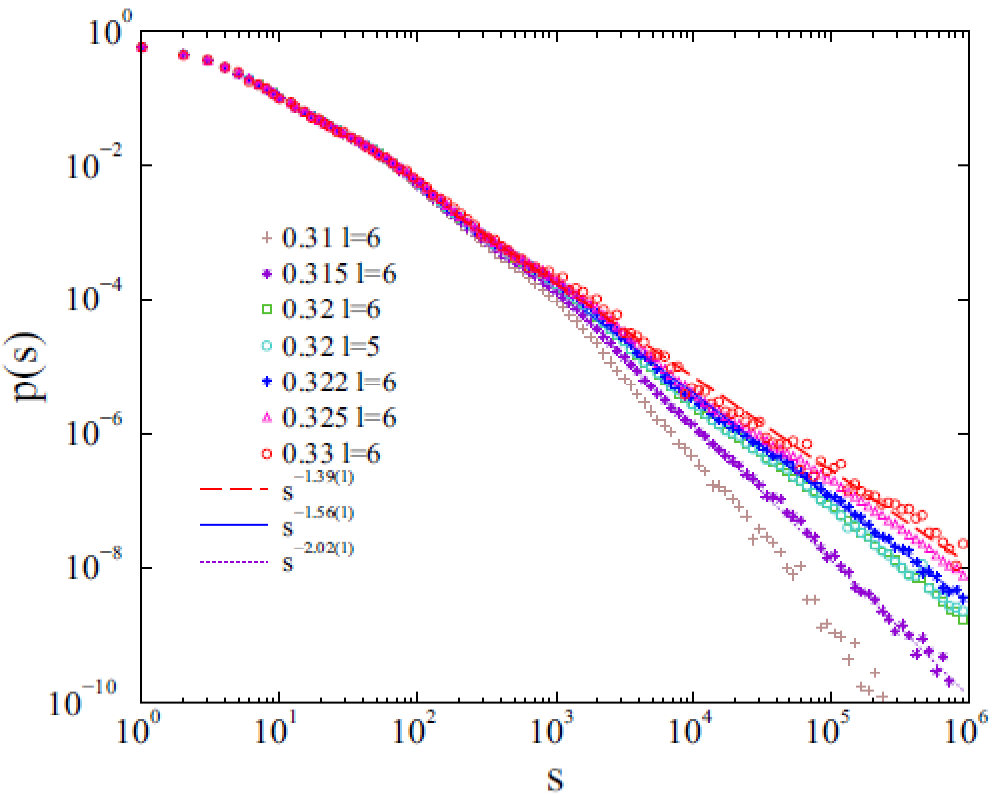

FIG. 3. Avalanche size distributions at different λ branching rates, denoted by the symbols, in the presence of excitatory links in the HMN2d with $l = 5, 6$ levels. From top to bottom curves: $\lambda = 0.33$, 0.325, 0.322, 0.32 ($l = 5$ cyan and $l = 6$ green), 0.315, 0.31. Dashed lines show PL fits for the tails: $s > 1000$ at $\lambda = 0.315$, 0.322, 0.33.

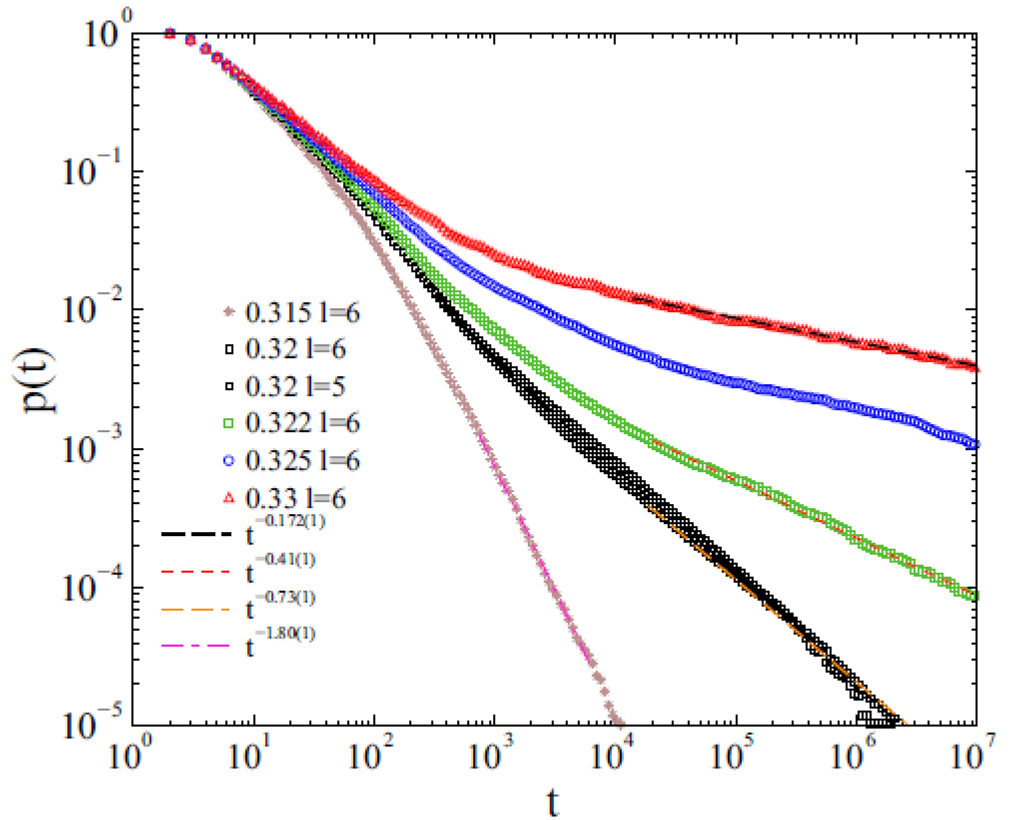

FIG. 4. Survival probability of the activity at different branching rates in the $K = 2$ threshold model with excitatory links. From top to bottom curves: $\lambda = 0.33$, 0.325, 0.322, 0.32 ($l = 5$ and $l = 6$), 0.315. Dashed lines show PL fits for the tails: $s > 10^4$ at $\lambda = 0.315$, 0.32, 0.322, 0.33.

Explanation for the Griffiths Phase

Explanation for the Griffiths Phase

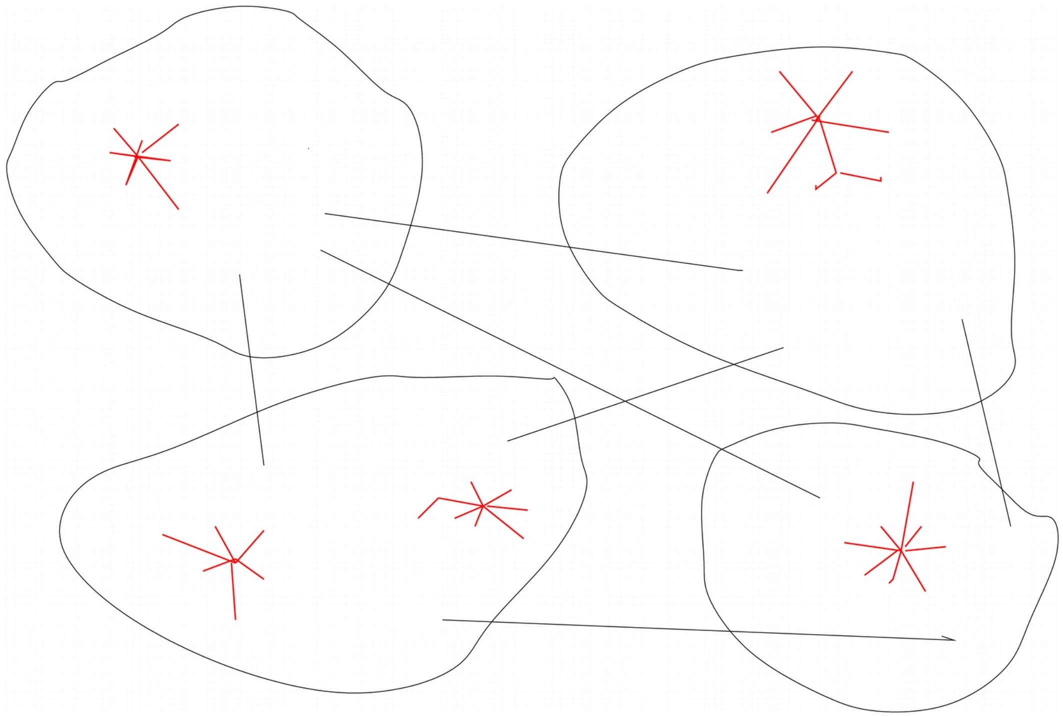

Explanation for the Griffiths Phase

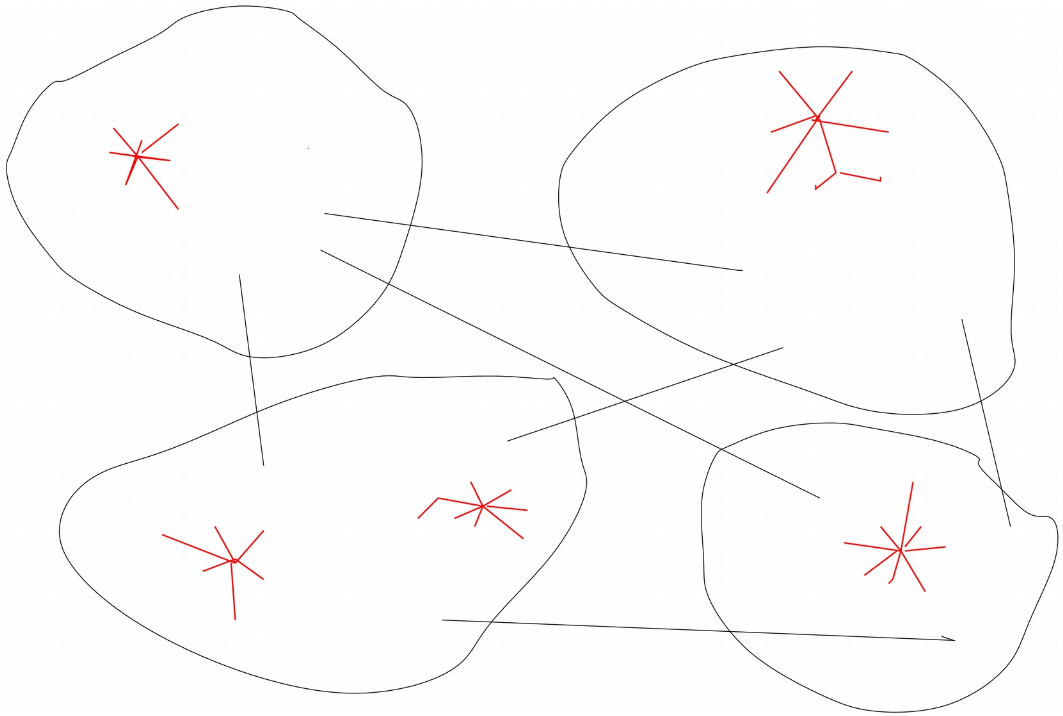

Hubs or cores in modules remain active which decay as: $\rho \sim \exp(-t/\tau_{ls})$

Random, inter-module connections with ***single links*** $\leftrightarrow$ ***K=2***
$\rightarrow$ *quasi unconnected, finite rare regions*

Conclusions

Conclusions

- **Griffiths phase (GP) can occur in high dimensional systems due to fragmentation of the activity propagation caused by the modules**
- **Nonuniversal PLs suggest that Griffiths effects are present**

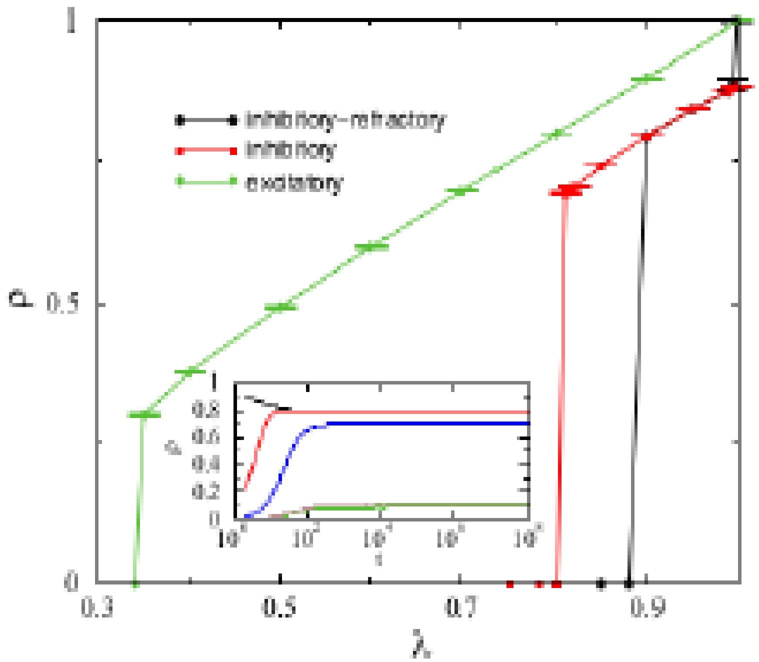

Fig. 5: Steady-state behavior for the excitatory, inhibitory, and refractory-inhibitory cases. Inset: evolution of ρ in an inhibitory HMN2d with $N = 4096$ for different initial activity densities: $\rho(0) = 0.0005, 0.001, 0.01, 0.1, 1$ (bottom to top curves).

- **Discontinuous jump in ρ, metastability and GP: Hybrid Phase Transition!**

Conclusions

- Griffiths phase (GP) can occur in high dimensional systems due to fragmentation of the activity propagation caused by the modules
- Nonuniversal PLs suggest that Griffiths effects are present

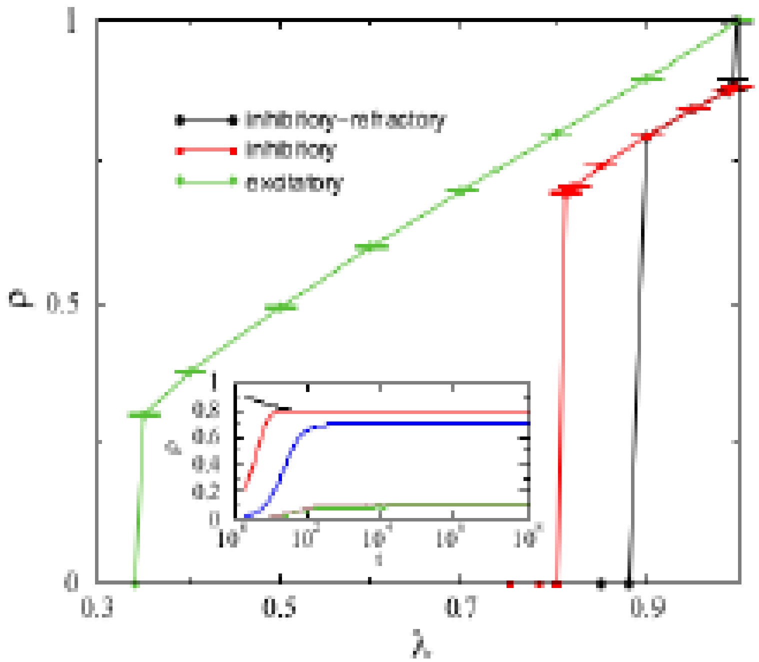

Fig. 5: Steady-state behavior for the excitatory, inhibitory, and refractory-inhibitory cases. Inset: evolution of ρ in an inhibitory HMN2d with $N = 4096$ for different initial activity densities: $\rho(0) = 0.0005, 0.001, 0.01, 0.1, 1$ (bottom to top curves).

- Discontinuous jump in ρ, metastability and GP: Hybrid Phase Transition!

May apply to other heretogeneous, excitable systems

G. Ó. & B. S. PHYSICAL REVIEW RESEARCH 3, 013106 (2021)

Thank you for your attention !

Inhibitory weights in the local homeostasis

Inhibitory weights in the local homeostasis

Inhibitory links (10-30%) generate Griffiths Phase

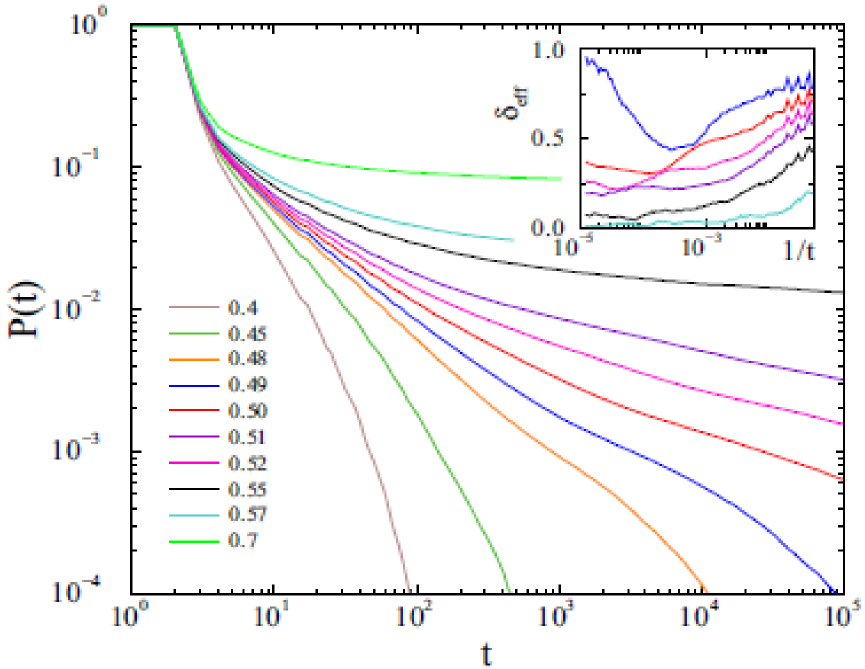

FIG. 5. Avalanche survival distribution of the relative threshold model with 30% inhibitory links at $K = 0.1$, for $\lambda = 0.95$ and $\nu = 0.4, 0.45, 0.49, 0.5, 0.51, 0.52, 0.550.57, 0.7$ (bottom to top curves). Inset: Local slopes of the same curves in opposite order.

Inhibitory weights in the local homeostasis

Inhibitory links (10-30%) generate Griffiths Phase
with non-universal power laws and ultra-slow dynamics at λ_c

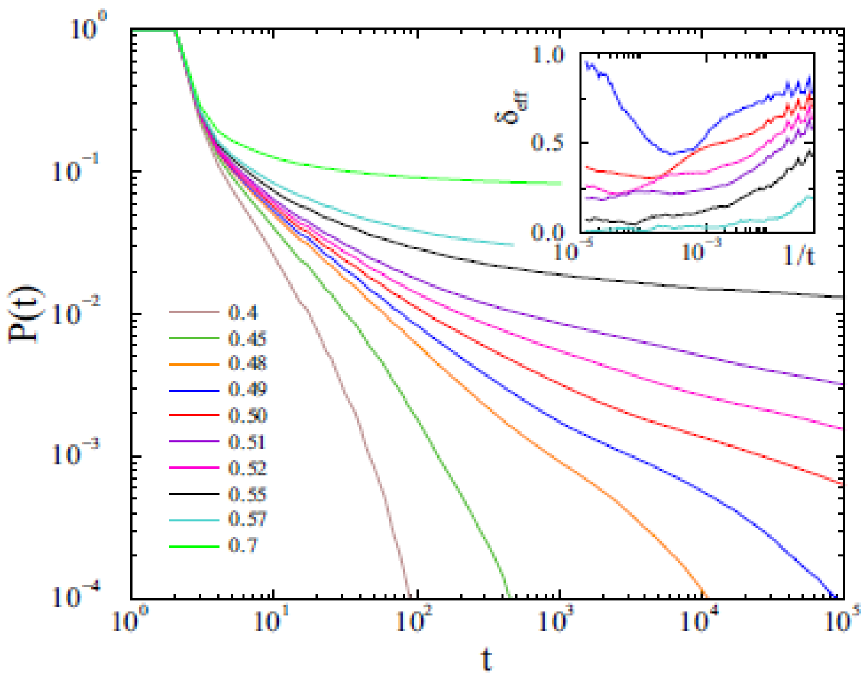

FIG. 5. Avalanche survival distribution of the relative threshold model with 30% inhibitory links at $K = 0.1$, for $\lambda = 0.95$ and $\nu = 0.4, 0.45, 0.49, 0.5, 0.51, 0.52, 0.550.57, 0.7$ (bottom to top curves). Inset: Local slopes of the same curves in opposite order.

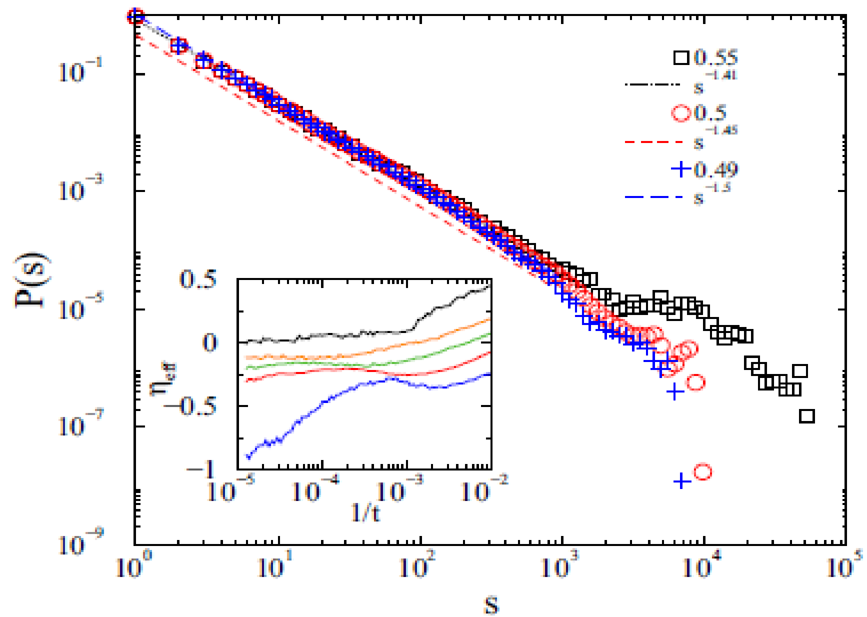

FIG. 6. Avalanche size distribution of the relative threshold model with 30% inhibitory links at $K = 0.1$, $\nu = 0.95$, and $\lambda = 0.49, 0.5, 0.55$. Dashed lines: PL fits. Inset: Effective η exponent for $\nu = 0.95$ and $\lambda = 0.49, 0.5, 0.51, 0.51, 0.55$ (bottom to top curves).

τ ~ 1.3 - 2

Inhibitory weights in the local homeostasis

Inhibitory links (10-30%) generate Griffiths Phase

with non-universal power laws and ultra-slow dynamics at λ_c

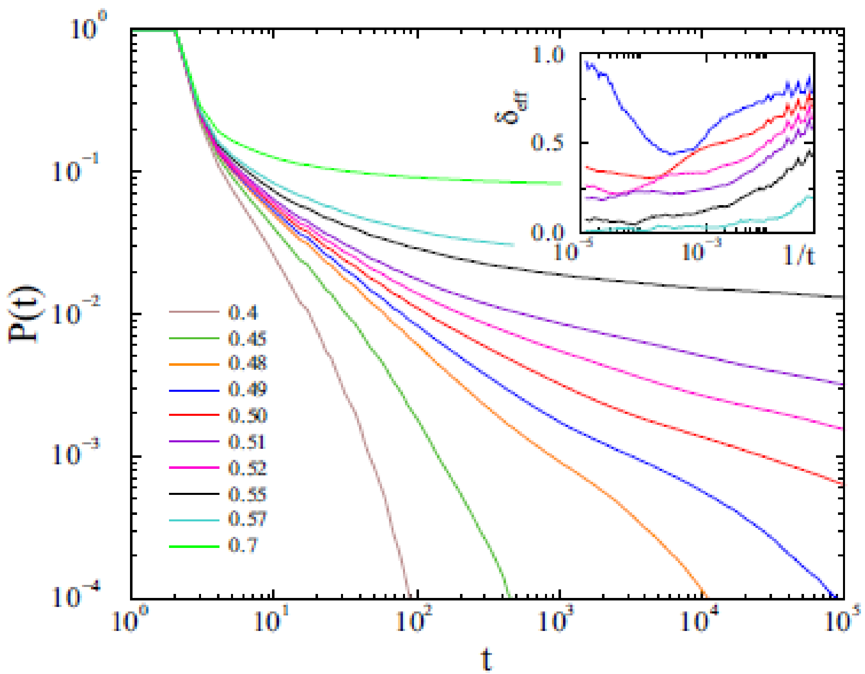

FIG. 5. Avalanche survival distribution of the relative threshold model with 30% inhibitory links at $K = 0.1$, for $\lambda = 0.95$ and $\nu = 0.4, 0.45, 0.49, 0.5, 0.51, 0.52, 0.55 0.57, 0.7$ (bottom to top curves). Inset: Local slopes of the same curves in opposite order.

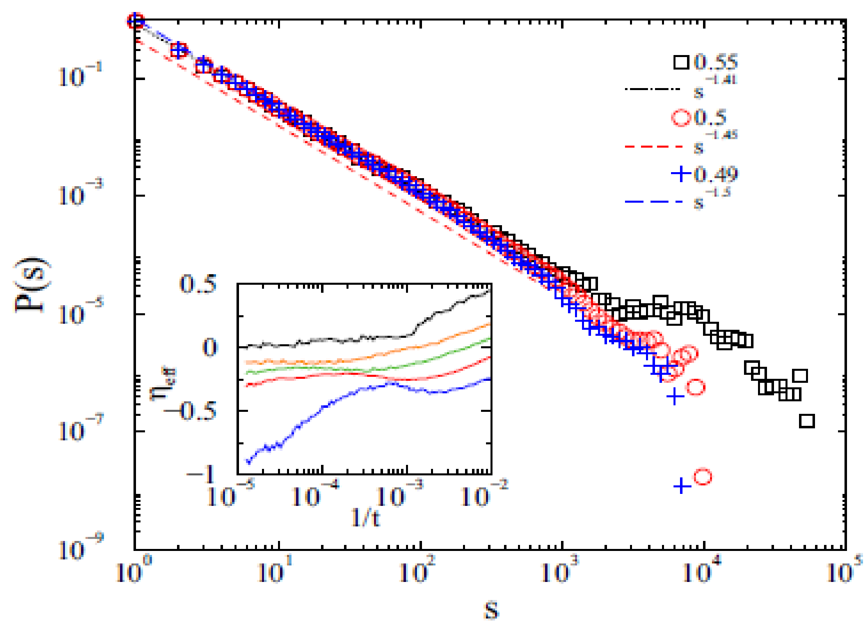

FIG. 6. Avalanche size distribution of the relative threshold model with 30% inhibitory links at $K = 0.1$, $\nu = 0.95$, and $\lambda = 0.49, 0.5, 0.55$. Dashed lines: PL fits. Inset: Effective η exponent for $\nu = 0.95$ and $\lambda = 0.49, 0.5, 0.51, 0.51, 0.55$ (bottom to top curves).

$\tau \sim 1.3 - 2$

G.Ó. Phys. Rev. E 94, 062411 (2016)

Inhibitory (negative) links compared to experiments

Inhibitions: 20% of links: $w_{ij} \rightarrow -w_{ij}$ randomly

Inhibitory (negative) links compared to experiments

Inhibitions: 20% of links: $w_{ij} \rightarrow -w_{ij}$ randomly

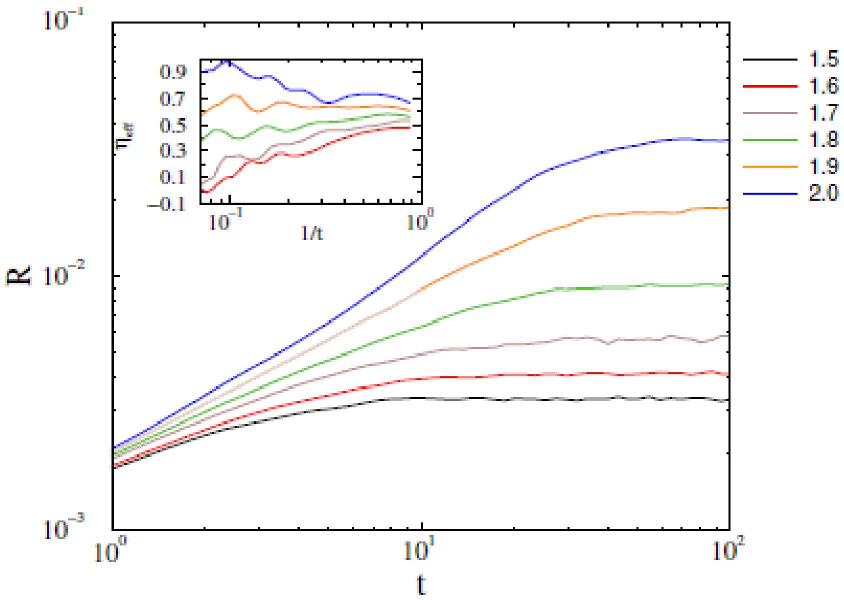

K_c increases to *1.9(1)*, but η = *0.6(1)* remains the same, and below it:

Inhibitory (negative) links compared to experiments

Inhibitions: 20% of links: $w_{ij} \rightarrow -w_{ij}$ randomly

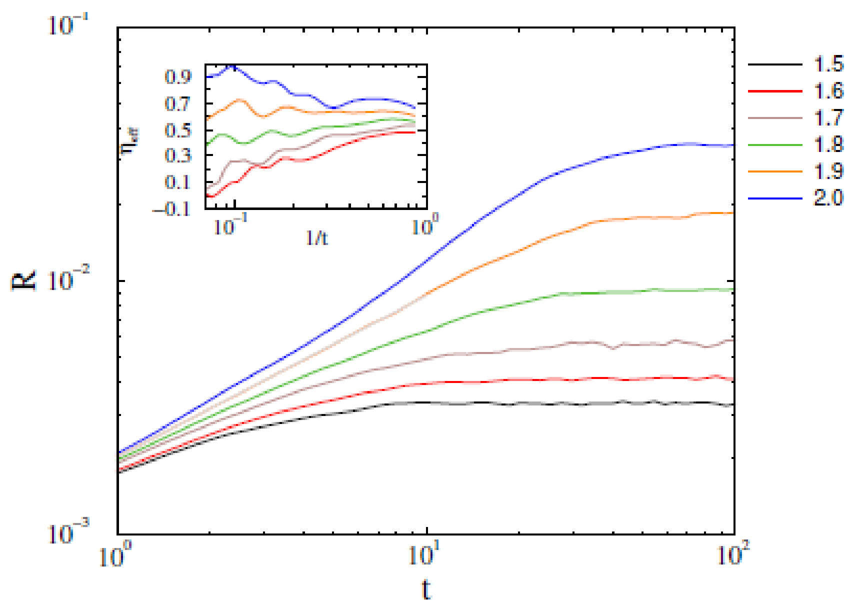

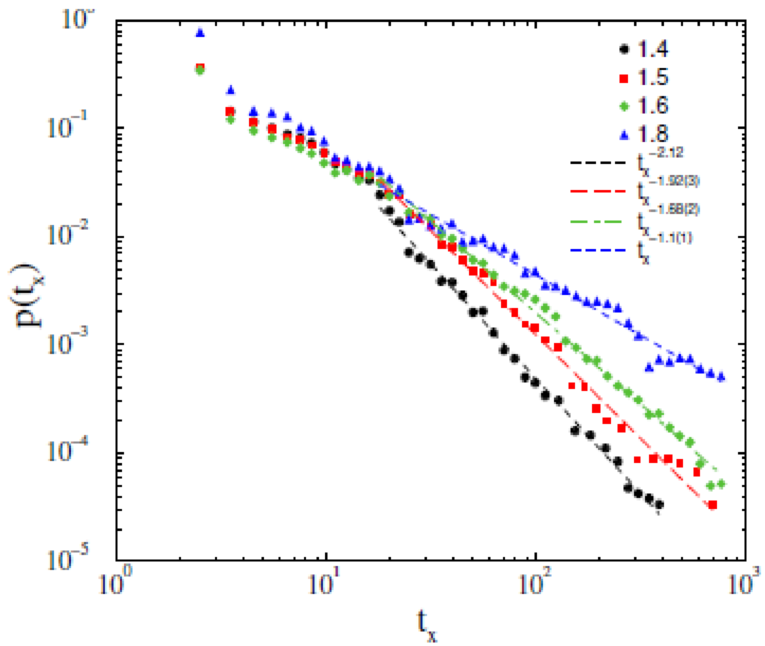

K_c increases to *1.9(1)*, but η = *0.6(1)* remains the same, and below it:

Duration scaling exponent within experimental range: ***1.5 < τ_t < 2.4***

J.M. Palva et al PNAS 110 (2013) 3585

Inhibitory model: $w_{ij}=1$ or $w_{ij}=-1$ (prob. 0.2)

Inhibitory model: $w_{ij}=1$ or $w_{ij}=-1$ (prob. 0.2)

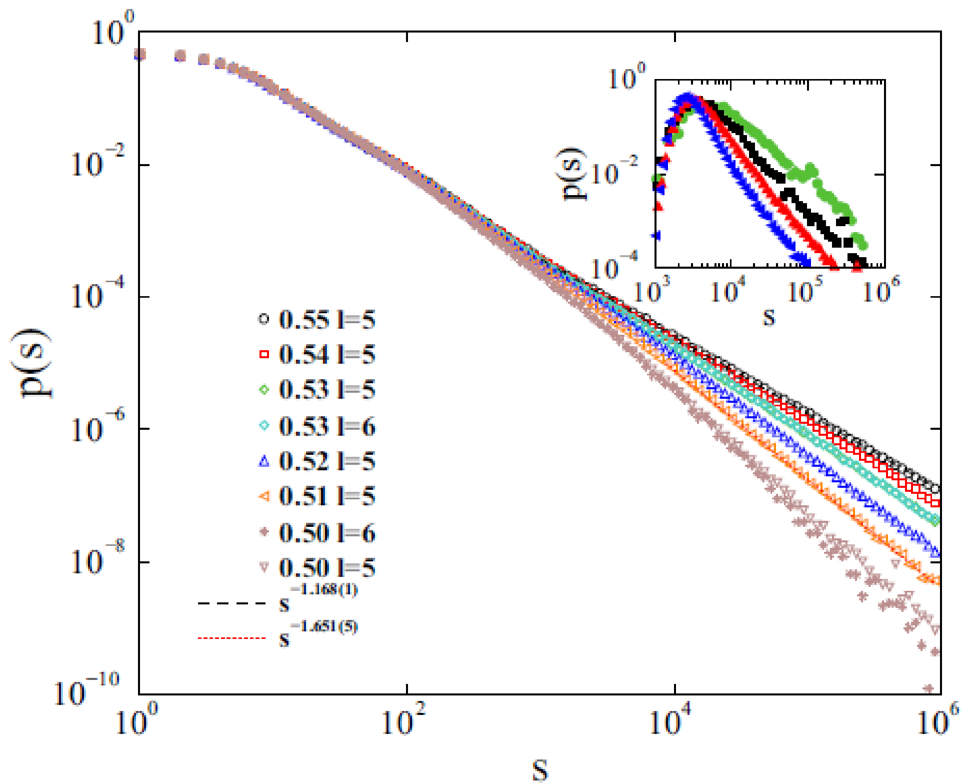

FIG. 5. Avalanche size distributions at different λ branching rates, denoted by the symbols, in the presence of inhibitory links in HMN2d with $l = 5, 6$ levels. From top to bottom curves: $\lambda = 0.55$, 0.54, 0.53 ($l = 5$ green and $l = 6$ cyan), 0.52, 0.51, 0.50 ($l = 5$ triangle and $l = 6$ diamond). Dashed lines show power-law fits for the tails of $\lambda = 0.55, 0.51$ cases, for $t > 1000$. Inset: overlapping avalanches case for half-filled initial condition at $\lambda = 0.51, 0.515, 0.52, 0.525$ (bottom to top symbols).

Inhibitory model: w_{ij}=*1* or w_{ij}=*-1* (prob. *0.2*)

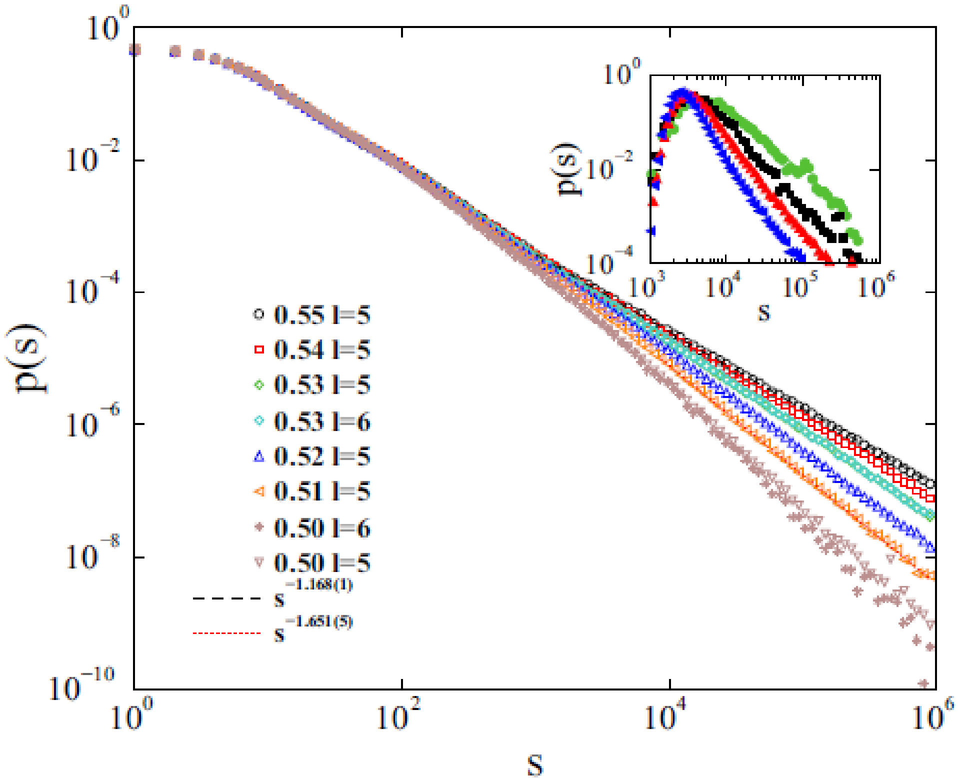

FIG. 5. Avalanche size distributions at different λ branching rates, denoted by the symbols, in the presence of inhibitory links in HMN2d with $l = 5, 6$ levels. From top to bottom curves: λ =0.55, 0.54, 0.53 ($l = 5$ green and $l = 6$ cyan), 0.52, 0.51, 0.50 ($l = 5$ triangle and $l = 6$ diamond). Dashed lines show power-law fits for the tails of $\lambda = 0.55, 0.51$ cases, for $t > 1000$. Inset: overlapping avalanches case for half-filled initial condition at $\lambda =$ 0.51, 0.515, 0.52, 0.525 (bottom to top symbols).

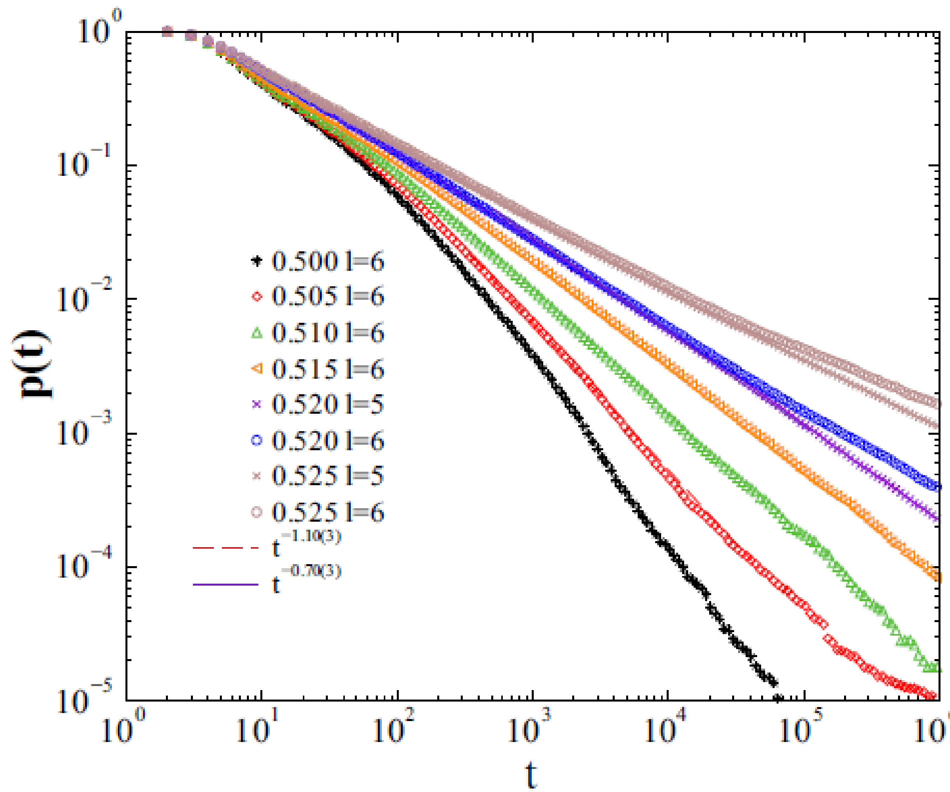

FIG. 6. Survival probability of the activity at different branching rates and $\nu = 1 - \lambda$ for the $K = 2$ threshold model with levels: $l = 5, 6$ for the case with 20% of inhibitory links. From bottom to top symbols: $\lambda = 0.5, 0.505, 0.510, 0.515, 0.520$ ($l = 5$ purple cross and $l = 6$ blue circle), 0.525 ($l = 5$ brown cross and $l = 6$ brown circle). Dashed lines are PL fits for the tails of $\lambda = 0.505$. 0.52 curves.

Inhibitory refractory: nodes cannot be reactivated for Δt time

Inhibitory refractory: nodes cannot be reactivated for Δt time

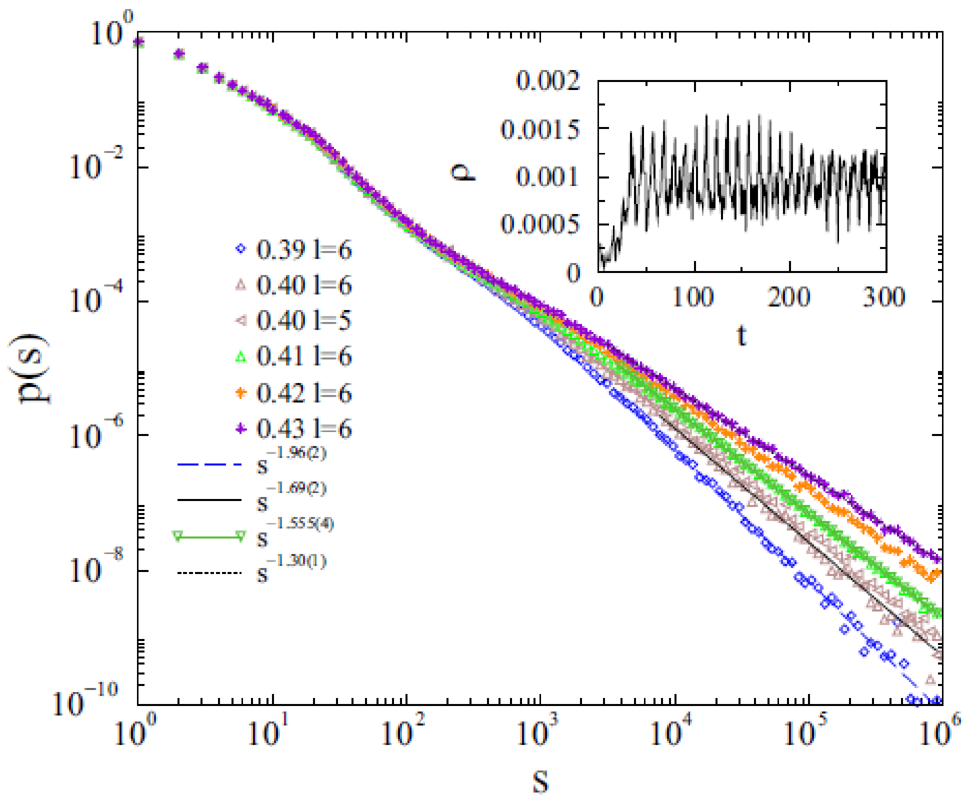

FIG. 7. Avalanche size distributions at different λ branching rates, denoted by the symbols, in case of the refractory model, in the presence of inhibitory links in HMN2ds with $l = 5, 6$ levels. From bottom to top symbols: $\lambda = 0.39, 0.40$ ($l = 5$ left triangle and $l = 6$ up triangle), 0.41, 0.42, 0.43. Dashed lines are PL fits for the tails of $\lambda = 0.39, 0.4, 0.41, 0.43$ cases for $t > 1000$. The inset shows the oscillatory behavior of $\rho(t)$ of a single run for $\Delta t = 10$.

Inhibitory refractory: nodes cannot be reactivated for Δt time

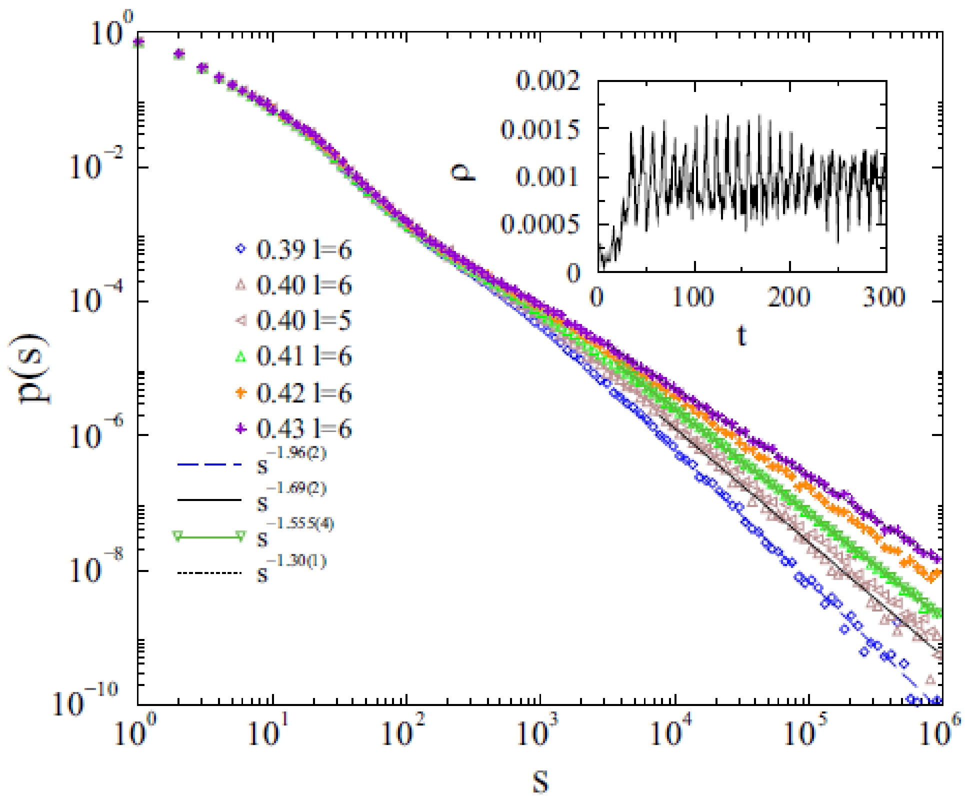

FIG. 7. Avalanche size distributions at different λ branching rates, denoted by the symbols, in case of the refractory model, in the presence of inhibitory links in HMN2ds with $l = 5, 6$ levels. From bottom to top symbols: $\lambda = 0.39$, 0.40 ($l = 5$ left triangle and $l = 6$ up triangle), 0.41, 0.42, 0.43. Dashed lines are PL fits for the tails of $\lambda = 0.39, 0.4, 0.41, 0.43$ cases for $t > 1000$. The inset shows the oscillatory behavior of $\rho(t)$ of a single run for $\Delta t = 10$.

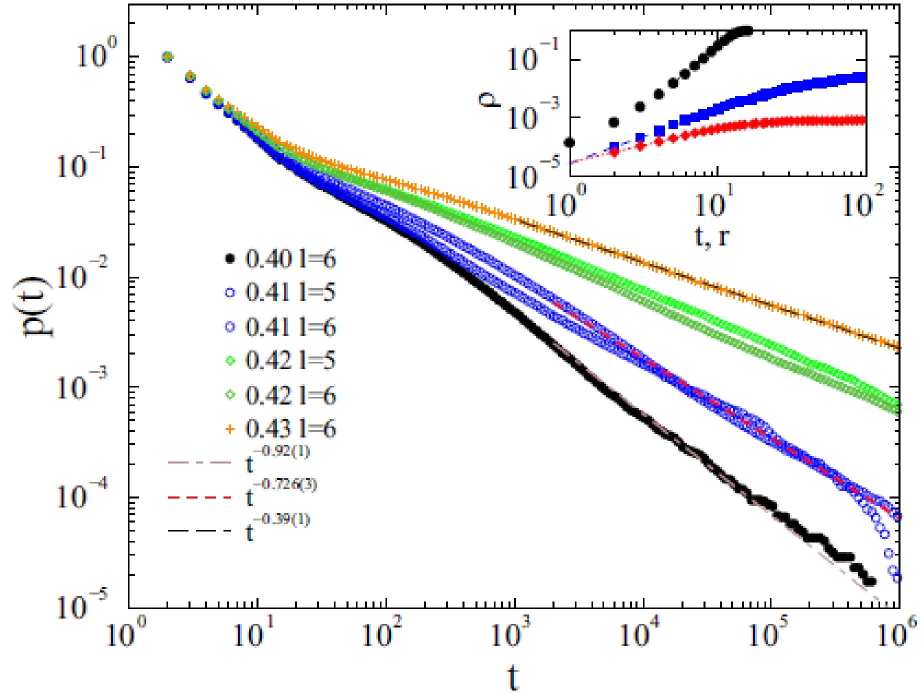

FIG. 8. Survival probability of the activity at different branching rates λ for the levels $l = 5, 6$, in the case of the inhibitory-refractory model. From bottom to top symbols: $\lambda = 0.40$, 0.41 ($l = 5$ and $l = 6$), 0.42 ($l = 5$ light green and $l = 6$ dark green), 0.43. Dashed lines show PL fits for $t > 1000$ for the $\lambda = 0.4, 0.41, 0.43$ cases. Inset: $\rho(t)$ at $\lambda = 1$, $l = 7$ averaged over 10^5 realizations. Blue boxes: excitatory; red diamonds: inhibitory. Black bullets: BFS $\rho(r)$ results. Dashed lines are PL fits for the initial regions: $1 \leqslant t < 10$) resulting in effective dimensions: $d_{\mathrm{eff}} = 1.84(3)$ (excitatory), $d_{\mathrm{eff}} = 1.19(1)$ (inhibitory), $d = 4.18(5)$ (graph dimension estimated for $5 < r < 10$).